THE HONG KONG POLYTECHNIC UNIVERSITY
DEPRTMENT OF COMPUTING

BIOMETRIC IDENTIFICATION USING CONTACT–FREE 3D HAND SCANS

By

Vivek Kanhangad

A DISSERTATION

SUBMITTED IN PARTIAL FULFILMENT OF THE REQUIREMENTS
FOR THE DEGREE OF

DOCTOR OF PHILOSOPHY

SEPTEMBER 2009

CERTIFICATE OF ORIGINALITY

I hereby declare that this thesis is my own work and that, to the best of my knowledge and belief, it reproduces no material previously published or written, nor material that has been accepted for the award of any other degree or diploma, except where due acknowledgement has been made in the text.

_____ (Signed)

Vivek Kanhangad (Name of student)

Dedicated to

My Family

ABSTRACT

BIOMETRIC IDENTIFICATION USING CONTACT–FREE 3D HAND SCANS

The hand identification problem has been extensively studied in the biometrics literature. Commercially available identification systems based on hand geometry features have gained high user acceptance and found wide ranging applications for personal verification tasks. Nevertheless, there are several critical issues that remain to be addressed in order to make hand identification systems more robust and user-friendly. Major limitations of current two dimensional image based hand identification include its high vulnerability to spoof attacks, inconvenience caused to the user by the constrained imaging set up, especially to elderly and people suffering from limited dexterity, and hygienic concerns among users due to the placement of the hand on the imaging platform. Obviating the need for hand position restricting pegs and the imaging platform, however, introduces a highly challenging problem of having to handle hand pose variations in three dimensional (3D) space. This dissertation explores the use of 3D contact-free hand scans and the possibility of integrating three dimensional shape and intensity information in order to overcome the above limitations. A two step, fully automatic, approach for hand matching that handles large changes in pose is developed. In the first step, the acquired 3D hand is utilized to robustly estimate its orientation based on a single detected point on the hand. The estimated orientation information is then used to normalize the pose of the 3D hand along with its texture. In the second step,

multimodal hand features extracted from the pose corrected range and intensity images are utilized to perform identification. The extracted palmprint and finger geometry features are combined using a new dynamic fusion strategy. It is shown that the dynamic fusion approach performs significantly better than the straightforward fusion using a weighted combination rule. In order to extract discriminatory features from the palmprint region of the 3D hand, two approaches that exploit local surface details have been developed. The proposed 3D palmprint matcher is shown to be more robust against spoof attacks. For the purpose of 3D finger matching, two representations that characterize the 3D finger surface features are extracted from the range images. The matching metrics proposed for the two finger geometry features effectively handle limited pose variations and perform partial feature matching in order to enhance the performance. Finally, an adaptive fusion framework based on hybrid particle swarm optimization (PSO) that chooses the optimal fusion rule and weight parameters for a desired level of security is developed. Experiments are performed on synthetic as well as real biometric matching scores to demonstrate that the proposed fusion approach consistently outperforms the existing framework based on decision level fusion.

LIST OF PUBLICATIONS BASED ON THE RESEARCH IN THIS DISSERTATION

1. A. Kumar, V. Kanhangad and D. Zhang, "Multimodal biometrics management using adaptive score-level combination", *Proc. ICPR 2008*, Tampa, Florida, pp. 1-4, Dec. 2008.
2. A. Kumar, V. Kanhangad and D. Zhang, "A new framework for adaptive multimodal biometrics management", *IEEE Trans. Info. Forensics & Security* (Accepted for publication), 2009.
3. D. Zhang, V. Kanhangad, L. Nan and A. Kumar, "Robust palmprint verification using 2D and 3D features", *Pattern Recognition*, vol. 43, pp. 358-368, 2010.
4. V. Kanhangad, A. Kumar and D. Zhang, "Combining 2D and 3D hand geometry features for biometric verification", *Proc. IEEE Workshop on Biometrics at CVPR 2009*, Miami, Florida, Jun. 2009.
5. V. Kanhangad, A. Kumar and D. Zhang, "Comments on an adaptive multimodal biometric management algorithm", *IEEE Trans. Systems, Man, and Cybernetics: Part C*, vol. 38, no. 5, pp. 438-440, Nov. 2008
6. V. Kanhangad, D. Zhang and L. Nan, "A multimodal biometric authentication system based on 2D and 3D palmprint features", *Proc. SPIE Biometric Technology for Human Identification V*, vol. 6944, Orlando, March 2008, pp. 69440C–69440C-9.

ACKNOWLEDGEMENTS

I have been privileged to have Dr. David Zhang as my chief supervisor. His unremitting quest for excellence and constructive criticism has inspired me to put my best efforts into this research work. I am extremely grateful to Dr. Zhang for his constant guidance and making my PhD experience an unforgettable one.

I owe a great deal to my co-supervisor Dr. Ajay Kumar for introducing me to the exciting area of biometrics. Had it not been for him, I would never have stepped out of my comfort zone to pursue research. No words are adequate to express my sincere gratitude to him, who on many occasions went out of his way to help me out. Nevertheless, I express my sincere thanks to him.

Special thanks to Dr. Lei Zhang for his thoughtful advices and suggestions during our weekly research group meetings. I am grateful to Nan Luo for all his help in the last three years, especially during my visits to the HIT Graduate School in Shenzhen. I would also like to thank Dr. Guangming Lu and his students for their help in arranging the biometric data collection sessions. I am also grateful to my friends Qijun Zhao, Denis Zhenhua Guo, Andy Wang, Wei Lei, Hu Yuan and Dr. Li Liu for their help in various ways during my three years of stay at the Biometrics Research Lab.

I would like to thank my roommates, Jiguang Yuan and Qinghao Meng for putting up with me during the times when I had to work late hours. Special thanks to Vaskar Raychoudhury for not just being a good friend, but also being a pillar of strength that I could fall back upon in times of need.

I very much appreciate the support and assistance rendered by Miu Tai and May Chu in administrative matters. I offer my sincere apologies to all those, who are inadvertently missed.

Last but by no means the least, I would like to express my deepest gratitude to my parents and sisters for their unstinted love and encouragement that enabled me to complete this work.

TABLE OF CONTENTS

LIST OF TABLES

LIST OF FIGURES

Chapter 1
Introduction

1.1 Biometrics

Biometrics refers to the methodologies for automated personal identification based on physical or behavioral traits. Traditional methods based on password and identity card provide simple ways to identify an individual. However, the major disadvantage of these techniques is that passwords and ID cards can be forgotten, stolen or lost leading to increased risk of them being fraudulently used. On the other hand, biometrics exploits biological traits that are unique and intrinsic to an individual and therefore provides a more robust (to circumvention) and reliable way of personal identification.

Biometrics such as fingerprint recognition has long been used for law enforcement and forensic applications. However, it is only recently that biometrics found a prominent place in our everyday life. Due to the increased security concerns in the past decade, biometrics has seen enormous growth and has been employed for a wide variety of civilian applications. Major applications include access control, time-attendance monitoring, automated teller machines (ATM), computer login and web security.

Based on their nature, biometric traits can be broadly classified into two categories:

1. Physiological characteristics: Include those biometric traits that are related to the physical shape of the body. Majority of the widely researched biometric traits fall into this category. Some of the examples for physiological characteristics include

fingerprint, face, iris, hand geometry, palmprint, palm vein and ear. Of these, face and hand geometry traits enjoy a very high user acceptance as these characteristics can be measured in a non intrusive manner, causing very little inconvenience to the user. Hand geometry systems are widely employed for personal authentication tasks because of its high user-friendliness and acceptance. Other hand based characteristics such as palmprint, palm vein and knuckle surface have drawn considerable attention from researchers only in the past few years and therefore these biometric traits have not yet established their presence in real world applications. Fingerprint, on the other hand, has been extensively researched and several major vendors are involved in developing fingerprint sensors and matching algorithms. Fingerprint identification remains the leading biometric technology in terms of revenue, despite it being relatively more intrusive than other hand based biometrics such as hand geometry.

2. Behavioral characteristics: Include those biometric traits that are associated with the behavior of a person. Examples for behavioral characteristic include gait, signature, keystroke and voice. However, voice is often considered a combination of both behavioral and physiological characteristics since certain parts of the body are involved in synthesis of voice. Voice biometrics is widely used for applications such as personal authentication (speaker identification) over the phone. Human gait, on the other hand, is one of the few biometrics traits that can be acquired covertly and without the cooperation of the users. This feature makes it an attractive biometric trait for surveillance applications along with other biometrics such as face.

A typical biometric system operates in two modes. In identification mode, the feature extracted from an individual is compared (matched) to template features belonging to all users in the database in order to establish the identity of the individual. This is often known as one-to-many matching. In the verification mode, a biometric system performs one-to-one matching to validate the claimed identity. A basic biometric system comprises the following five major processing modules (refer to figure 1.1):

1. Data acquisition module: This module comprises a device that detects (senses) the biometric data of an individual. Typical outputs of a sensor module in biometric systems include 1-D data (e.g., speech), 2-D data or image (e.g., face and fingerprint images) or 3-D data (e.g., 3D face and 3D ear).
2. Preprocessing module: This module processes the acquired data in order to perform operations such as de-noising, enhancement and normalization prior to feature extraction. The preprocessing may also include localizing and cropping a region of interest for feature extraction.
3. Feature extraction module: The data from the preprocessing stage is further processed by this module to extract discriminatory features for an individual. During enrolment, the extracted features are stored in the database as template features.
4. Feature matching module: This module computes the similarity between a pair of features. Specifically, the extracted feature is compared to the one stored in the database and a matching score that indicates the similarity/dissimilarity between the features is generated as the output.

5. Decision module: The similarity score generated in the matching stage is compared to the threshold of the system in order to either accept or reject the identity claim. In the identification mode, identity of the user is determined based on the highest similarity score among the set of scores generated by one-to-many matching.

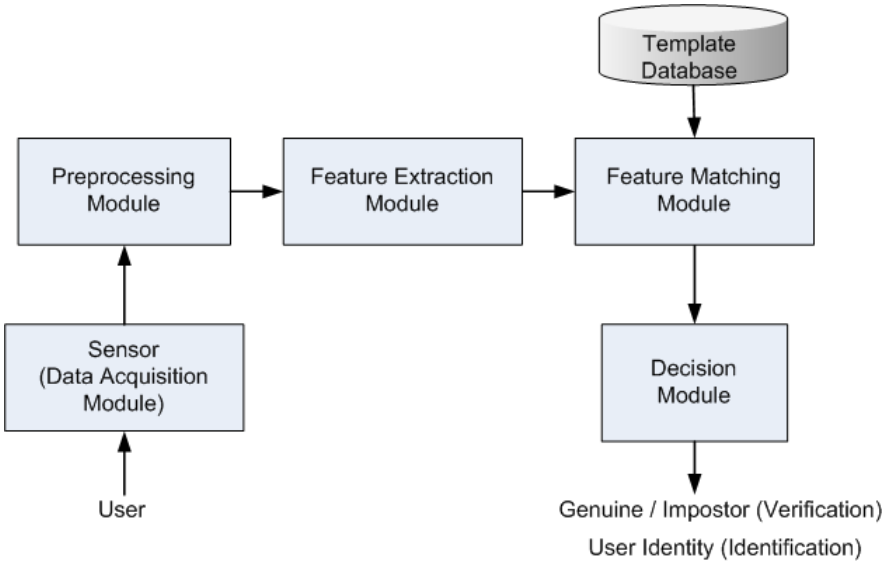

Figure 1.1: The block diagram of a typical biometric system showing the five major processing modules.

Performance of a biometric system is generally specified in terms of a set of performance plots and indices. In the verification mode, the performance of the system is evaluated based on the Receiver Operating Characteristics (ROC) curve. The ROC is a plot of False Reject Rate (FRR) or Genuine Acceptance Rate (GAR) against False Acceptance Rate (FAR) (refer to figure 1.2(a)). FRR is the probability of a genuine user being rejected as impostor, while FAR is the probability of an impostor being accepted as genuine user by the system. FRR and FAR are usually computed for a range of values of the system threshold. Equal Error rate (EER), the rate at which FAR and FRR are equal,

is often used as scalar performance index to evaluate and compare the accuracy different matchers. In the identification mode, Cumulative Match Characteristics (CMC) curve is commonly used to evaluate the accuracy of the system. A CMC curve is obtained by plotting the rank against the percentage of correct identification (refer to figure 1.2(b)), where rank-n is the number of top-n matching scores reported.

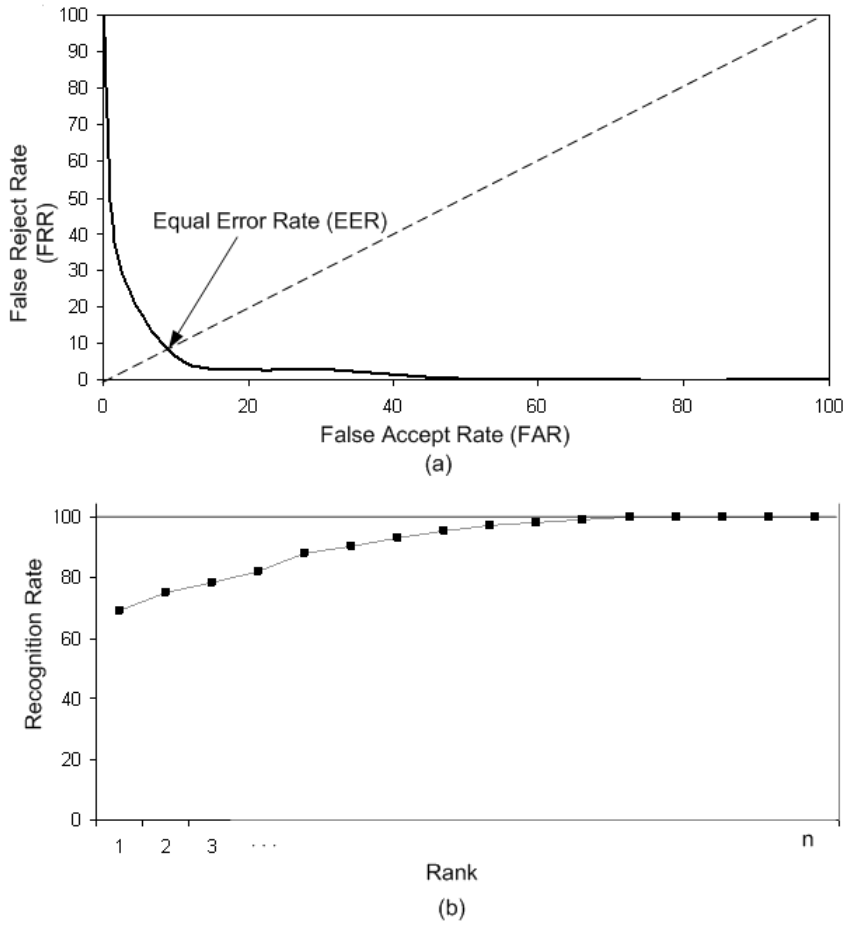

Figure 1.2: Performance curves. Typical (a) Receiver Operating Characteristic (ROC) and (b) Cumulative Match Characteristic (CMC) curves.

1.2 Hand Biometrics

Human hand is rich with several unique and stable characteristics that can be useful for biometric identification. Figure 1.3 shows the inner and the dorsal surface of the hand.

This figure also depicts the regions where various biometric traits are located on the hand. The following sections provide a detailed description of the hand based biometric modalities, namely, fingerprint, palmprint, hand geometry, hand vein and finger surface.

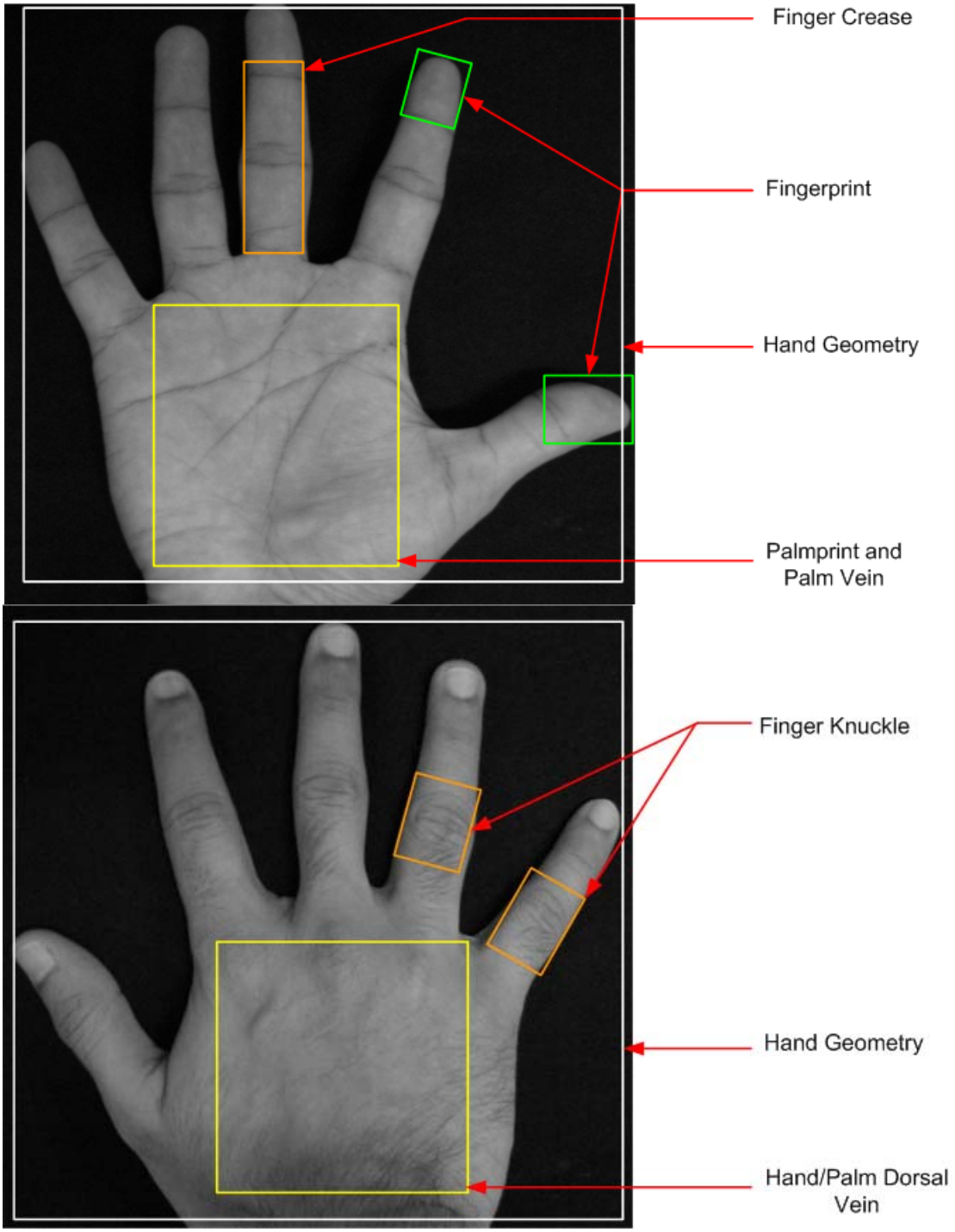

Figure 1.3: Two sides of the hand with locations of various biometric traits marked on it.

1.2.1 Fingerprint

Fingerprint is the pattern of ridges and valleys found on a fingertip. Fingerprint, as a biometric trait, has been extensively researched and widely used for forensic applications. The stigma associated with fingerprints due to its widespread use in criminal investigations has (to some extent) hampered its penetration and acceptability for civilian applications. However, with fingerprint scanners getting miniaturized it has become the preferred choice for personal authentication in portable devices such as laptops and mobile phones. Moreover, fingerprint identification continues to enjoy the highest market share among all biometric technologies. Fingerprint features are believed to be highly stable and discriminatory. However, the major disadvantage of the current fingerprint systems is that the images are acquired by pressing the finger against the sensing surface. Such contact based image acquisition systems not only cause hygienic concerns but also carry potential security threats. The fingerprint impressions left (by the users) on the imaging surface can easily be lifted and used to fabricate fake fingerprints.

Features on the fingerprint are defined at three levels (refer to figure 1.4). Level 1 features comprise the ridge pattern and its type (e.g., loop, arch and whorl), while the level 2 features include frictional ridge characteristics such as bifurcations and endings (minutiae). Level 3 features are the pores, incipient ridges and other details. While Level 1 and Level 2 features can be extracted from the standard 500 ppi fingerprint images (refer to figure 1.4), Level 3 features requires fingerprint images of higher resolution (1000 ppi or higher). Although Level 3 features have long been used by forensic experts for identification, the majority of the current automated fingerprint identification systems

(AFIS) utilize only Level 1 and Level 2 features as these systems are based on 500 ppi fingerprint images. However, recently, researchers [7] have shown that incorporating Level 3 features into the matching framework significantly improves the performance of the fingerprint matcher.

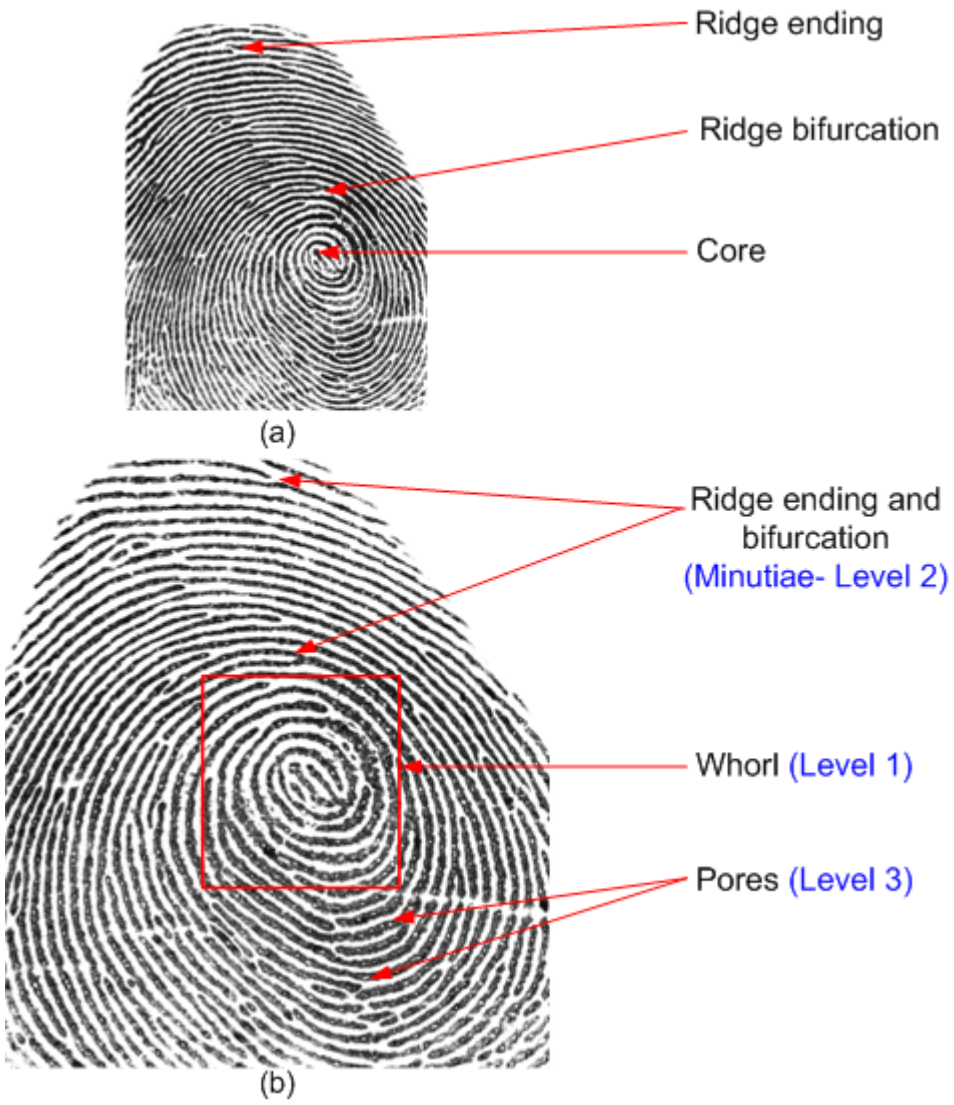

Figure 1.4: Fingerprint impressions (of the same finger) captured at two different image resolutions. (a) Features on a 500 ppi fingerprint image mainly include Level 1 and Level 2 details while (b) Level 3 features (pores, incipient ridges) can also be extracted from a 1000 ppi fingerprint image.

1.2.2 Palmprint

Palmprint is the part of the inner surface of the human hand from the wrist to the base of the fingers. Much like fingerprints, this region contains highly discriminatory features such as palmlines, wrinkles, frictional ridges and minutiae. Palmprints have long been used by forensic experts in criminal investigations where latent palmprints picked up from the crime scenes are matched to the inked impressions captured on paper. Early research in this area also focused on identification using images of the palmprint impressions. These images were obtained by digitizing the inked impressions on the paper using a digital scanner. However, majority of the current research in the literature utilize low resolution images (about 100 ppi) of the palmprint acquired using a digital camera. Palmprint identification using low resolution images has certain distinct advantages over other popular hand based biometrics such as fingerprints and hand geometry. In contrast to fingerprint identification systems, the image acquisition in palmprint systems can be done in a contact-free manner. In addition, the quality of acquired palmprint image is less affected by factors such as dry skin and bruises/cuts, which can adversely affect the performance of the fingerprint systems. On the other hand, since a larger area needs to be captured, the image acquisition devices are often bulky. Therefore the physical size of the palmprint identification systems makes them impractical to be embedded into portable electronic devices. Palmprints provide more distinctive features and as a result, personal identification system based on palmprints achieves significantly higher accuracy than the one based on hand geometry features. The major drawback of a palmprint identification system is its high vulnerability to spoof

attacks. Fake palmprint can be easily generated by printing palmprint images on paper. However it may not be possible to obtain a good quality palmprint image without user's cooperation.

Discriminatory features on the palmprint include ridge characteristics (such as minutiae, pore and delta point) and palmar flexion creases (principal palm lines and wrinkles). Figure 1.5 shows palmprint images from the same hand at two different resolutions. While all palmprint features described above can be extracted from the high resolution image of the palmprint, only major palm lines and wrinkles (flexion creases) are visible in the low resolution image. However, texture features extracted from the low resolution palmprint images have been shown to be highly distinctive and useful for personal authentication.

1.2.3 Hand Geometry

Hand geometry, along with the fingerprint and palmprint, is one of the widely researched hand based biometric modalities. Hand geometry based biometric systems exploit various geometric features extracted from hand images to perform personal authentication. Due to limited discriminatory power of these features, hand geometry systems are rarely employed for applications that require performing identity recognition from a large scale database or applications where the highest level of security is desired. Moreover, hand geometry based biometric systems are highly vulnerable to impostor attacks, since fake hands created using paper is adequate to circumvent the system. Nevertheless, these systems have gained immense popularity and public acceptance as evident from their extensive deployment for applications in access control, time and attendance applications

and several other verification tasks. Major advantages of hand geometry systems include simple imaging requirements (features can be extracted from low resolution hand images), ability to operate under harsh environmental conditions (immune to dirt on the hand and other external factors), and low data storage requirements. In addition, hand geometry acquisition and verification is extremely fast. These distinct advantages over other biometrics helped the hand geometry systems capture a niche market.

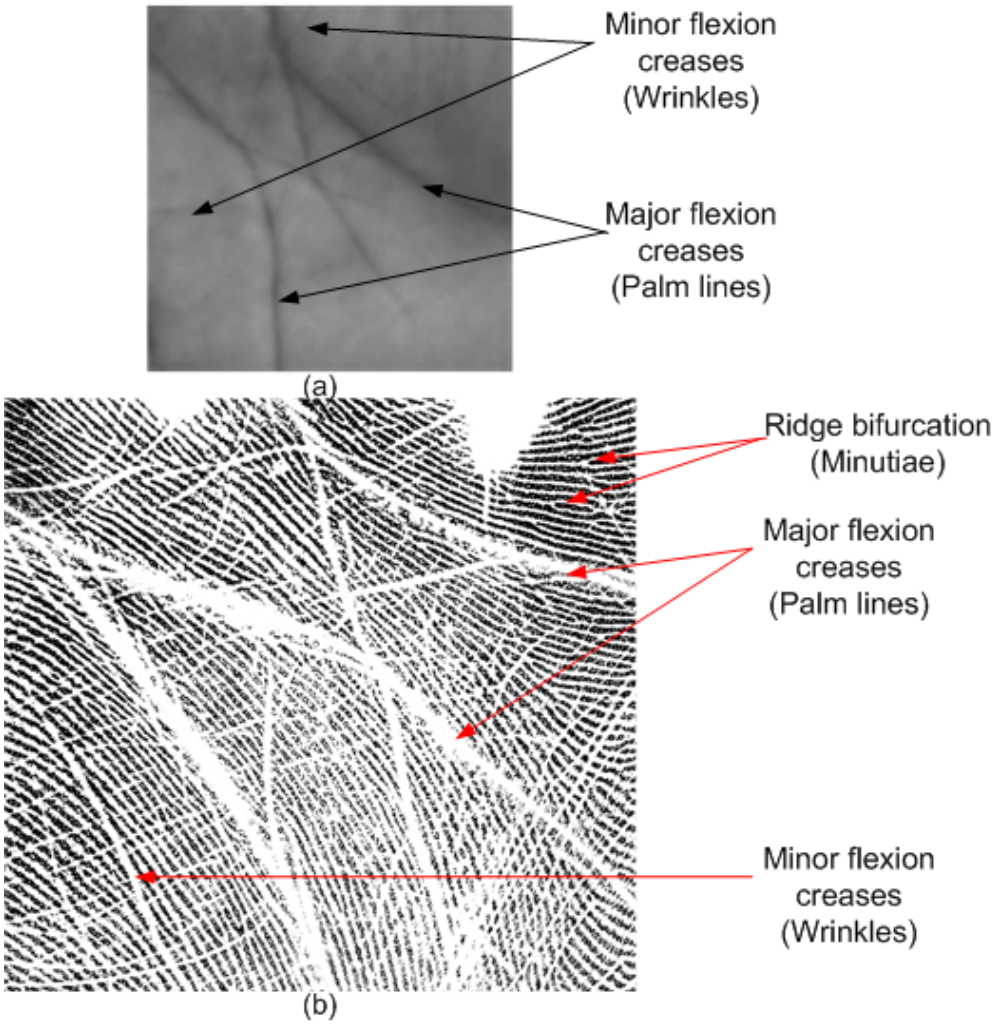

Figure 1.5: Human palmprint (of the same palm) captured at two different image resolutions. (a) Features on a low resolution (about 75 ppi) palmprint image include major flexion creases and a few minor creases while (b) finer features such as ridge pattern, minutiae and pores are also visible in a high resolution (1000 ppi) palmprint image.

Figure 1.6 shows typical hand geometry features extracted from the contour of the hand. Finger length is computed as the distance from the finger tip to its base along the orientation of the finger. Finger width measurements are made at a number of evenly spaced points along the finger length. Finger perimeter refers to the number of pixels on the finger contour. All the measurements shown in figure 1.6 are usually made in terms of pixels. In addition to these geometric measurements from the hand, the hand contour (silhouette) can also be used (as a shape feature) in establishing the identity.

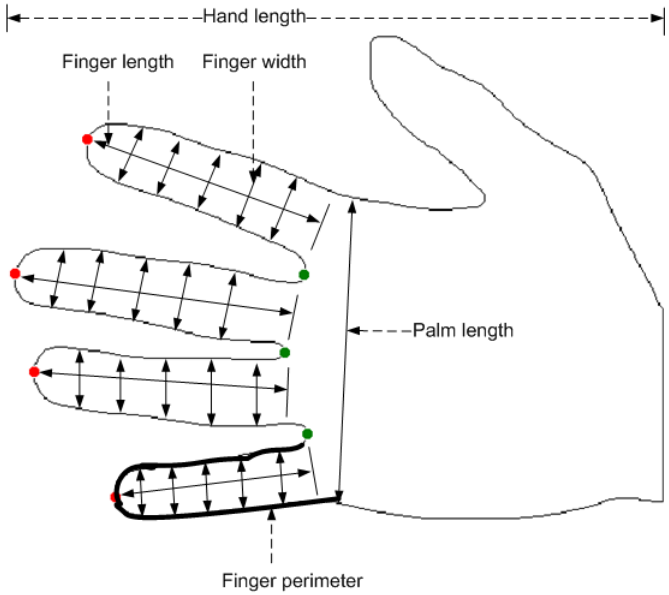

Figure 1.6: Typical hand geometry features marked on a hand silhouette.

1.2.4 Hand Vein

Human hand, in particular, the palmar region is abundant with blood vessels. These blood vessels (veins), which form an intricate and unique vascular pattern has attracted a lot of attention from biometric researchers [80],[72]. In addition, personal identification systems based on palm vein features are now available in the market [48]. Vein pattern

on the dorsum of the hand has also been investigated and found useful as a biometric identifier [29],[73],[16]. Much like the palmprint and hand geometry features, palm vein pattern can be acquired in a contract-free manner. This feature helps avoid the hygienic concerns among users, especially when a large number of people use the device. In addition, hand vein pattern has a distinctive feature of being internal to the human body, which makes them is extremely difficult to spoof and thereby enabling an extremely high level of security. Moreover, these features are highly stable and are unaffected by external wounds and injuries and other external factors.

Vascular pattern of an individual's hand can be acquired using either active NIR (Near Infrared) or passive IR (thermal) imaging. Active NIR imaging of hand vein is based on the fact that hemoglobin in the deoxygenated blood flowing through the veins absorbs the NIR illumination and therefore the vein vessels appear prominently dark in the acquired NIR images (refer to figure 1.7). Thermal imaging, on the other hand, exploits the temperature gradient that exists between the vein and the surrounding tissues. Various discriminatory features like lines, minutiae points (vein ending and bifurcation) and texture can be extracted from the acquired IR images of the palm.

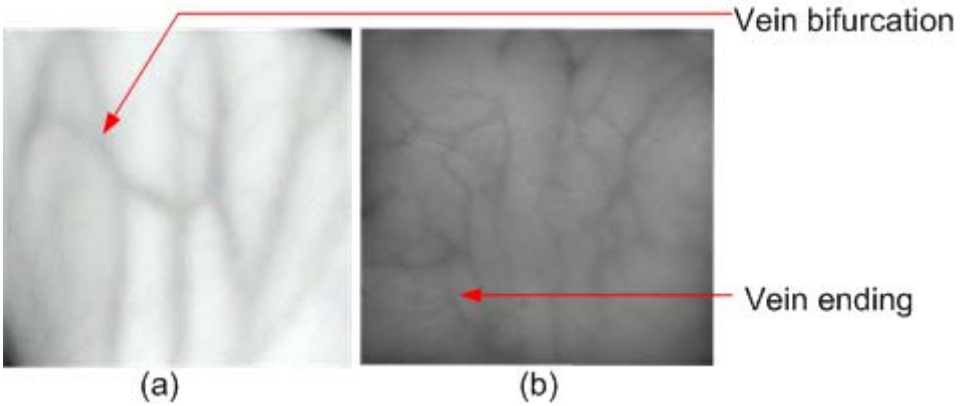

Figure 1.7: NIR images of the hand showing vein pattern on (a) the dorsal surface and (b) the inner surface (palm-side) of the hand.

1.2.5 Finger Surface

In addition to the above discussed major hand based biometric modalities, other characteristics such as finger creases (on inner surface of the finger) [103],[128] and finger knuckle (on back surface of the finger) [11] have also been investigated for its utility as biometric identifiers (refer to figure 1.8). Inner surface of the finger contain limited number of creases and therefore is more suitable to be used in combination with other hand characteristics such as palmprint and hand geometry to build a highly accurate biometric system. The pattern of wrinkles and creases on the finger dorsum surface (finger knuckle), on the other hand, have been found to be highly distinctive [11].

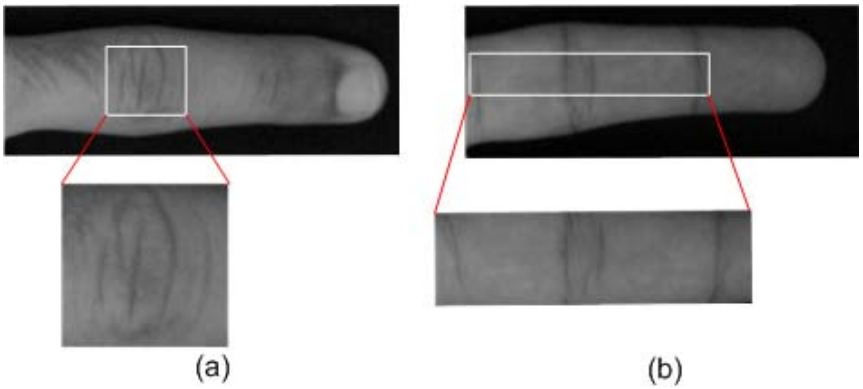

Figure 1.8: Finger surface images. (a) Finger dorsal surface and (b) the inner surface captured at about 100 ppi image resolution. Respective regions of interest are zoomed in to show the details.

Texture features extracted from even a single finger knuckle carry enough discriminatory information to perform personal verification for a relatively large population. The major advantage of these finger based biometric traits, in particular, the finger knuckle is that only a small area on the finger surface needs to be captured. In addition, feature extraction can be performed using the finger surface images acquired at relatively lower resolutions (as compared to fingerprint). Small sensing area and low

image resolution help reduce the overall size of the biometric system and achieve faster processing of the acquired images.

1.2.6 Challenges in Contact-free Hand Identification

Over the past decade, hand based biometrics have received tremendous attention from researchers. As a result, the problem of hand identification using hand geometry and palmprint features have been extensively studied. However, most of the existing works in the literature employ image acquisition modules that constrain the position and placement of the hand. In an attempt to address hygienic concerns and make the hand biometrics more user-friendly, researchers have proposed to acquire images in a contact-free manner. This, however, leads to a number of issues that need to be addressed before such approaches can be adopted in real world applications. Some of the major challenges in contact-free hand identification include:

1. Pose variation: Contact-free hand identification systems offer more freedom to the users in terms of the hand placement. A user is only expected to present his/her hand at a certain distance from the camera. The increased freedom, however, leads to large variations in 3D pose of the acquired hands. Figure 1.9 illustrates the pose changes in the acquired (textured) 3D hands. The variation in 3D pose of the hand is major issue in hand based identification systems, since it causes significant deterioration in matching performance of the 2D as well as 3D matchers. Large pose variation is also likely to impede the process of extraction of the region of interest. It is, therefore, necessary to normalize the pose of the acquired hand images (range and intensity) prior to feature extraction.

2. Deformation/bending: Human hand is not strictly rigid and therefore the deformation due to the elasticity of the skin cannot be ignored. Movement and bending of the fingers can introduce considerable deformation in the hand, and is a major concern in the absence of any pegs or the imaging platform. The performance of the hand geometry matchers suffers the most in the presence of hand deformation. Palmprint features on the other hand are relatively less affected, since the palmprint region of the hand is not prone to large skin deformations.

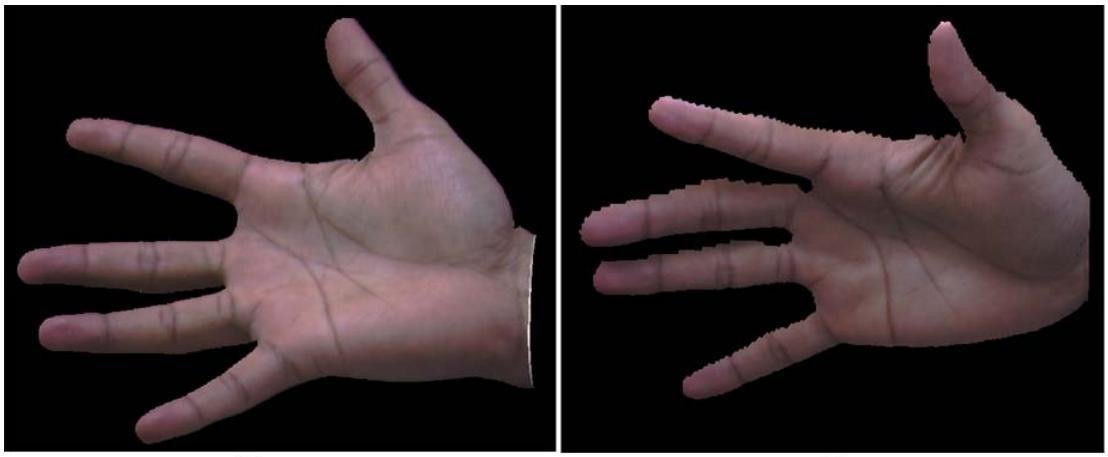

Figure 1.9: Effect of hand pose variations. (a) Textured 3D hand acquired from a user during enrolment. (b) Textured 3D hand acquired from the same user during verification. Large change in hand pose poses challenges for hand matching.

3. Illumination variation: The contact-free hand identification systems also need to deal with illumination changes, since it may be impractical to acquire images in uniformly illuminated environments. 2D palmprint matching performance is adversely affected by the illumination variations present in the acquired palmprint images. The problem is further compounded by changes in the hand pose, since the user hand presented at certain poses can introduce illumination changes in the

palmprint region due to shadowing effects (refer to figure 1.10), especially when a single light source is employed. The acquired palmprint images need to be re-lighted with frontal lighting (illumination normalization) in order to enhance the 2D palmprint matching performance.

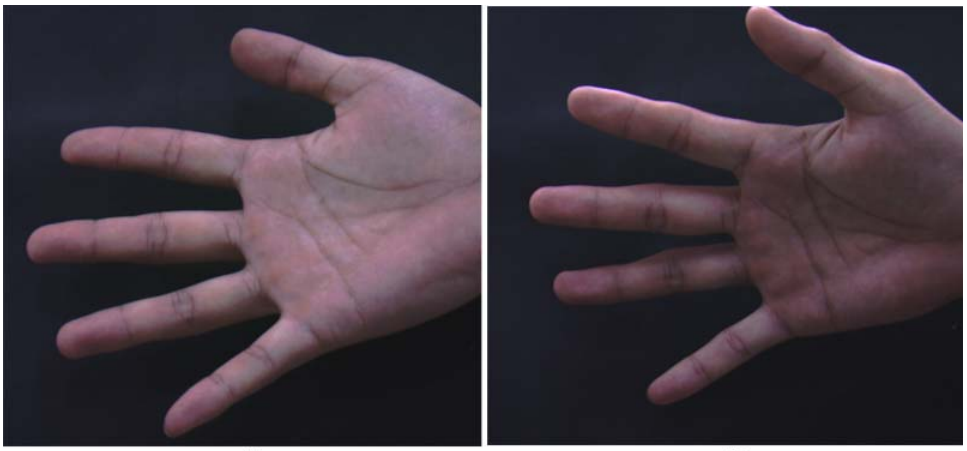

Figure 1.10: Effect of illumination variations. (a) 2D hand image (color) acquired from a user during enrolment. (b) 2D hand image acquired from the same user during verification. Large change in 3D hand pose results in illumination changes due to shadow effects and possible erroneous results for 2D palmprint matching.

4. Vulnerability to impostor attacks: Hand identification systems based on two dimensional palmprint and hand geometry features can be effortlessly circumvented using fake hands generated by printing hand images on paper (refer to figure 1.11). It is, therefore, essential to develop anti spoofing measures to increase the robustness of the system against such attacks. Another approach would be to augment two dimensional palmprint and hand geometry features with other hand features that are simultaneously acquirable and extremely difficult to spoof.

5. Selection of the optimal fusion strategy: Hand geometry features extracted from the hand are not known to be very distinctive. Therefore, often these features are combined with palmprint, finger surface or knuckle surface features in order to enhance the hand matching performance. However, since there are several combination strategies available in the literature, it is difficult to choose the one that provides the best performance. Therefore it is important to develop an approach that chooses a fusion rule that is optimal in some sense.

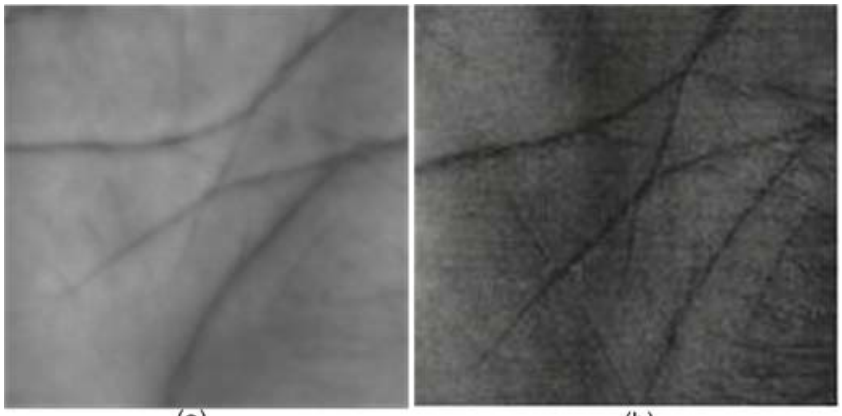

Figure 1.11: (a) A two dimensional palmprint image. (b) A fake palmprint generated by printing the palmprint image in (a) on a paper.

1.3 Contributions of this Dissertation

This dissertation attempts to address some of the issues (discussed in the previous section) associated with hand based identification systems. The proposed approach utilizes textured three dimensional hand scans to perform personal identification. Figure 1.12 plots the existing approaches in the area of hand identification along the two axes that represent the nature of image acquisition and the biometric modality (2D and 3D) utilized for identification. It should be noted that this figure only provides a few

representative and relevant approaches for each category. It may be observed from the figure 1.12 that the research work presented in this dissertation investigates into unexplored area of hand identification using textured 3D hand scans that are acquired in an unconstrained and contact-free manner. Moreover, none of the existing work addresses the problem of hand pose variations in the context of 3D hand identification.

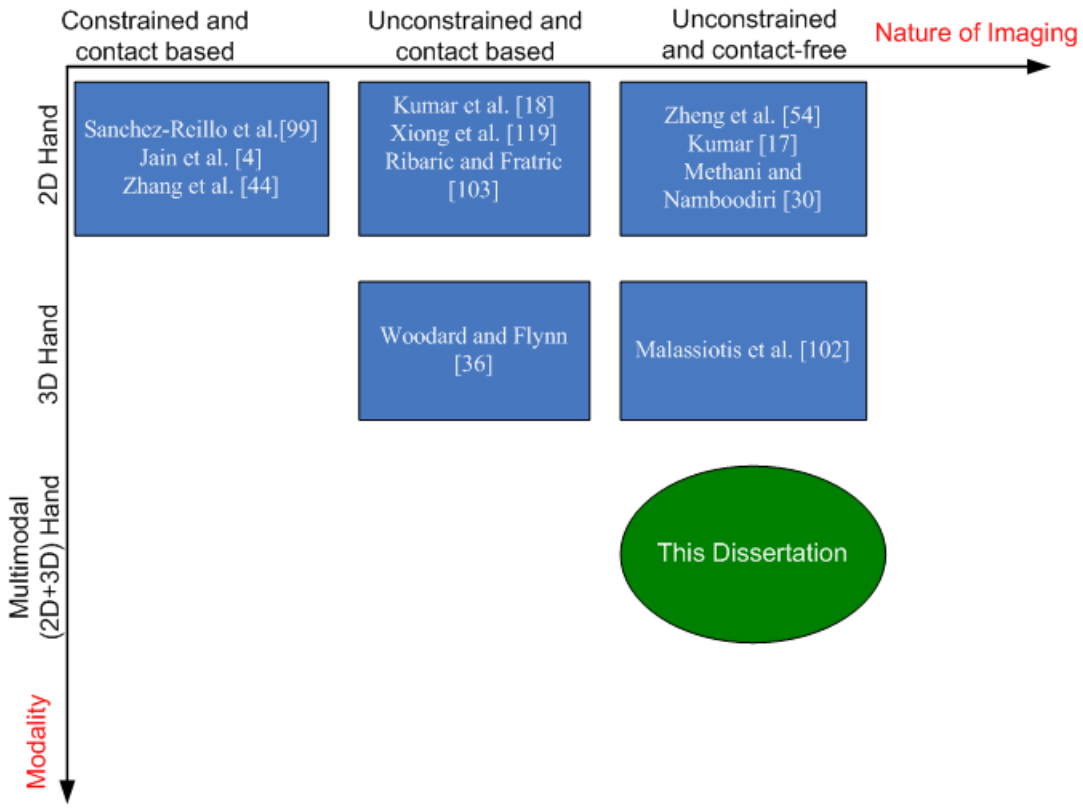

Figure 1.12: Illustration of current research in the area of hand biometrics.

The major contributions of this dissertation can be summarized as follows:

1. A fully automatic hand identification approach that can reliably authenticate individuals even in the presence of significant hand pose variations (in 3D space) is presented. The acquired 3D hand data is utilized to automatically estimate its pose based on a single detected point on the palm. The estimated 3D orientation

information is then used to correct the pose of both the 3D and the corresponding intensity image of the hand. The approach also employs a new dynamic fusion strategy to combine palmprint and hand geometry matching scores.

2. Two feature representations, namely, surface curvature and unit normal vector that characterize finger surface details are suggested for their usage in personal authentication based on 3D geometry of user hands. These representations explicitly capture local surface information by computing the local features for every data point on cross sectional segments extracted from the individual fingers. The proposed matching techniques perform a *sliding* match in order to handle partial cross sectional features and limited pose variations in the acquired hand images.
3. In order to perform 3D palmprint matching, two representations that characterize the rich surface details present in the palm region of the acquired 3D hand are presented. The first representation for 3D palm surface is based on the local curvature features, while the second representation namely *SurfaceCode*, is based on the quantization and binary encoding of the shape index feature. The key advantage of the proposed SurfaceCode lies in its compact and effective representation of 3D palm features.
4. An adaptive score level fusion framework based on hybrid particle swarm optimization (PSO) is developed for combination of multiple biometric modalities. The proposed fusion framework chooses the optimal rule from a pool of fixed combination rules and the corresponding weight parameters for a desired

level of security. This framework can be easily scaled up to accommodate any number of fusion rules and biometric modalities.

1.4 Organization of this Dissertation

This dissertation begins with a literature review of hand geometry and palmprint biometrics, detailed in Chapter 2. Various approaches available in the literature for image acquisition, feature extraction and feature matching are discussed in detail in this chapter. The chapter concludes with remarks on the status as well as the trend of research in this area.

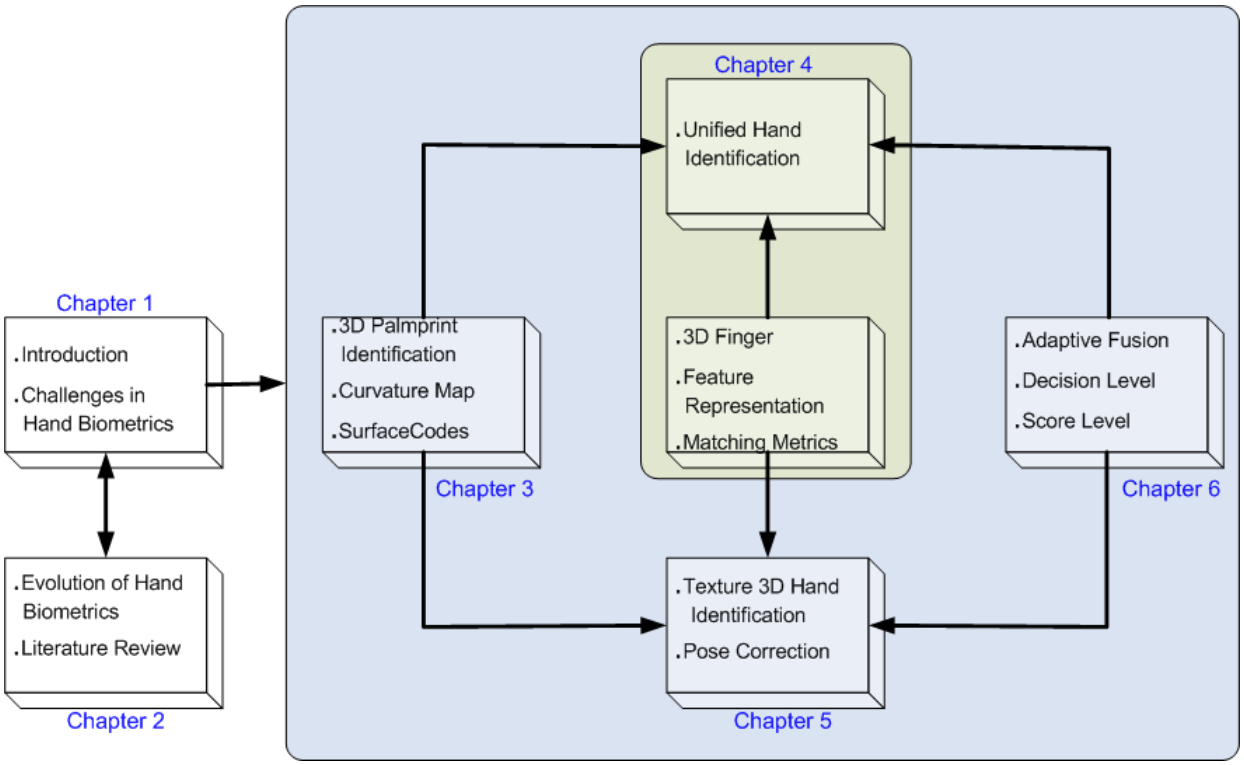

Figure 1.13: An Overview with links between the chapters of this dissertation.

Chapter 3 introduces novel approaches for 3D palmprint identification. A multilevel framework is presented to efficiently combine 2D and 3D palmprint features. A novel representation, namely the curvature map that characterizes the 3D palm surface is presented, along with the corresponding matching metric. This chapter also investigates the vulnerability of existing 2D palmprint verification approaches to sensor level attacks using fake palms.

Chapter 4 presents a unified framework for hand identification using 3D hand scans that are acquired in a contact-free manner. This chapter also presents novel representations and matching metrics for 3D hand geometry verification. Multimodal palmprint and hand geometry features extracted from the frontal hand scans are matched and the resulting matching scores are consolidated to build a highly accurate personal verification system.

Chapter 5 addresses the highly challenging problem of 3D hand pose variations in contact-free hand identification. A simple but efficient pose normalization approach is presented to obtain the frontal scan from any arbitrary pose of the hand. A new dynamic approach is introduced to combine palmprint and hand geometry matching scores based on the quality of the features extracted from the pose corrected images.

Chapter 6 presents a general framework for score level fusion that is adaptive to the security level requirement. Matching scores generated by matching individual hand features are combined using the optimal fusion rule and the corresponding optimal parameter set in order to achieve a desired level of security. The usefulness of the approach is first ascertained on a synthetic dataset followed by performance evaluation on two different hand databases.

Chapter 7 summarizes this dissertation with conclusions and presents directions for future work.

Figure 1.13 summarizes the chapters in this dissertation. This figure also provides an overview with major contributions of each chapter and illustrates how the chapters are linked to each other.

Chapter 2
Related Work

2.1 Evolution of Hand Biometrics

Hand based biometric systems, especially hand/finger geometry based verification systems are amongst the highest in terms of user acceptability for biometric traits. This is evident from their widespread commercial deployments around the world. Despite the commercial success, several issues remain to be addressed in order to make these systems more user-friendly. Major problems include, inconvenience caused by the constrained imaging set up, especially to elderly and people suffering from limited dexterity [5], and hygienic concerns among users due to the placement of the hand on the imaging platform. Moreover, shape features (hand/finger geometry or silhouette) extracted from the hand carry limited discriminatory information and therefore are not known to be highly distinctive.

Over the years, researchers have proposed various approaches to overcome these problems. Several research systems have been developed to simultaneously acquire and combine hand shape and palmprint features and thereby achieving significant performance improvement. Furthermore, a lot of researchers have focused on eliminating the use of pegs used for guiding the placement of the hand [82]. Recent advances in hand biometrics literature is towards developing systems that acquire hand images in a contact free manner. Essentially, hand identification approaches available in

the literature can be classified in to three categories based on the nature of image acquisition:

1. *Constrained and contact based*: These systems employ pegs or pins on the platform to constrain the position and posture of the hand. Image acquisition is usually done under controlled environments, with uniform illumination. Hand images acquired using such systems require minimum processing prior to feature extraction and thereby considerably reducing the time required for the process of authentication. Typical hand geometry features extracted from the acquired hand images include finger length, finger width, finger thickness, and palm width. Finger thickness features are computed from the lateral view of the hand, which can be easily acquired using a mirror with this kind of constrained imaging set up. Majority of the commercial systems and early research systems [99],[4],[3],[44] fall under this category.

2. *Unconstrained and contact based*: Hand images are acquired in an unconstrained manner, often requiring the users to place their hand on flat surface [18],[36],[11] or a digital scanner [31],[119],[103],[45]. Some researchers have even employed a backlit surface with camera mounted on top to acquire high contrast hand images [49]. Landmark points (finger tips and finger valleys) on the hand image are commonly used to align images prior to feature extraction. An alternate approach is to extract features that are invariant to image plane transformations of the acquired hand images.

3. *Unconstrained and contact-free*: This approach does away with the need for any pegs or platform during hand image acquisition. Users are given the freedom to hold their hand freely in the 3D space, usually at a fixed (approximately) distance from the

camera. The absence of any mechanism to constrain the placement of the hand introduces additional challenges in terms of variations in scale and out-of-plane transformations (3D pose) in the acquired hand images. Images acquired in cluttered backgrounds may also require sophisticated segmentation algorithms to localize the hand in the image. This mode of image acquisition is believed to be more user-friendly and have recently received increased attention from biometric researchers [102],[54],[17],[111],[30].

2.2 Hand Geometry

History of hand geometry biometric technology/systems dates back over three decades. In fact, the hand geometry system – Identimat developed by Identimation is one of the earliest reported implementations of a biometric system for commercial applications. Since then, the hand geometry biometric systems have found applications in wide variety of fields ranging from airports to nuclear power plants [39]. Recognition systems [101] offers various time and attendance and access control solutions based on hand geometry biometrics. Their access control solution HandKey extracts over 90 measurements from the user's hand image and stores the information into a 9 byte template. VeryFast access control terminal [25], manufactured by BioMet partners, captures the image of user's two fingers. Features extracted by processing this image are encrypted and stored as a 20 byte template. Accu-Time systems manufactures a similar access control device based on user's finger geometry [23]. Several units of the above mentioned systems have been installed at various places around the world. USPASS (formerly known as INSPASS) is the first and the largest hand geometry based biometric verification program undertaken by the US government to accelerate the process of immigration for authorized and

frequent travelers [39]. HandKey scanners were installed at certain airports in the US to accelerate the process of immigration for frequent fliers. Another large scale deployment was at 1996 Olympics Games in Atlanta, where hand geometry scanners were installed to restrict access to the Olympic Village.

Despite the commercial development and success of the hand geometry technology, there was not much literature available in the public domain until late nineties. However, since as early as 1970, several U.S. patents have been issued for personal identification devices based on hand/finger geometry measurements [96],[58],[98],[40]. Table 2.1 summarizes the inventions described in these patents. Most of the early work in the hand geometry literature was based on 2D images (intensity and color) of the human hand. However, with advancements in range image acquisition technology, a few researchers have also explored the utility of features extracted from range images of the hand. In the following sections, we describe in detail various methodologies proposed in the literature for 2D as well as 3D hand biometrics.

Table 2.1: Summary of inventions on hand/finger geometry identification systems.

Patent	Invention
[96]	Mechanical device (using bars and springs) to measure length and width measurements of the hand, placed palm down on a flat surface
[98]	Mechanical contact members are employed to measure outer dimension of fingers, while photoelectrical sensing devices compare the measurements with the ones stored in an identity card
[58]	Optical scanning device to measure finger lengths of four fingers (thumb not considered). Optical sensors are embedded on the flat surface to sense measurements, with a light source on top
[40]	Device captures virtual 3D image of the hand using a mirror to reflect the side view. Flat surface has four pegs with an illumination source on top. Various measurements including finger lengths/widths, hand thickness, surface area and perimeter are computed

2D hand geometry technology is based on the features extracted from two dimensional image of the human hand. Major processing modules in a 2D hand geometry

system are: Image acquisition system, preprocessing and feature extraction, feature matching and decision making. Following sections provide a detailed discussion on various approaches available for these processing tasks.

2.2.1 Imaging Techniques

A typical imaging set up for a two dimensional hand geometry system would involve the following components: A CCD camera, illumination source and a flat surface. CCD camera employed is usually low to medium resolution as the hand geometry features can be extracted from binary images of the hand. Joshi *et al.* [34] are one of the earliest researchers to build a prototype hand based biometric system. Their system mainly comprised a CCD camera for imaging finger creases and a fluorescent tube for illumination. In order to minimize variations in imaging and subsequent performance deterioration, the placement of the fingers was constrained using a metal strip and a micro-switch, which also activates the frame grabber to capture images of the fingers. Another prototype hand geometry system developed by Jain *et al.* [4] employs image acquisition module that includes a camera, an illumination source and a flat surface with five pegs (similar to the one in patent [40]). A mirror was employed to project the lateral view of the hand on to the CCD. This enables the system to acquire top and lateral view of the user's hand in a single image of 640 × 480 resolution. The hand geometry system developed by Sanchez-Reillo *et al.* [99] employs an image acquisition module similar to the one in [4],[3]. Pegs in their system, however, are equipped with pressure sensors to trigger the camera when a hand is detected on the platform.

Most of the early work in the literature employ pegs (on the flat surface where the user is required to place his/her hand) to restrict the position and movement of the hand during image acquisition. Though use of such constraints helps avoid registration/alignment of hand images before feature extraction, such systems cause inconvenience to the user and therefore are less user friendly. For example, elderly or people with arthritis and other conditions that limit dexterity may have difficulty placing their hand on a surface guided by pegs. Hence, a lot of researchers have focused their efforts to eliminate the use of pegs. Kumar *et al.* [18] employed a peg free imaging set up to acquire hand images. Users were requested to place their hand on the imaging table, with a digital camera mounted on top. They did not employ any special illumination, as the images were acquired in a well lit indoor environment. Authors in [49] employ an image acquisition system that includes a flat surface (for hand placement) with a VGA resolution CCD camera mounted on top. A uniform illumination is provided underneath the flat surface. Such an arrangement helps to acquire high contrast hand images which can binarized by simple thresholding. A few researchers [74],[45] have even used low resolution digital scanners to acquired hand images in a peg free manner. Though the approaches discussed above do not use pegs to constrain hand placement, they require the user to place his/her hand on a flat surface. Such contact may give rise to security as well as hygienic concerns among users. Fingerprint or palm-print impressions left on the surface by the user may actually be picked up and used to fabricate fake biometric samples. Zheng *et al.* [54] have addressed this problem by proposing a hand geometry technique using a non-contact, peg free imaging set up that allows users the freedom of

presenting their hands at any orientation, as long as the major part of the hand is captured. They employ a digital color camera to acquire hand images.

A few researchers have also employed 3D scanners to acquire range images of the hand. Active 3D scanners are usually preferred as they can effectively capture dense and accurate 3D data. Woodard *et al*. [36] are perhaps the first researchers to work on the range images of the hand for biometric identification. Their approach uses laser based vivid 910 3D scanner [81] to simultaneously acquire color and registered range images of the hand. In order simplify the hand segmentation process, users were requested to place their right hand against a wall covered with black cloth. In another system developed by Malassiotis *et al.* [102], users were asked to hold their hand in front their face while an in-house developed low cost 3D sensor was used to capture color and range images of the dorsal surface of the hand. 3D sensor employed in their system consisted of a color camera and a standard video projector.

2.2.2 Preprocessing and Feature Extraction

Prior to feature extraction, acquired hand images are usually processed to obtain a binary image of the hand or in some cases, a hand contour. In most cases, a simple thresholding scheme followed by morphological operations can be used to segment the hand from the background. Typical geometry features extracted from the hand include finger lengths, widths, finger area, finger perimeter and palm width. Please note that measurements from thumb have been found to be unreliable [102] and therefore, in most cases hand geometry features are extracted only from the remaining four fingers. This is especially

true in the case of peg free image acquisition systems where the variations in measurements of the thumb are extremely large.

Hand geometry system described in [4] measures features such as finger length, finger width and thickness of the hand along 16 different axes. Finger thickness features is computed from the lateral view of the hand. Authors propose to model the gray level profile along the measurement axis for feature extraction. Instead of explicitly measuring geometry features on the hand, authors in [3] and [119] propose to align finger shapes (contours) from a pair of hand images. In order to deal with the deformation of the hand shape (contour) caused by the movement of fingers, authors individually align respective pairs of fingers from the hand images. Sanchez-Reillo *et al.* [99] extracted an extended set of geometry features from the contour of the hand. In addition to the length and width features from the fingers, various angles and deviations at specific points on the fingers are extracted. A feature selection scheme, based on the discriminatory power of the features, is used to reduce the dimension of the feature vector.

Hand geometry systems that do not employ pegs to register/align hand images usually locate key points (commonly finger tips and valleys) in the hand image. This information can be used to align hand images prior to feature extraction. An alternate approach would be to extract features that are invariant to translation and rotation of the hand in the image plane. Authors in [31] explored one such method by modeling finger contours using implicit polynomials and computing algebraic invariants (features) from polynomial coefficients. The approach proposed in [49] represents hand shapes using Zernike moments that are invariant to transformation and scale. The resulting high dimensional feature vector undergoes a dimensionality reduction technique - PCA. Yörük *et al.* [45]

applied dimensionality reduction techniques on the binary images of the hand that are pre aligned using orientations of the fingers. Zheng *et al.* [54] proposed hand geometry technique using projective invariant hand features. Feature points detected on the fingers creases are used to compute the projective invariant hand features. Kumar *et al.* [12] demonstrated that discretization of the hand geometry features leads to significant improvement in performance. Various hand geometry features such as finger lengths/widths, palm length/width, hand length and perimeter are extracted and discretized before matching.

Segmentation of the hand in the acquired range images can be made simple by making use of the simultaneously captured (and registered) color or intensity image. Woodard *et al.* [36] worked on a combination of edge and skin detection algorithms to segment hand from the uniform background. Convex hull of the hand contour was used to locate finger valleys and to extract index, middle and ring fingers from the range image of the hand. Malassiotis *et al.* [102] employed a more complex approach to segment the hand from other parts of the body appearing in the image. Working solely on range images, authors use mixture of Gaussians to model and to subsequently segment hand.

The approach proposed in [131] investigates the pattern distorted by the shape (or curvature) of the hand. The distorted pattern captured by a CCD camera is coded by quad-tree to extract one dimensional binary feature. Though this approach does not extract 3D features from the range image of the hand, it essentially utilizes the 3D surface features in an indirect manner. Woodard *et al.* [36] computed shape index, defined in terms of principal curvatures, at every pixel in the range images of fingers and stored as feature templates for matching. The approach presented in [102] extracts two signature

functions, namely, 3D width and mean curvature for each of the four fingers (thumb excluded). Features computed for four fingers are concatenated to form a feature vector.

2.2.3 Feature Matching

Feature matching process computes the similarity (or dissimilarity) between the user's feature vector and the one stored during the enrolment. Various matching metrics proposed in the literature include Euclidean distance [99],[4],[49],[54], absolute distance [4], hamming distance [99], normalized correlation [18], cosine similarity [45] and Mahalanobis distance [31]. In addition to these simple matching metrics various trainable classifiers such as radial basis function (RBF) [99], support vector machine (SVM) [12] and Gaussian mixture model (GMM) [99] have also been used to classify the user's feature vector in to genuine or impostor class. Approaches based on alignment of hand contours use metrics such as mean alignment error [3], goodness of alignment [119] (based on finger width measurements) to compare a pair of hand shapes.

Match score generated from feature matching process is used to make a decision as to whether the user is a genuine or an impostor. This decision is usually made based on whether the match score is above or below a given threshold.

2.2.4 Performance

Hand geometry biometric systems based on 2D as well as 3D features have been shown to offer sufficiently high accuracy to reliably authenticate individuals. Researchers have been exploring various approaches (such as combining hand geometry features with other

biometric modalities) to improve the performance of the existing systems. Table 2.2 provides a comparative summary of major hand geometry approaches discussed in this chapter. This table also shows the performance achieved and the size of database employed for the experiments. However, one should also note that a one-to-one comparison of the approaches cannot be made as these performance statistics are obtained on different datasets, with non-standard experimental configurations.

As can be seen from the Table 2.2, early research [4],[3],[99] in the hand geometry literature employed pegs fixed on a flat surface to guide the placement of the hand. Most of the approaches [4],[99],[18],[12] shown in this table are based on the extraction of limited number of geometric features and hence achieve relatively high error rates. Moreover, the matching algorithms presented in [4],[3],[99],[31],[102],[49], [54] have only been evaluated on small databases (in terms of the number of users) and therefore the reported results may not provide a reliable measure of their performance. A few researches [6],[102] have investigated the utility of 3D features for hand matching. Both of these approaches are based on the features extracted from the dorsal surface of the hand. Major drawback of such approaches is that they do not facilitate the combination of the extracted 3D features and with other hand based features (such as palmprint) located on the palmar surface of the hand. Moreover, the authors in [6],[102] have not examined the possibility of integrating 3D features with 2D features (such as finger knuckle) that can be extracted from the dorsal surface of the hand. Instead, their approaches rely entirely on the 3D features with limited discriminatory information and hence result in moderate performance as evident from the reported experimental results. Moreover, the approach proposed in [102] does not take into account the changes in 3D pose of the user hand. Therefore the performance of this approach is likely to deteriorate in the presence of considerable pose variations that are expected in a contact-free imaging scenario.

Table 2.2: Comparative summary of some of the major approaches for hand geometry authentication

Reference	Methodology	Imaging		Database size (Users)	Performance (EER %)
		Modality	Pegs		
[4]	Measurements are made along 16 different axes, and matched using weighted Euclidean distance	2D	YES	50	6[1]
[3]	Individual finger shapes are aligned and a *shape distance* (Mean alignment error) is computed as match score	2D	YES	53	2.5-3[1]
[99]	Feature vector comprises several width, height and angle measurements. GMM is used for matching	2D	YES	20	6[1]
[18]	Feature vectors comprising 16 geometry measurements are matched using normalized correlation	2D	NO	100	8.5
[31]	Fusion of invariants from implicit polynomials and geometric features	2D	NO	28	1
[119]	Individual finger shapes are aligned using a elliptical model and finger tip/valley information	2D	NO	108	2.4
[6]	Shape index image is extracted from range images of fingers and is matched using normalized correlation coefficient	3D	NO	177(probe) 132(gallery)	5.5
[102]	Feature vectors comprising 96 curvature and 3D finger width measurements are matched using L_1 distance	3D	NO[2]	73	3.6
[45]	Independent Component Analysis (ICA) on binary images of the hand. Feature vectors are matched using cosine similarity measure	2D	NO	458	2
[49]	Principal Component analysis (PCA) on extracted higher order Zernike moment features. Reduced feature vectors are matched using Euclidean distance	2D	NO	40	2
[12]	Discretization of hand geometry features to improve the performance	2D	NO	100	1.9
[54]	Feature points on finger creases are detected and used to compute projective invariant features. Feature vectors are matched using normalized Euclidean distance	2D	NO[2]	23	0

[1] Equal error rate has been approximated from the ROC plot reported in the paper

[2] System acquires hand images in a completely contact free manner

2.3 2D Palmprint

Over the recent years, personal recognition based on two dimensional palmprint images has received tremendous attention from researchers. As a result, several approaches have been proposed in the literature [10]. Following sections provide a detailed discussion on various approaches available in the literature for palmprint recognition.

2.3.1 Imaging Techniques

Early research in this area utilized scanners to digitize the palmprint impression captured on a paper [42],[83]. Majority of the recent research, however, are focused on utilizing low resolution images of the palm. Researchers have developed ad hoc CCD based palmprint scanners [44], [26] that acquire palmprint images in a controlled environment. These devices also employ pegs on the scanning platform to restrict the position of the hand. In order to eliminate the use of pegs, researchers have proposed to employ digital cameras [18], and digital scanner [104],[103],[27] for hand image acquisition. In addition to being more user-friendly, these approaches have the advantage (over the ad hoc palmprint scanners) that a complete image of the hand can be acquired. Multiple discriminatory features including palmprint, hand geometry and finger surface can be simultaneously extracted (from such hand images) and combined to enhance the performance. The prototype system developed by Rowe *et al*. [97] acquires multispectral images of the whole hand. Multiple discriminatory features including fingerprint are extracted and combined in order to improve the performance. In an attempt to address

hygienic concerns, researchers have proposed to acquire hand images in an unconstrained and contact-free manner. While Kumar [17] has employed a simple set up for palmprint imaging in the visible spectrum, the work presented in [130],[129] designed a dedicated imaging system that captures multispectral palm images.

2.3.2 Preprocessing and Palmprint Extraction

Prior to feature extraction, the acquired hand images are preprocessed to extract a region of interest (palmprint) from the center of the palm. Firstly, the acquired images are processed to localize the hand. This step usually involves a simple thesholding followed morphological operations, especially when the hand images are acquired in a controlled environment with uniform illumination. Most of the approaches in the literature use interfinger (valley) points as reference points to localize a rotation invariant region of interest [116]. Researchers, however, have proposed different methods to detect the interfinger points on the hand contour. The popular method (especially with images acquired using peg-free set up) involves traversing the hand contour (boundary pixels on the localized hand) to detect local minima and maxima corresponding to finger joints and finger tips [103],[88]. An alternative method detects high curvature points on the hand contour [27],[18]. Another approach [36] employs convex hull of the hand contour to locate finger valleys. Figure 2.1 shows a hand contour with finger valley and finger tip points marked on it. This figure also shows the localization of the region of interest (palmprint region) using the two finger valley points. An exception to the interfinger point based approach is proposed in [14], which uses distance transform and ellipse fitting to estimate the center of the palm and orientation of the hand respectively. Once

the center of the palm is located, a square [27],[18], circular [15] or half elliptical [32] region of interest is extracted from the hand image. The approaches [17],[130] that employ unconstrained and contact-free imaging set ups extract a variable size ROI (usually the largest palmprint region that can be extracted in the acquired image) and then normalize it to a predetermined size. This is done in order to take into account the scale variations that are inevitable in such imaging set ups.

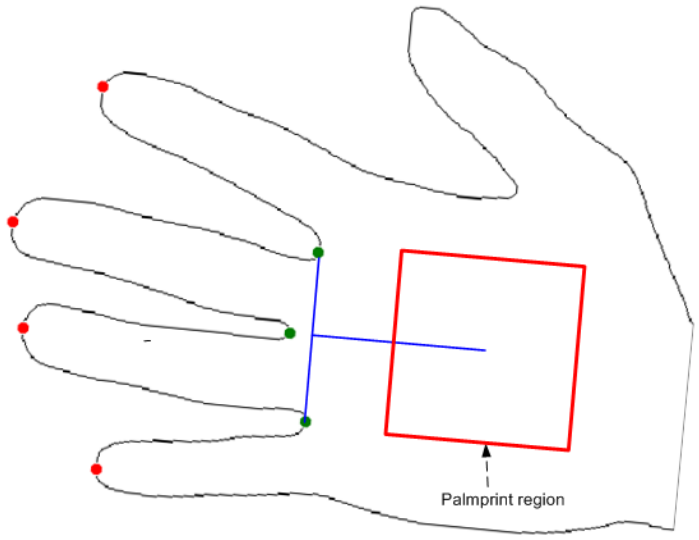

Figure 2.1: A hand silhouette with fingertips, finger valleys and the palmprint region marked on it. Two finger valley points are used to crop a sub image for the palmprint feature extraction.

2.3.3 Feature Extraction and Matching

The extracted region of interest is further processed for palmprint feature extraction. Various palmprint representation methods proposed in the literature can be roughly classified in to line feature, point feature, dimensionality reduction techniques, frequency domain transform [117],[127], wavelets [126],[75],[76] and Gabor feature coding based

approaches. Line based approaches [27],[123],[124],[125],[118],[70],[41],[115] employ edge detectors (such as canny edge detector or sobel operator) in order to extract principal lines and/or wrinkles on the palmprint. These approaches, however, do not utilize the crucial texture information present in the palmprint images. A few researchers have also studied feature point based matching for palmprints. The approach proposed in [83] extracts a set of feature points along the palm lines by binarizing a smoothed palmprint image and perform matching using a point set alignment algorithm. Another approach proposed in [2] explicitly utilizes ridge and minutiae features extracted from the high resolution (500 dpi) palmprint images. However, the applicability these approaches are largely limited to high resolution or latent palmprint matching, since the low resolution palmprint images lack well defined feature points for matching. Nevertheless, a SIFT (scale invariant feature transformation) feature point based approach has been investigated for matching a pair of low resolution palmprint images [59]. Dimensionality reduction based approaches simply employ linear [52],[122],[103],[71],[53],[107] and non linear subspace methods [50] (such as principal component analysis (PCA), linear discriminate analysis (LDA) and kernel PCA) in order to reduce the dimension of palmprint images or the extracted features. The computation of matching distance is performed using metrics such as Euclidean distance, cosine similarity or classifiers such as neural networks and support vector machines (SVM). The major disadvantage of dimensionality reduction techniques is that a large training set may be required to reliably learn the subspace coefficients. Moreover, small inaccuracies in the extraction of palmprint images may lead to significant performance deterioration as these approaches assume perfect alignment between a pair of palmprint images being compared. The

texture features extracted using Gabor filters have often performed well for recognition tasks including iris, face, and fingerprint. In the case of palmprint recognition, it has been shown to outperform line based and appearance based approaches [13]. Several approaches have been proposed for palmprint identification based on binary encoding of quantized Gabor features [44],[8],[9],[132]. These approaches have gained popularity due to its efficient and compact representations, which are more suitable for online applications. Binary encoding of orientation information extracted from palmprint images using have also been shown to perform well for palmprint identification [22],[132],[115]. Coding based approaches generally employ hamming distance in order to compute the matching distance between two binary features. In order to take into account small transformations (rotation and translation) between the pair of palmprint images being matched, multiple matches are performed by translating horizontally and vertically one of the 2D binary feature matrices over the other. The best matching score among all the computed scores is considered as the final matching score.

2.3.4 Performance

Table 2.3 provides a summary of some of the major palmprint recognition techniques reported in the literature. As can be seen in this table, the palmprint matching algorithms presented in [44],[132],[103],[88],[115] and [78] achieve significantly low error rates on considerably large databases. However, the majority of these techniques employ contact based (either constrained or unconstrained) image acquisition modules. A few of the approaches in the literature [27], [103] even use digital scanners to acquire hand images.

Table 2.3: Comparative summary of some of the major approaches for palmprint recognition.

Reference	Methodology		Imaging		Database size (Users)	Performance (EER %)
	Features	Matching metric	Modality	Pegs		
[42]	Line features represented as end points of straight line segments	Euclidean distance, angle	2D (Inked impression)	NO	20	0[3]
[27]	Line-like features extracted using Sobel and morphological operations	Correlation function, Neural network	2D	NO	50	Not Reported
[44]	Texture features (Binary encoded phase) extracted using Gabor filter	Normalized Hamming distance	2D	YES	386	0.6
[18]	Standard deviation of line map computed using four directional masks	Normalized correlation	2D	NO	100	11-12[3]
[132]	Binary encoding of the sign of ordinal comparison using a set of three orthogonal Gaussian filters	Hamming distance	2D	YES	283	0.22
[22]	Binary encoding of dominant orientation extracted using a bank of six Gabor filters	Angular distance	2D	YES	386	Not Reported
[103]	Subspace projection of palmprint images based on PCA	Euclidean distance	2D	NO	237	0.58
[88]	Two class correlation filters	Peak-to-correlation energy ratio	2D	YES	385	0.08
[115]	Binary encoding of orientation extracted using the finite radon transform	Pixel-to-area comparison	2D	YES	386	0.4
[78]	Texture features extracted using Local Binary pattern (LBP) on the directional map	Chi-square static, Probabilistic neural network (PNN)	2D	NO[4]	320	0.74
[17]	Integrating cohort information with texture features	Hamming distance	2D	NO[4]	235	8[3]

The slow acquisition speed and the large size of the digital scanners are likely to make them impracticable for real world applications. In order to address the problems associated with contact based imaging modules (such as hygienic concerns and inconvenience to the users), researchers have developed contact-free palmprint matching approaches [78], [17]. These approaches tackle a few challenges such as the changes in

[3] Equal error rate has been approximated from the ROC plot reported in the paper

[4] System acquires hand images in a completely contact free manner

scale [17] and the segmentation of the hand image acquired in dynamic and uncontrolled environments [78]. However, there are major issues (such as variation in 3D pose of the hand) yet to be addressed in the literature for contact-free palmprint identification. Moreover, as evident in the table, all existing approaches for palmprint recognition are based on the two dimensional images of the palmprint. In other words, none of the existing research work in the palmprint literature has investigated the utility of 3D features for palmprint matching. The combination of 2D and 3D palmprint features is expected not only to enhance the matching performance but also to make the palmprint systems more robust against spoof attacks. Therefore, exploration of novel approaches for 3D palmprint feature extraction and matching offers a promising direction for future work in this area.

2.4 Summary

This chapter provided a discussion on various methodologies/techniques available for the hand geometry and palmprint biometrics. While the history of commercial hand geometry systems dates back over three decades, academic research addressing critical issues lagged behind and appears to have begun only in late nineties. However, literature currently available in the public domain clearly shows that the research has now caught up with and has in fact transcended the commercially available systems. Majority of the early systems employed pegs to restrict hand placement in order to simplify the subsequent processing steps. This, however, caused inconvenience to the users. Several researchers have addressed this problem by proposing approaches to do away with pegs

and thus contributed to the increase in user friendliness of the hand based biometric systems. Recently, a few researchers have gone even further and proposed techniques that allow users to simply hold their hand in front of the camera, in a completely unconstrained manner, in order to get authenticated. However, these systems need to be rigorously evaluated on larger databases before they can be deployed for real world applications. In addition, only a few researchers have explored the use of 3D features for hand biometrics. Three dimensional hand features can be simultaneously extracted and combined to significantly improve the performance of the system. Therefore there is tremendous scope for further research in this direction. Finally, there is a pressing need to develop anti spoofing measures for hand based biometric systems, especially in view of the ease with which researchers have been able to circumvent a commercially available hand geometry system [57]. Anti spoofing measures proposed in the literature [38], [92] to detect fake fingerprints based on liveness detection can very well be employed in hand geometry systems. However, further research needs to be done to adapt these techniques and design hand geometry systems that can thwart attacks based on fake hands.

Chapter 3
Three Dimensional Palmprint Identification

The existing techniques for automatic palmprint identification are based on two-dimensional palmprint images. These approaches primarily suffer from changes in imaging factors such as pose and illumination, which can adversely affect the performance of the system. Moreover, 2D image based palmprint recognition systems are vulnerable to various kinds of attacks. For instance, if one could draw some lines on the palm and make it look like another person's palm, then a 2D palmprint recognition system could easily be circumvented. It may also be possible for an impostor to present a genuine user's fake palmprint image to gain access to restricted services. However, the capability of current palmprint authentication systems against such spoof attacks has not yet been investigated. One of the possible ways to overcome the limitations associated with 2D palmprint authentication systems is to use 3D imaging devices for capturing surfaces of human palm and use this data in performing user identification. Such observations are relatively invariant to illumination and provide more information on depth and curvature of lines and wrinkles on the palm surface.

This chapter presents a new personal authentication approach that simultaneously exploits 2D and 3D palmprint features. The objective of this work is to improve accuracy and robustness of existing palmprint authentication systems using 3D palmprint features. A multilevel framework for personal authentication that efficiently utilizes the robustness

(against spoof attacks) of the 3D features and the high discriminating power of the 2D features is presented. The approach uses an active stereo technique, structured light, to simultaneously capture 3D image or range data and a registered intensity image of the palm. A curvature based representation is investigated for 3D palmprint feature extraction while Gabor feature based competitive coding scheme is used for 2D palmprint matching. The 2D and 3D palmprint representations are comparatively analyzed for their individual performance and an attempt is made to achieve performance improvement using the proposed multilevel matcher that utilizes fixed score level combination scheme to integrate information. It is shown that improvement in performance can be achieved with the integration of 3D features as compared to the case when 2D palmprint features alone are employed. The experimental results also demonstrate that the proposed biometric system is extremely difficult to circumvent, as compared to the existing palmprint authentication approaches. The experiments reported in this chapter are based on a 3D palmprint range image database of 108 subjects.

3.1 Background

The automatic palmprint recognition has extensively been researched in recent years and several techniques have been proposed in the literature. Depending on the information they make use of, palmprint recognition techniques can be broadly classified into three types [13], namely texture, line and appearance based techniques. Most of these techniques are based on ideas from 2D image analysis [88], [66], [34], [44]. Although these methods have been shown to perform well on relatively large databases, efforts are

still required to achieve an automated, robust, and high accuracy palmprint recognition system capable of being deployed for high security applications.

There are a few works in the field of hand geometry recognition that exploits 3D features of the hand/finger. Even though a typical hand geometry recognition system [4],[99]utilizes 3D features such as height of the finger and the palm, these systems rely entirely on intensity images of the hand for feature extraction. The authors in [36] investigated the use of finger back surface as a biometric feature. A laser triangulation based range scanner is used to capture the range image of the back surface of the hand. They report a recognition rate of 99.4% using data obtained on the same day, while it reduced to 74% when gallery and probe images were obtained on different days. The US patent [46] illustrates the process of acquisition of 3D finger and palmprint information using multi camera and light projection system. However, this patent does not describe any method for verification/ recognition using the acquired biometric information. Malassiotis *et al.* [102] have developed a biometric authentication system based on measurements of user's 3D hand geometry. A low-cost 3D sensor is used to capture the range image of the user's hand. Furthermore, in order to improve the performance, biometric researchers have combined 2D and 3D features for face [120],[67] and ear biometrics [94]. However, there has not been any previous study in the biometric literature that investigated the utility of 3D palmprint features.

A robust biometric system has to deal with a number of security threats. Among various kinds of attacks [84], one of the simplest ways to attack a biometric system is to present a fake biometric to the acquisition device. Researchers have shown that biometric traits such as fingerprint [108] and gait [35] are vulnerable to spoof attacks. As a result,

various approaches have been proposed for fake fingerprint detection [1],[105],[92]. However, there has not been any attempt so far in the literature to analyze the vulnerability of palmprint systems to such attacks. This has motivated us to explore the utility of 3D palmprint features and the possibility of combining them with 2D features for palmprint recognition in order to enhance the accuracy as well the robustness of the resulting biometric system.

3.2 System Description

The image acquisition device is based on the principle of structured light. Figure 3.1 shows acquisition of a sample hand image using the 3D scanner.

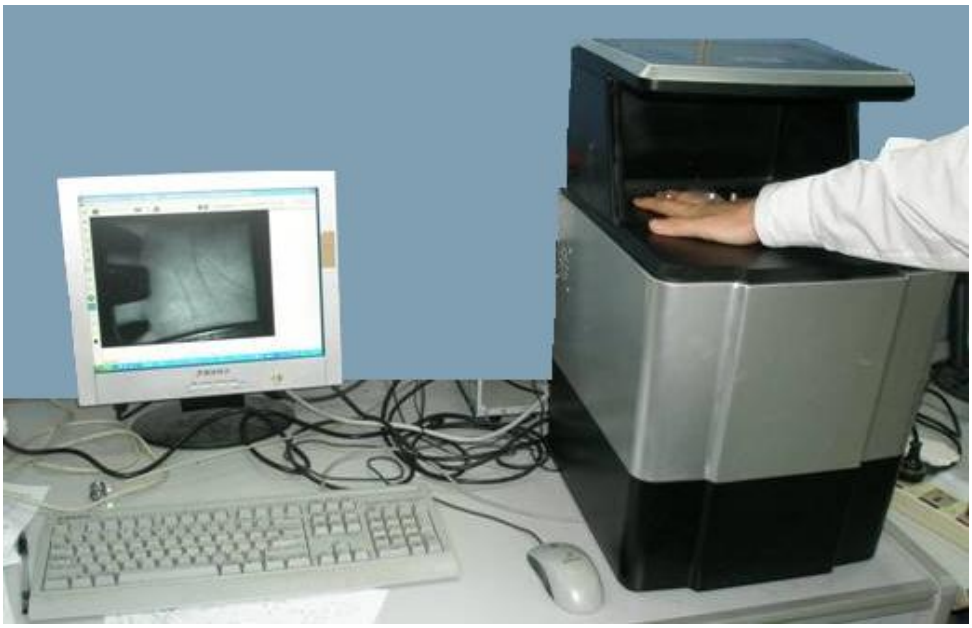

Figure 3.1: Palmprint range and intensity image acquisition using the device.

Infrared sensors are employed to detect the presence of the hand on the acquisition device (see figure 3.2). When a hand is detected the device projects multiple light patterns onto the palm surface and acquires depth information using active triangulation.

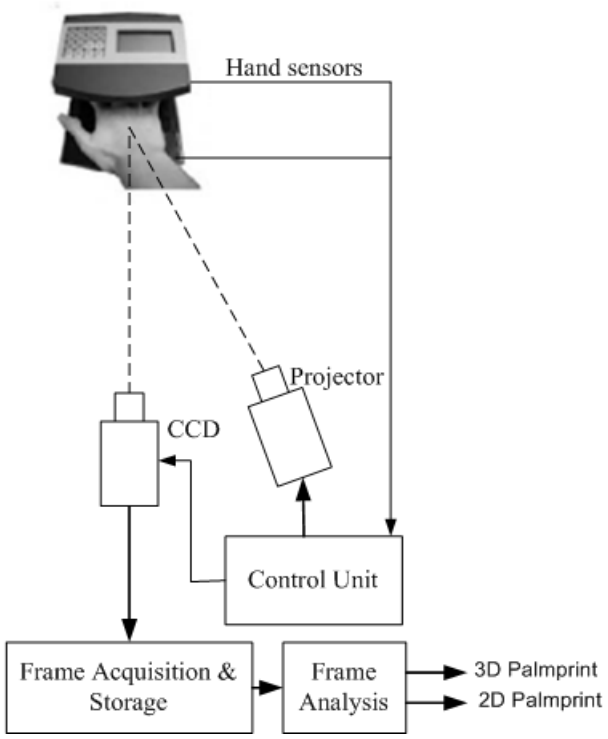

Figure 3.2: Block diagram of the image acquisition module.

Figure 3.3 illustrates a basic active triangulation system [87]. The origin of the reference 3D coordinate system lies at the center of the lens, with its z - axis aligned along the optical axis of the camera. The projector, located at a distance b (baseline distance) from the camera, illuminates a 3D point (x, y, z) on the surface of the object. The point (x, y, z) is projected (through the aperture of the camera) onto the image plane

at the pixel (u,v), as shown in the figure 3.3. Based on the similar triangles in this figure, we obtain the following equations:

$$\frac{u}{f}=\frac{x}{z} \text{ and } \frac{v}{f}=\frac{y}{z} \tag{3.1}$$

where f is the focal length of the camera. Given the parameters (f,b) and the pixel coordinates (u,v), the 3D coordinates of the point can be computed as:

$$x=\frac{b}{(f\cot\phi+u)}.u,\ y=\frac{b}{(f\cot\phi+u)}.v \text{ and } z=\frac{b}{(f\cot\phi+u)}.f \tag{3.2}$$

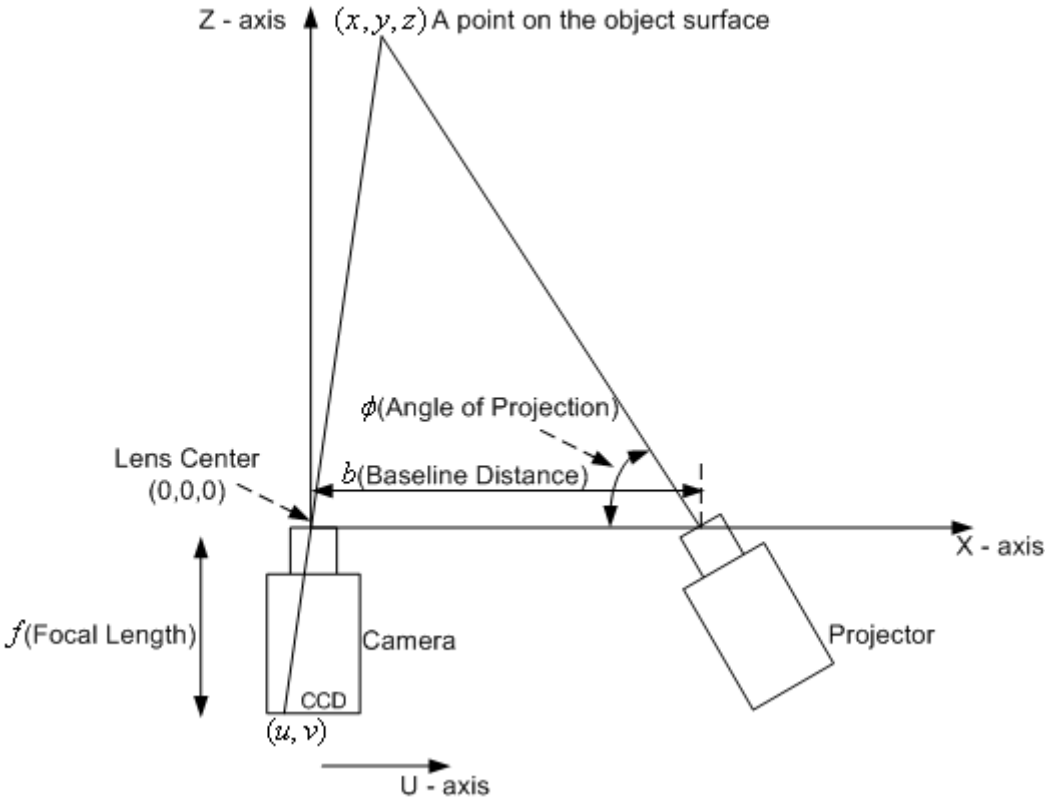

Figure 3.3: Illustration of active triangulation geometry.

The above process computes the 3D coordinates for a single point on the surface of the object. In order to obtain dense 3D coordinate data and to speed up the computation of range values, a specific light pattern (structured light) is projected on to the scene. The system employed in this work uses a computer controlled Liquid Crystal Display (LCD) projector that generates stripe patterns and projects onto the surface of the object. A CCD camera is used to capture the images formed on the object. The sequence of images captured by the CCD camera is processed using the active triangulation technique to obtain the 3D palm data. This device acquires 3D data in point cloud form. It also acquires a registered (captured near simultaneously) intensity image in the course of its normal operation. The size of these images are set to 768×576 pixels.

Each of the acquired 2D images is processed to extract the region of interest (ROI) using the method described in reference [44]. This method establishes a coordinate system with the gaps between the fingers as reference points and extracts a sub image of fixed size located at the central part of the palmprint. Since the 2D and the 3D data are acquired simultaneously, the two images are registered and the pixel coordinates of the 2D sub image can be used to locate the ROI and extract the 3D sub image.

Figure 3.5 shows samples of 3D and corresponding 2D sub images in our database. These 3D and 2D sub images are further processed to extract surface curvature (3D palmprint feature) and competitive code (2D palmprint feature) [22] respectively. The similarity between two curvature maps is then calculated using the local correlation method. If the matching score is greater than the threshold of Decision Module I, the query is rejected as a fake palm or an impostor and the process is terminated. This constitutes Level 1 of the proposed multilevel authentication approach. On the other hand, if the

matching score computed at Level 1 is below the threshold, matching proceeds to Level 2 where the matching score from the 2D palmprint feature is combined with the 3D matching score from Level 1 to obtain a final matching score. This score is used to make a decision as to whether the claimant is a genuine user or impostor. The entire process of the system is illustrated in Figure 3.4.

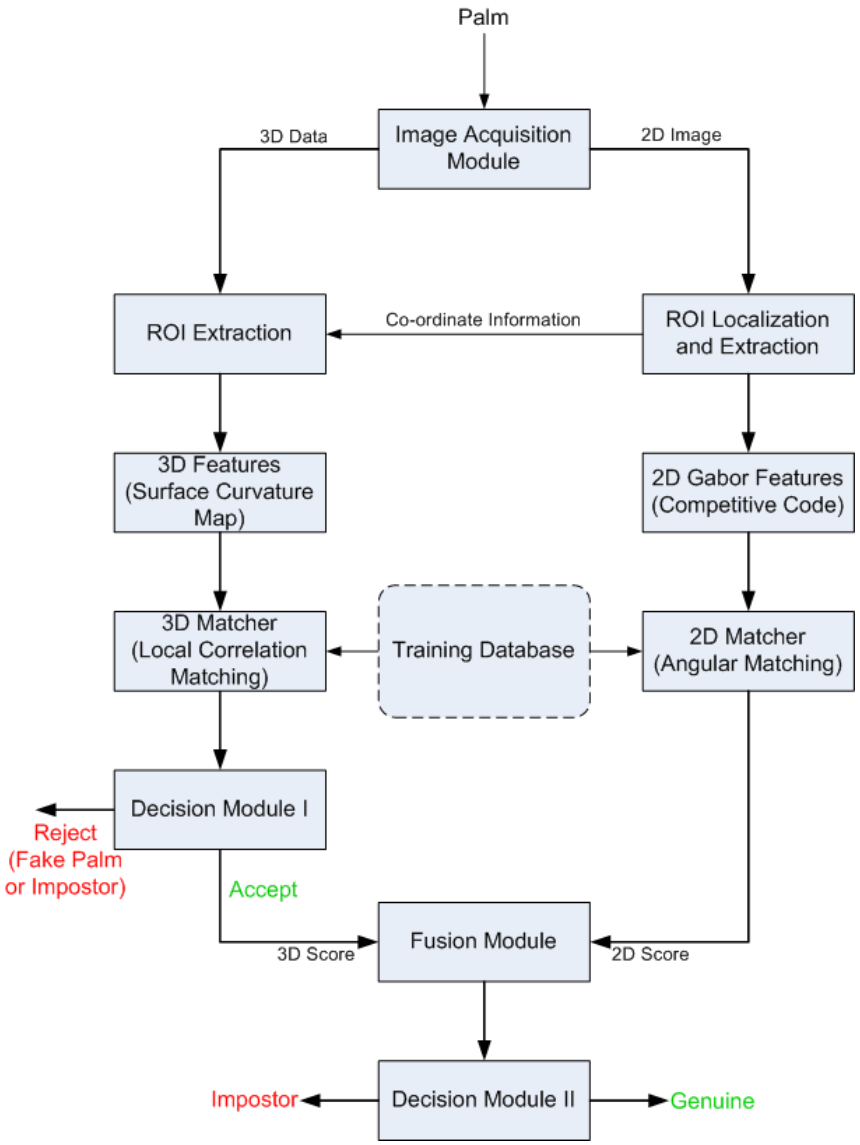

Figure 3.4: Block diagram of the multimodal palmprint authentication system.

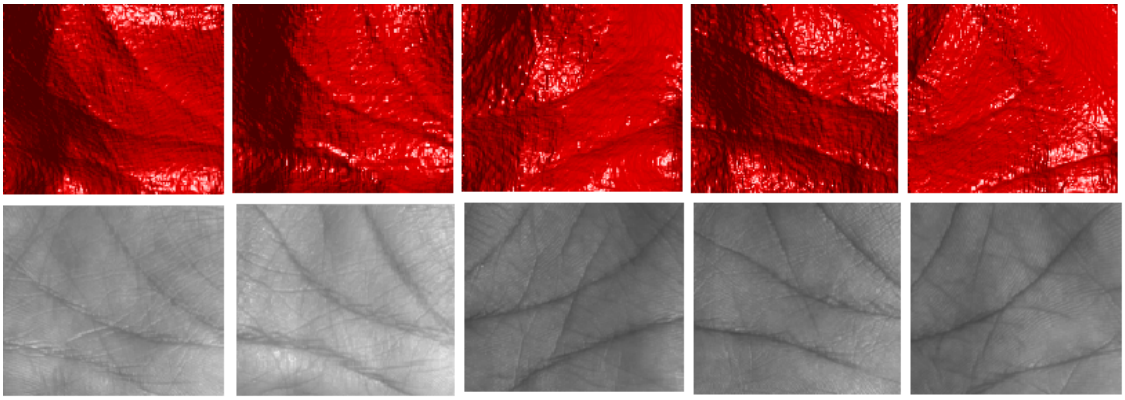

Figure 3.5: Samples of 3D (first row) and 2D (second row) palmprints in the database.

3.3 3D Palmprint Matching

The 3D palmprints offer unique and highly discriminatory information resulting from depth of palm lines and creases. As can be seen in figure 3.5, the range images of the palmprint (3D palmprint) are rich in local structural features. The surface curvature properties have been widely used to represent and recognize various surfaces. Properties such as mean and Gaussian curvatures are also used to classify points on a surface to different classes [55]. The following section presents a representation, namely, curvature map for 3D palmprint matching.

The localized region of interest, i.e., 3D palmprint, is processed to extract principal curvatures at every data point. The principal curvatures are computed by fitting a surface over a local neighborhood and then estimating its partial derivatives. For an image patch surrounding a pixel, represented by $X(u,v) = (u, v, f(u,v))$, Gaussian curvature (K) and mean curvature (H) are calculated as follows [24]:

$$K(X) = \frac{f_{uu} f_{vv} - f_{uv}^2}{(1 + f_u^2 + f_v^2)^2} \quad \text{and} \quad H(X) = \frac{(1 + f_u^2) f_{vv} + (1 + f_v^2) f_{uu} - 2 f_u f_v f_{uv}}{(1 + f_u^2 + f_v^2)^{3/2}} \qquad (3.3)$$

where, f_u, f_v and f_{uu}, f_{vv}, f_{uv} are first and second order partial derivatives of $f(u,v)$. Once the values of K and H are computed at every point on the 3D palm surface, the principal curvatures k_1 and k_2 can be determined as:

$$k_1, k_2 = H \pm \sqrt{H^2 - K} \tag{3.4}$$

In practice, these principal curvature values are computed by fitting a surface over a local neighborhood and then estimating first and second derivatives of the surface at the center pixel [90]. The key factor is to choose a 2D polynomial of appropriate order (at least twice differentiable, since we have to estimate its second order derivatives). While higher order polynomial, such as bicubic, better approximates the local surface shape, it can make the surface fit more sensitive to noise or outliers in the data. Therefore, we perform local surface fitting with a biquadratic polynomial of the following form:

$$f(u,v) = a_{00} + a_{10}u + a_{01}v + a_{11}uv + a_{20}u^2 + a_{02}v^2 \tag{3.5}$$

The first and second derivatives of the fitted polynomial, evaluated at the center of the image patch ($u = 0, v = 0$) are given by:

$$f_u = a_{10}\ ,\ f_v = a_{01}\ ,\ f_{uv} = a_{11}\ ,\ f_{uu} = 2a_{20}\ ,\ f_{vv} = 2a_{02} \tag{3.6}$$

Therefore the process of polynomial fitting and computing partial derivative estimates reduces to solving equation (3.5) for polynomial coefficients using least squares. Solving a matrix formulation of equation (3.5), we obtain image filter like rectangular window operators which can be convolved with the range image to obtain its partial derivative estimates. Some specific examples of these window operators are discussed in [89],[86].

Since the above mentioned process involves the estimation of second order derivates, the estimated curvature values are sensitive to noise in the input 3D data. This problem

can be overcome by increasing the size of the local neighborhood used for fitting the surface. However, a large window size can smooth the image, resulting in the loss of minute details in the 3D palmprint image. In our experiments, we empirically fixed the size of window to be 9×9.

3.3.1 Curvature Map Representation

In order to represent the curvature of every point on the 3D palmprint image by a scalar value, we utilized the curvedness (C) introduced in [63]. The positive value C is a measure of how sharply or gently curved a point is [55]. It is defined in terms of principal curvatures k_1 and k_2, as:

$$C = \sqrt{(k_1^2 + k_2^2)/2} \tag{3.7}$$

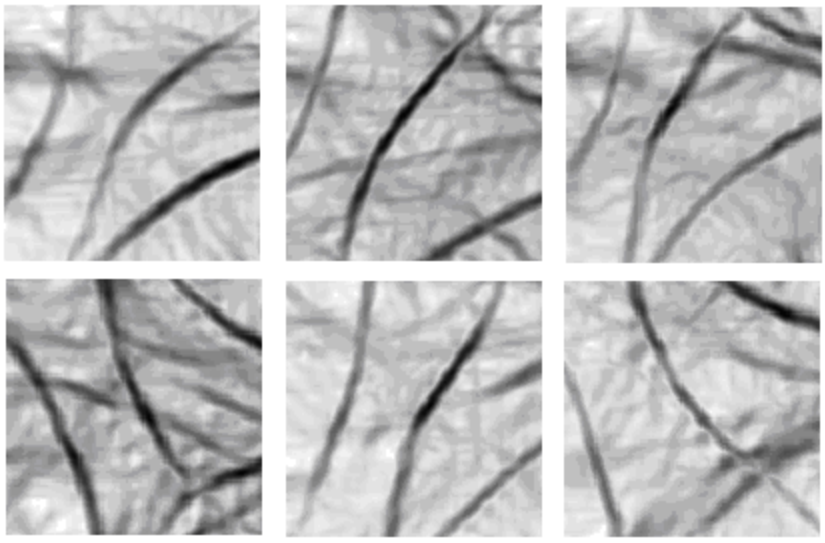

Figure 3.6: Surface curvature maps for six different subjects.

Thus a scalar value of curvature is obtained for every point on the 3D palmprint image and this can be stored in a 2D matrix or an image. A set of such scalar values is referred

to as surface curvature map. Figure 3.6 shows curvature maps for some of the 3D palmprint images in the database. It can easily be observed that the surface curvature maps obtained by the proposed feature extraction algorithm closely resembles the palm lines, especially the strong principal lines.

The inputs for the matching algorithm are two sets of curvature maps of size 128 × 128. The feature matching process establishes the similarity between the gallery and the probe templates. In this work, we employ an image matching technique, normalized local correlation for comparing two curvature maps. Result of this matching is a correlation value for every point in the input curvature maps. Average of these correlation values is considered to be the matching score. The expression for normalized local correlation is given by:

$$C = \frac{\sum_{i=-N}^{N}\sum_{j=-N}^{N}(P_{ij}-\overline{P})(Q_{ij}-\overline{Q})}{\sqrt{[\sum_{i=-N}^{N}\sum_{j=-N}^{N}(P_{ij}-\overline{P})^2][\sum_{i=-N}^{N}\sum_{j=-N}^{N}(Q_{ij}-\overline{Q})^2]}} \tag{3.8}$$

where P_{ij} and Q_{ij} are curvature values in the neighborhood of the points being matched in gallery and test curvature maps, respectively, and $\overline{P}$ and $\overline{Q}$ are the mean curvature values in those neighborhoods. $(2N+1) \times (2N+1)$ is the size of the neighborhood in pixels. Clearly, the value of C lies in the range of [-1, 1] with values 1 and -1 indicating a perfect match and mismatch, respectively. Figures 3.7 and 3.8 illustrate the process of matching two curvature maps of the same and different users, respectively. Red (dark) colored pixels in the correlation map represent high values of correlation while blue (light) represents low correlation. Final matching score is the average of pixel values in

the correlation map. It can be observed from Figure 3.7 that genuine matching results in a correlation map with large regions of red colored pixels, indicating high correlation between the two curvature maps being matched.

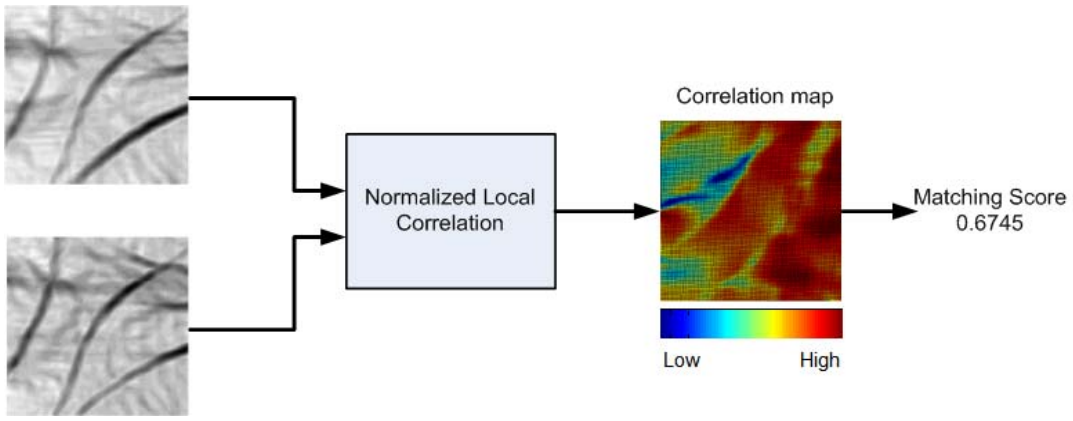

Figure 3.7: Matching curvature maps from the same subject.

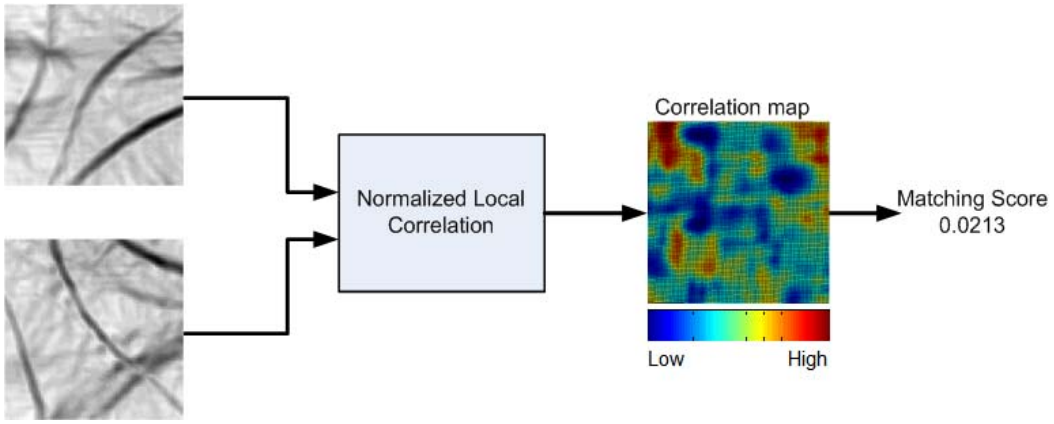

Figure 3.8: Matching curvature maps from different subjects.

3.4 2D Palmprint Matching

In this work, we acquire low resolution hand images and employ a 2D Gabor filter based competitive coding scheme [22] to extract features from the 2D palmprint. This approach uses a bank of 2D Gabor filters to extract information on the orientation of lines and

creases in the palmprint. A family of 2D Gabor wavelets, satisfying wavelet theory and the neurophysiological constraints can be derived from general complex 2D Gabor function as [109]:

$$\psi(x, y, \omega_o, \theta) = \frac{\omega_o}{\sqrt{2\pi}\kappa} e^{\frac{-\omega_o^2}{8\kappa^2}\left(4(x\cos\theta + y\sin\theta)^2 + (-x\sin\theta + y\cos\theta)^2\right)} \left[e^{i(\omega_o x\cos\theta + \omega_o y\sin\theta)} - e^{\frac{-\kappa^2}{2}} \right] \tag{3.9}$$

where ω_o is the radial frequency in radians per unit length and θ is the wavelet orientation in radians. κ is a constant, value of which depends on the frequency bandwidth. The center frequency ω_o of the Gabor filters can be derived to be $\frac{\kappa}{\sigma}$ [109]. Each of the extracted sub images is convolved with Gabor filters oriented in six different directions and a competitive rule is formulated to select the dominant orientation, θ_p. This orientation is selected to be the one with minimum filter response and is defined as:

$$p = \arg\ \min_j (I(x, y) * \psi_R(x, y, \omega, \theta_j)) \tag{3.10}$$

where I is a 2D sub image, ψ_R represents the real part of the Gabor filter, and '*' denotes discrete convolution. Orientations of the filters are chosen to be $\theta_j = j\pi/6,\ j = \{0,1,...,5\}$. Since we considered only six orientations, the computed features (orientation index) are binary encoded using three bits. Figure 3.9 shows sample palmprint images from our database and their corresponding CompCode representations. The three parameters of the Gabor filter ($filterSize, \sigma, \omega$) are empirically determined to be $(35, 2.6, 0.7)$ respectively.

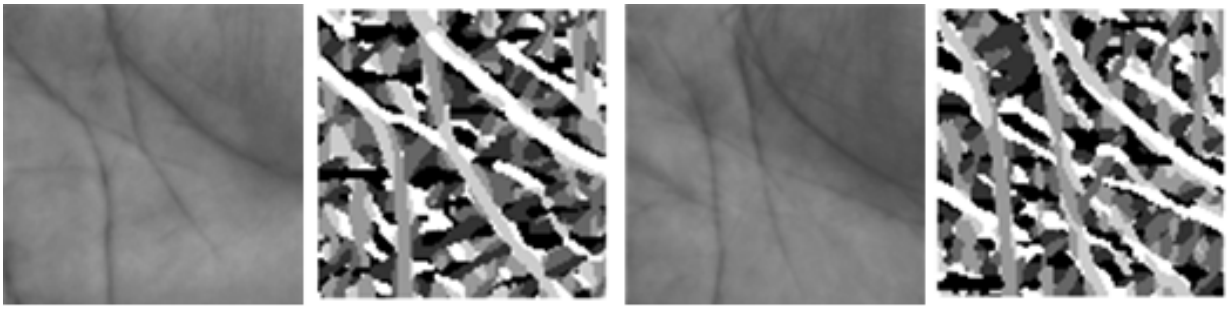

Figure 3.9: Sample 2D palmprint (intensity) images in (a) and (c), corresponding gray level CompCode representations in (b) and (d) respectively.

.

Angular distance described in [22] is employed for comparing features extracted from 2D palmprint images. Let P and Q be the two feature matrices (competitive codes). P_M and Q_M are the corresponding masks used for indicating the non palmprint pixels obtained by binarizing the palmprint images. Angular distance $D(P,Q)$ is defined by the following equation:

$$D(P,Q) = \frac{\sum_{y=0}^{N}\sum_{x=0}^{N}\sum_{i=1}^{3}(P_M(x,y) \cap Q_M(x,y)) \cap (P_i^b(x,y) \otimes Q_i^b(x,y))}{3\sum_{y=0}^{N}\sum_{x=0}^{N} P_M(x,y) \cap Q_M(x,y)} \qquad (3.11)$$

where $\cap$ and $\otimes$ denote the bitwise AND and XOR operations respectively. $P_i^b(Q_i^b)$ is the i^{th} bit plane of $P(Q)$. In order to take into account the possible translations in the extracted sub image (with respect to the one extracted during the enrolment), multiple matches are performed with one of the features translated in horizontal and vertical directions. Minimum of the resulting matching scores is considered to be the final score.

3.5 Experimental Results

3.5.1 Verification Experiments

In order to evaluate the performance of the proposed system, verification experiments are performed on a database of 108 subjects. This database was collected at the Biometric Research Center, the Hong Kong Polytechnic University over a period of two months. The database was collected in two sessions, with an interval of 2 weeks and mainly consisted of volunteers and students from our university. Ideally, the database should include some fake palmprints to test the robustness of the proposed system. However, in this set of experiments, the primary focus is on analyzing 2D and 3D palmprint features. The main objective was to achieve performance improvement by combining 2D and 3D palmprint features that are simultaneously acquired from the imaging setup. However, the utility of our approach is not only limited to the performance improvement. In the next section, we illustrate the experiments performed to analyze the robustness of the 3D palmprint features against spoof attacks. The database for the experimental results reported in this section includes only real palmprint images. All images were acquired using the capture device [43] shown in figure 3.1. For each subject, six samples of 2D and 3D palmprint images were captured and stored in the database. Thus, there are a total of 648 palmprint images in our database. Therefore there are 1,620 genuine and 208,008 impostors matching scores for each of the two modalities. Figure 3.10 shows a scatter plot of the genuine and impostor score distributions obtained from 2D and 3D palmprint features. It can be observed that the two distributions are well

separated and a linear classifier would be able to discriminate the genuine and impostor classes.

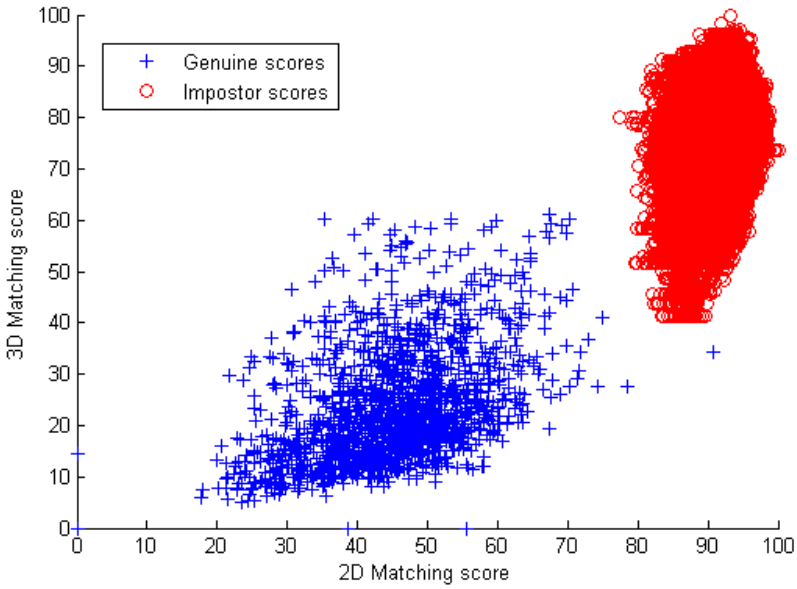

Figure 3.10: Genuine and impostor score distribution in 2D space.

We first analyzed the individual achieved performance from 2D and 3D palmprint representation. Figure 3.11(a) and 3.11(b) show the performance, in terms of False Acceptance Rate (FAR) and False Rejection Rate (FRR) characteristics obtained from 2D and 3D features respectively. The Equal Error Rate (EER) achieved from the two separate experiments using 2D and 3D features are illustrated in Table 3.1. In figures 3.11(a) and 3.11(b), it is important to note that the 2D palmprint representation clearly outperforms 3D in terms accuracy.

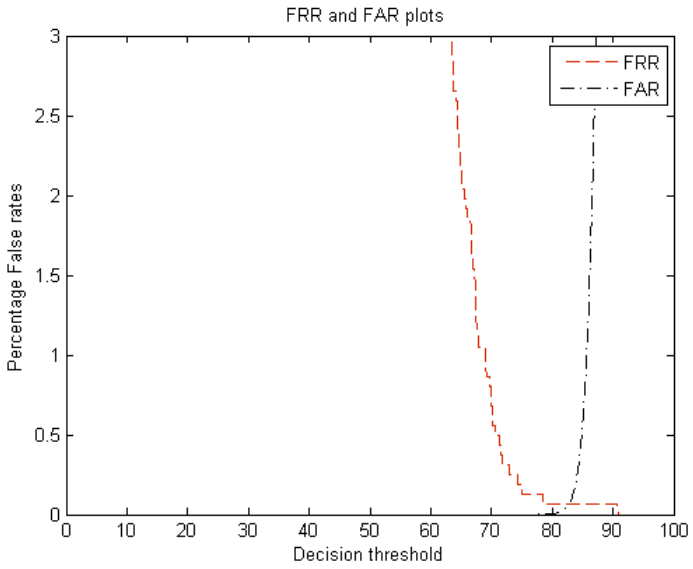

(a)

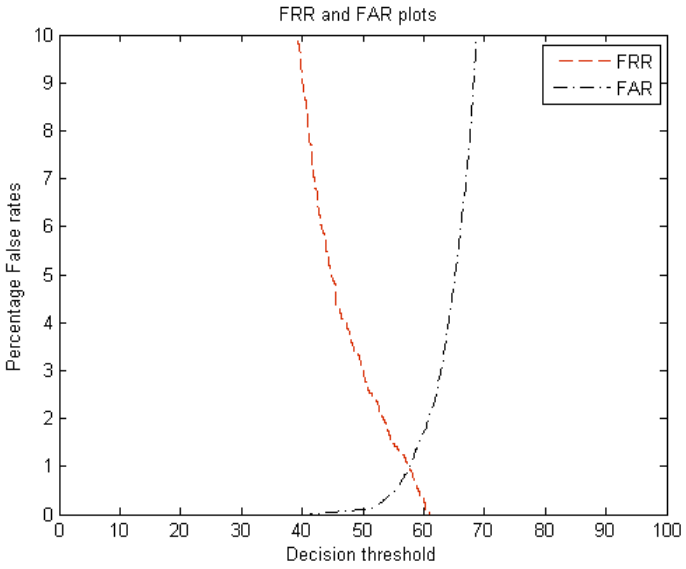

(b)

Figure 3.11: FAR and FRR plots. (a) 2D CompCode features. (b) 3D Curvature map features.

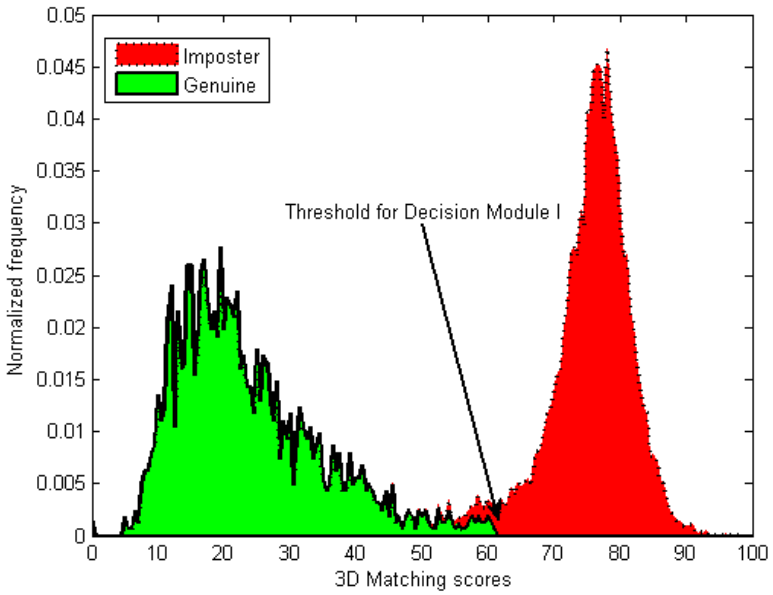

Figure 3.12: The selection of threshold for Decision Module I.

Further experiments were carried out to ascertain the possible performance improvement by combining two (2D+3D) palmprint representations using the proposed multilevel matching framework. The threshold of the Decision Module I was selected such that no genuine users are rejected at Level 1. This can be achieved by setting the threshold to the operating point at which FRR for 3D palmprint features becomes zero. The value of this threshold was found to be 61.03 (refer to figure 3.12). All 3D matching scores (genuine as well as impostor) above this threshold are rejected at Level 1. After rejection at Level 1, there were 1620 genuine and 203,667 impostor scores for each of the two modalities. These scores were carried over to the next level. At this level (Level 2), since the genuine and impostor distributions are originally well separated (refer to figure 3.10), we employ a simple weighted sum rule to combine the 2D and 3D matching scores. The combined score (Level 2 match score) is computed as:

$$S_{2D+3D} = w_1 S_{2D} + w_2 S_{3D} \tag{3.12}$$

where S_{2D} is the 2D matching score normalized to (0,100) range. The 3D matching score, which originally is a dissimilarity score, is firstly normalized to (0,100) range and then converted to a similarity score to obtain S_{3D}. The weights w_1 and w_2 are tuned to provide the best verification results. The optimal values of w_1 and w_2 were empirically calculated and found to be 0.56 and 0.44 respectively.

Results of our experiments are summarized in Table 3.1. Decidability index (d') is used as a measure to quantify the improvement in the separability of impostor and genuine matching score distributions. It is computed as:

$$d' = \frac{|\mu_1 - \mu_2|}{\sqrt{\frac{\sigma_1^2 + \sigma_2^2}{2}}} \tag{3.13}$$

where μ_1 and μ_2 are the mean values and σ_1^2 and σ_2^2 are the variances of the genuine and impostor score distributions respectively.

It can be observed from the Table 3.1 that the proposed multilevel approach for combination of 2D and 3D features achieves the best performance, i.e., Equal Error Rate (EER) of 0.0022% and decidability index of 7.45. This performance is significantly higher as compared to the case when either 2D or 3D palmprint features alone are used. Figure 3.13 shows the FAR and FRR plots for the case when both 2D and 2D features are employed.

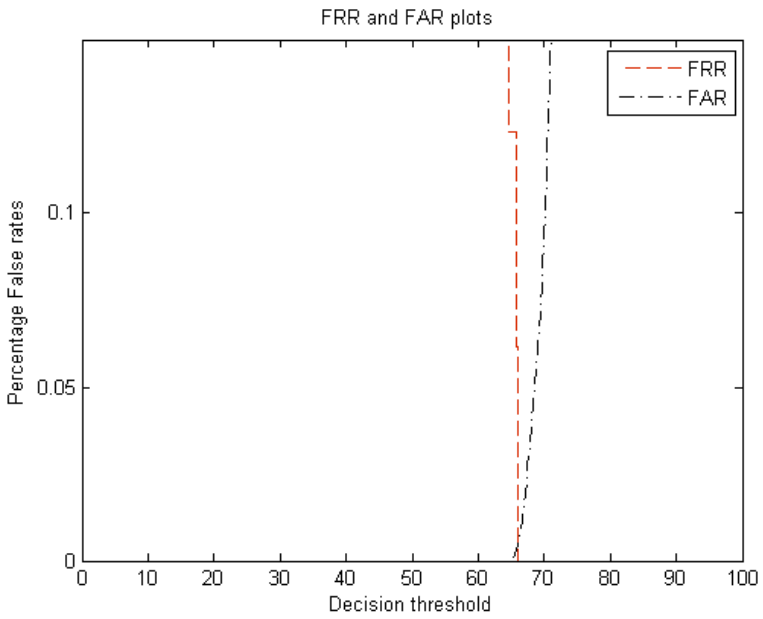

Figure 3.13: FAR, FRR plots for (2D + 3D) features.

A comparative Receiver Operating Characteristics (ROC) obtained from the three different sets of experiments is shown in figure 3.14. It can be ascertained from figure 3.14 that the combination of 2D and 3D features for palmprint verification outperforms each individual scheme.

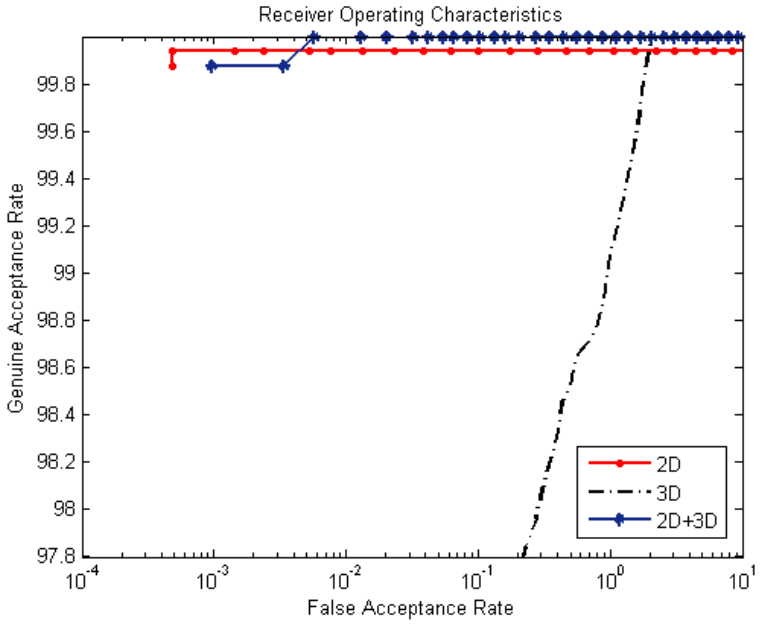

Figure 3.14: The ROC curves for 2D, 3D and the proposed multilevel (2D+3D) features.

Table 3.1: Performance indices for 2D, 3D and the (2D+3D) palmprint representations.

Palmprint Matcher	EER (%)	Decidability Index (d')
2D	0.0621	6.50
3D	0.9914	5.97
Multi level (2D+3D)	0.0022	7.45

3.5.2 Spoof Experiments

In this set of experiments, we investigate the robustness of the 3D palmprint features against the sensor level spoof attacks. We also analyze the vulnerability of 2D image based authentication system against such attacks. Our experiments involved collecting data from five subjects, in two stages. In the first stage, subjects were asked to present their "real" hand, while in the second, images of the same users' hand (palm side) printed on a paper were presented to the capture device. Figure 3.15 shows fake palmprints used for our experiments. The fake palmprints generated from genuine users' palmprint images (Figure 3.15(a)-(d)) were simply pasted on one real palm, as shown in Figure 3.15(e). This real hand, with fake palmprint, was presented to the image acquisition system (refer to figure 3.1) that can acquire both 2D and 3D palmprint images. Again, experiments were performed in a verification scenario, i.e., a user's palmprint image captured in the first stage is matched to the one captured in the second stage. A match is counted as correct if the resulting matching score is less than the system threshold. For the purpose of analysis we consider this threshold to be the operating point of EER as it represents commonly preferred operating point for most of the practical deployments. The results from this set of experiments are summarized in Table 3.2.

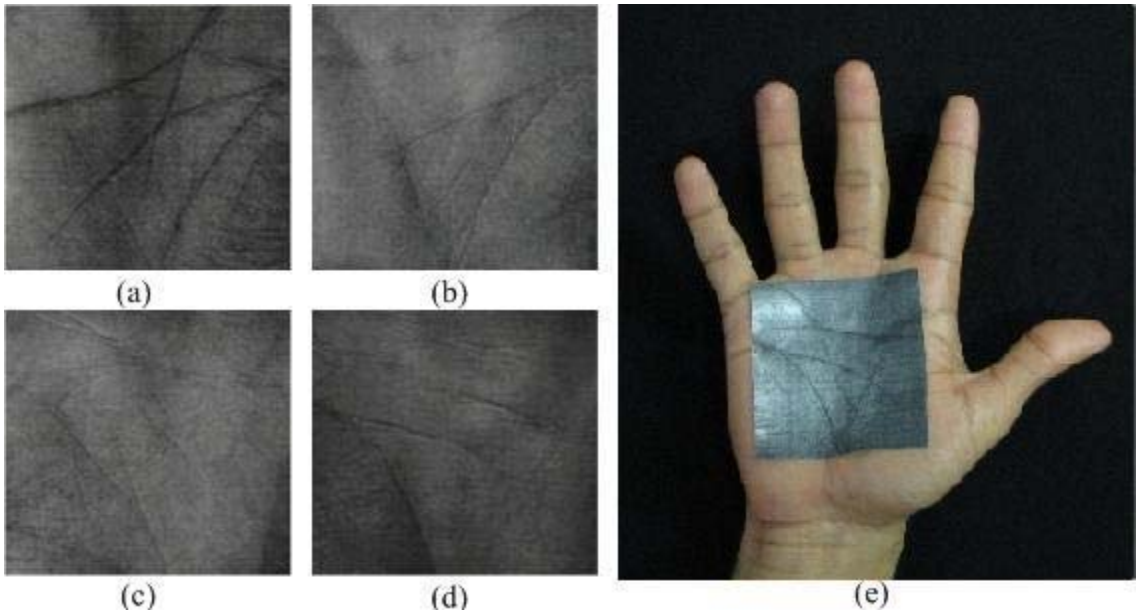

Figure 3.15: Fake palmprints. (a) - (d) Show the palmprint images printed on the paper to use as spoofs. (e) Shows a fake palmprint pasted on the hand to spoof the system.

Table 3.2: Matching scores from fake palmprints (spoof attack analysis).

User ID	2D Matching Score (Threshold = 82.69)	3D Matching Score (Threshold = 58.19)	2D+3D Matching Score (Threshold = 66.01)
1	63.75	72.42	67.56
2	66.69	75.68	70.65
3	67.09	81.89	73.60
4	59.46	74.59	66.10
5	60.26	76.79	67.5

The experimental results in Table 3.2 show that the user verification using 2D palmprint features fails to discriminate between real and fake palmprint samples for all users. As seen from the Table 3.2, matching scores for 2D palmprint features are well below the threshold at EER, which suggest that the system considers all matches as correct. On the other hand, Table 3.2 indicate that for the 3D and (2D+3D) features, the system would count all matches as incorrect or negative as the matching scores for 3D and 2D+3D are above their corresponding thresholds. In fact, 3D performs better than

2D+3D (matching scores for 3D are well above the threshold, while 2D+3D scores are relatively closer to the threshold). This is why we rely entirely on 3D features to reject fake palmprints at Level 1 of the multilevel matching algorithm. It may be noted that the threshold for Decision Module I was set to 61.03, and all the 3D match scores in Table 3.2 are above this threshold. This suggests that the proposed system will be successful in rejecting all fake palms at Level 1. The experimental results presented in Table 3.2 demonstrate the utility of 3D palmprint features for enhancing the robustness (against spoof attacks) of the palmprint matching system.

3.6 Discussion

The previous section has presented experimental results from a multimodal palmprint authentication system that can simultaneously acquire and combine 2D and 3D palmprint features. Experimental results on a real palmprint database of 108 subjects demonstrate that with proper selection of weight parameters of fusion scheme, considerable performance improvement (over individual 2D and 3D representations) can be achieved. The experimental results presented in Section 3.5.1 illustrate a relative performance gain of 96% in EER (over the 2D palmprint matcher) and 14.6% in decidability index when the simultaneously acquired 3D features are combined with traditional 2D palmprint features. However, our comparative analysis, where 2D features achieve lower error rates compared to the 3D features, suggests that the 2D features are more discriminative than 3D features for palmprint representation.

The experiments performed in section 3.5.2 to investigate the robustness of 2D image based approaches, expose the vulnerability of such systems to spoof attacks. On the other

hand, palmprint authentication systems based on 3D features, as well as combination of (2D+3D) features, utilize depth information from the palm surface, therefore making them extremely difficult to circumvent. It may also be noted that the proposed system is more robust to noise such as some text or lines drawn on the palmprint. This is because the 3D depth features extracted from such palms are unaffected by noise and therefore results in a more robust system compared to the 2D image based palmprint authentication systems.

In fact, most 2D image based biometric systems have been shown to be vulnerable to sensor level spoof attacks. For example, the popular biometric trait, fingerprint can be easily reproduced by lifting the latent impressions left by the users [108]. In addition, experimental results in [113] have shown that iris, considered to be highly reliable biometric modality, is highly vulnerable to direct spoof attacks with fake iris generated by printing iris images on a piece of paper. Therefore there is compelling need to investigate the security of existing 2D palmprint systems against such attacks. However, it is important to note that the palmprint system [44] uses central part of human palm (acquires these images in a touch free manner) for recognition/authentication task, and therefore ruling out the possibility of users leaving any impressions on the scanner, which can be used to reproduce synthetic palmprints. It may also be noted that, 2D images of palmprint cannot be easily acquired as other biometric traits such as face, iris, which can be acquired covertly from a distance [51]. Despite the difficulty in covertly acquiring palmprint images, we have investigated the vulnerability of 2D palmprint systems without actually considering how these images can be acquired for printing on the paper.

The experimental results presented in this chapter has led us to believe that the proposed system effectively combines the high discriminatory power of 2D and robustness of 3D palmprint representations, resulting in a biometric system that has the potential to be deployed for security critical applications. Future research should be directed towards developing better 3D palmprint representations and exploring different fusion strategies.

3.7 Summary

This chapter has investigated the utility of 3D palmprint features and proposed a multilevel approach for the personal authentication using 3D and 2D palmprint images of the user. The surface curvature based feature, namely, curvature map is employed to represent the discriminatory information in the captured 3D palmprint images, while normalized local correlation is used to match a pair of curvature maps. The decision at Level 1 of the multilevel authentication approach is entirely based on the matching of 3D features. If the resulting match score is above a particular threshold, the query is rejected as a fake palm or an impostor and the matching process is terminated at Level 1. Otherwise matching proceeds to Level 2 where 2D and 3D matching scores are combined to decide if the user is a genuine or impostor. The experimental results presented in Section 3.5 demonstrate that the proposed combination of 2D and 3D matching scores results in significant performance improvement over the case when either 2D or 3D features are alone employed (relative improvement in EER of 96% and 99% over the 2D and 3D matchers respectively). We have also investigated the robustness (against spoof

attacks) of a 2D palmprint matcher and presented experimental results to demonstrate the utility of 3D palmprint features for enhancing the robustness of the proposed system.

Chapter 4
Contact-free 3D Hand Geometry Identification

The personal verification technique introduced in Chapter 3 employs a contact based image acquisition module in order to acquire 3D and 2D palmprint images. The approach requires the user to place his/her hand on the imaging platform guided by pegs. As indicated earlier in the introduction chapter, the practicality of contact based image acquisition is limited by factors such as low user acceptance due to the hygienic concerns and inconvenience caused to the users. Moreover, the verification approach presented in Chapter 3 is entirely based on the palmprint region of the hand, while other parts of the hand such as fingers also contain highly discriminatory information that can be used in combination with palmprint to enhance the performance. The primary focus of the work presented in this chapter is to explore 3D hand/finger geometry features and to build a robust and reliable hand biometric system, without sacrificing user friendliness and acceptability.

This chapter presents a new approach to achieve performance improvement by simultaneously acquiring and combining three dimensional (3D) and two dimensional (2D) features from the human hand. The approach utilizes a 3D digitizer to simultaneously acquire intensity and range images of the presented hands of the users in a completely contact-free manner. Two new representations that effectively characterize the local finger surface features are extracted from the acquired range images and are

matched using the proposed matching metrics. The proposed approach is evaluated on a database of 177 users acquired in two sessions. The experimental results suggest that the 3D hand geometry features have significant discriminatory information to reliably authenticate individuals. Our experimental results demonstrate that consolidating 3D and 2D hand geometry features results in significantly improved performance that cannot be achieved with the traditional 2D hand geometry features alone. Furthermore, this chapter also investigates the performance improvement that can be achieved by integrating five biometric features, *i.e*. 2D palmprint, 3D palmprint, finger texture, along with 3D and 2D hand geometry features, that are simultaneously extracted from the user's hand presented for authentication.

4.1 Background

A number of techniques have been proposed in the literature for the personal verification based on hand geometry features. Often, users are required to place their hand on flat surface fitted with pegs to minimize variations in the hand position. Although such constraints make the feature extraction task easier and consequently result in lower error rates, such systems are not user friendly. In order to overcome this problem, a few researchers have proposed to do away with hand position restricting pegs. Feature extraction algorithm in their approaches takes care of possible rotation or translation of the hand images acquired without guiding pegs. However, users are still required to place their hand on a flat surface or a digital scanner. Such contact may give rise to hygienic as well as security concerns among users. Security concern on the contact based approaches arises from the possibility of picking up fingerprint or palm-print impressions left on the

surface by the user and thereby compromising the user's biometric traits. Moreover, most of the hand geometry systems/techniques proposed in the literature is based on users' gray level hand images. These approaches extract various features from the binarized version of the acquired hand image. Unique information in such binary images is very limited, leading to low discriminatory power from the hand geometry biometric systems.

Despite the advances in hand geometry research, very few researchers have explored the use of 3D surface features on the hand or fingers. Woodard and Flynn [36] investigated 3D finger surface as a potential biometric modality. Convex hull of the hand contour was used to locate finger valleys and to extract index, middle and ring fingers from the range image of the hand. Shape index, defined in terms of principal curvatures and computed at every pixel in the range images of fingers, is utilized as feature representation. Correlation coefficient is used to determine the matching distance between a pair of shape index images. Score level fusion of matching scores from individual fingers is then performed to obtain the final matching score. Authors achieved promising results when experiments were performed on data collected in a single session. However, rank one recognition rates dropped significantly when gallery and probe images were collected with a time lapse of one week. One of the limitations of this technique is the usage of large sized feature templates, as shape images of size 80×240, corresponding to each fingers, are required to be stored. In addition, the data acquisition method adopted in [36] is not completely contact free and raises hygienic concerns.

Malassiotis *et al*. [102] proposed a biometric system based on measurements extracted from user's 3D finger. Mixture of Gaussians is used to model and to

subsequently segment hand from other parts of the body appearing in the acquired range images. 3D width and mean curvature of cross sectional segments are computed for four fingers (thumb excluded) and concatenated to form a feature vector. Finally, L_1 distance was employed for feature matching. The work detailed in [102] is promising but was evaluated on relatively smaller database and authors did not make any attempt to use the finger back surface features (2D features) that can be simultaneously extracted from the presented hands.

There exists another class of hand shape based authentication approaches that do not explicitly acquire depth information from the hand [131], [21]. These approaches project a pattern onto the back surface of the hand and employ a CCD camera to capture the pattern distorted by the shape (or curvature) of the hand. Features extracted from the acquired 2D image are then used to perform identity verification. Although these approaches are relatively simpler in computation, they fail to explicitly characterize surface details and solely rely on the coarse-level hand shape features. More importantly, since a projector and a camera are employed, the cost of such systems when used for real world applications is identical to a 3D acquisition system based on structured light principle.

4.2 System Description

The block diagram of the proposed approach for biometric authentication that simultaneously employs multiple 2D and 3D hand features is shown in figure 4.1. Major computational modules of the proposed approach involve - image normalization (in the pre-processing stage), feature extraction and feature matching. The intensity and range

images of the user's hand, acquired by a 3D digitizer, are processed to locate and extract individual fingers and palmprint. Feature extraction modules further process the respective regions of interest in order to extract the discriminatory features. Individual matching modules compute the matching distance by comparing the extracted features with the corresponding feature templates enrolled in the database. Multiple matching scores generated by the preceding stage are then combined at the fusion module, to obtain a consolidated match score. Finally, the decision module compares the consolidated match score with the pre-set threshold to determine whether the claimant is genuine or an impostor. The details of these key processing stages appear in the following sections.

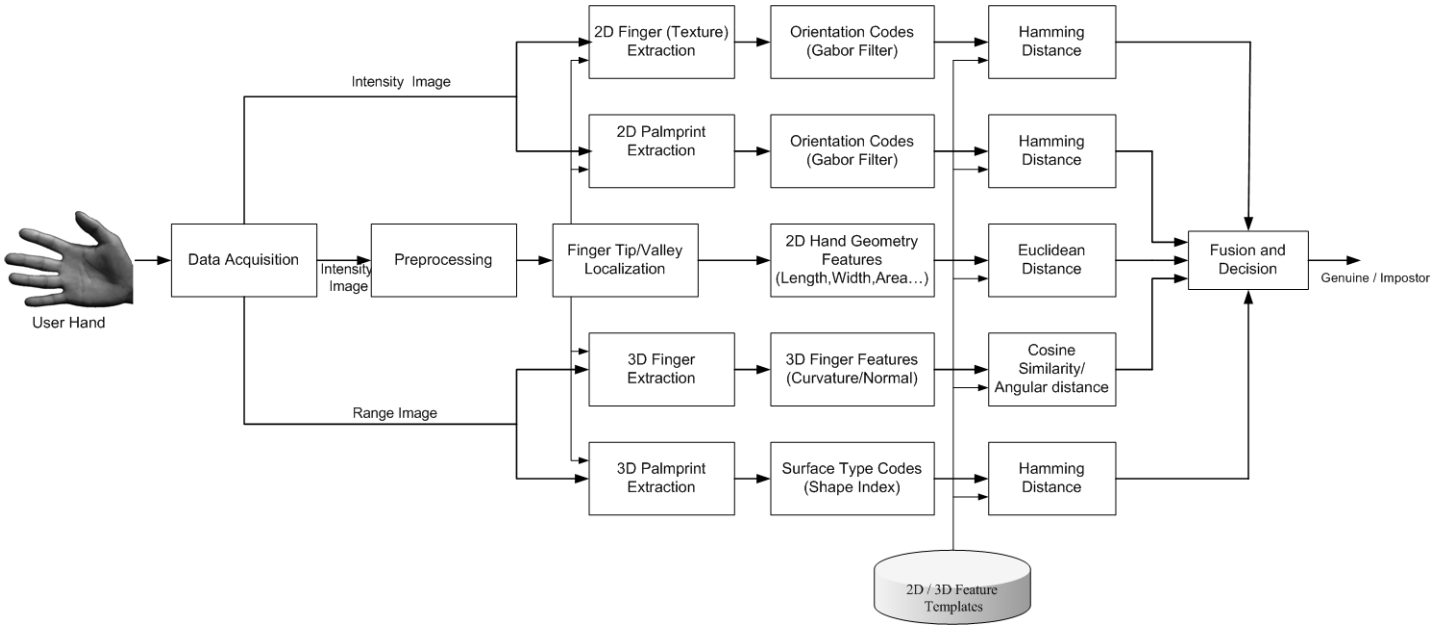

Figure 4.1: Block diagram of the personal authentication using 2D and 3D hand features.

4.3 Preprocessing and Finger Extraction

The acquired intensity images are first processed to automatically locate the finger tips and finger valleys. These reference points are then used to determine the orientation of

each finger and to extract them from the acquired hand image. Since the acquired intensity and range images are registered, we work only on the intensity image to determine the key points and the finger orientation. The key processing steps involved in the automated extraction of fingers are illustrated in figure 4.2. The gray level intensity images are firstly binarized using Otsu's threshold [85]. Simple thresholding scheme is employed for the hand segmentation, as images are acquired with a uniform black background. The resulting binarized image is passed through a morphological opening operation to remove isolated regions that can sometimes appear as noise. Boundary pixels of the hand in the processed binary image are then identified using the 8-connected contour tracing of binary pixels [79]. Traversing the extracted hand contour, local minima and local maxima points, which correspond to finger tips and finger valleys, are located. In order to estimate the orientation of each finger, four points on the finger contour (two points each on both sides of the fingertip) at fixed distances from the finger tip are identified. Two middle points are computed for corresponding points on either side and are joined to obtain the finger orientation (refer to figure 4.2(d)). This approach is similar to the one employed in [103], which automatically finds the line of symmetry. However, differing from their approach, we only consider points on the finger contour that are close to the finger tip. Points at the center and bottom part of the finger are not considered for the estimation of orientation, as some of the fingers are found to be non-symmetric at these parts. Once the finger orientation and finger tip/valley points are determined, it is straightforward task to extract a rectangular region of interest from the fingers. Similarly, based on the two finger valley points (between little-ring and middle-index fingers) a

fixed ROI representing palmprint can be extracted [116]. Figure 4.2(e) shows the extracted region of interests for four fingers.

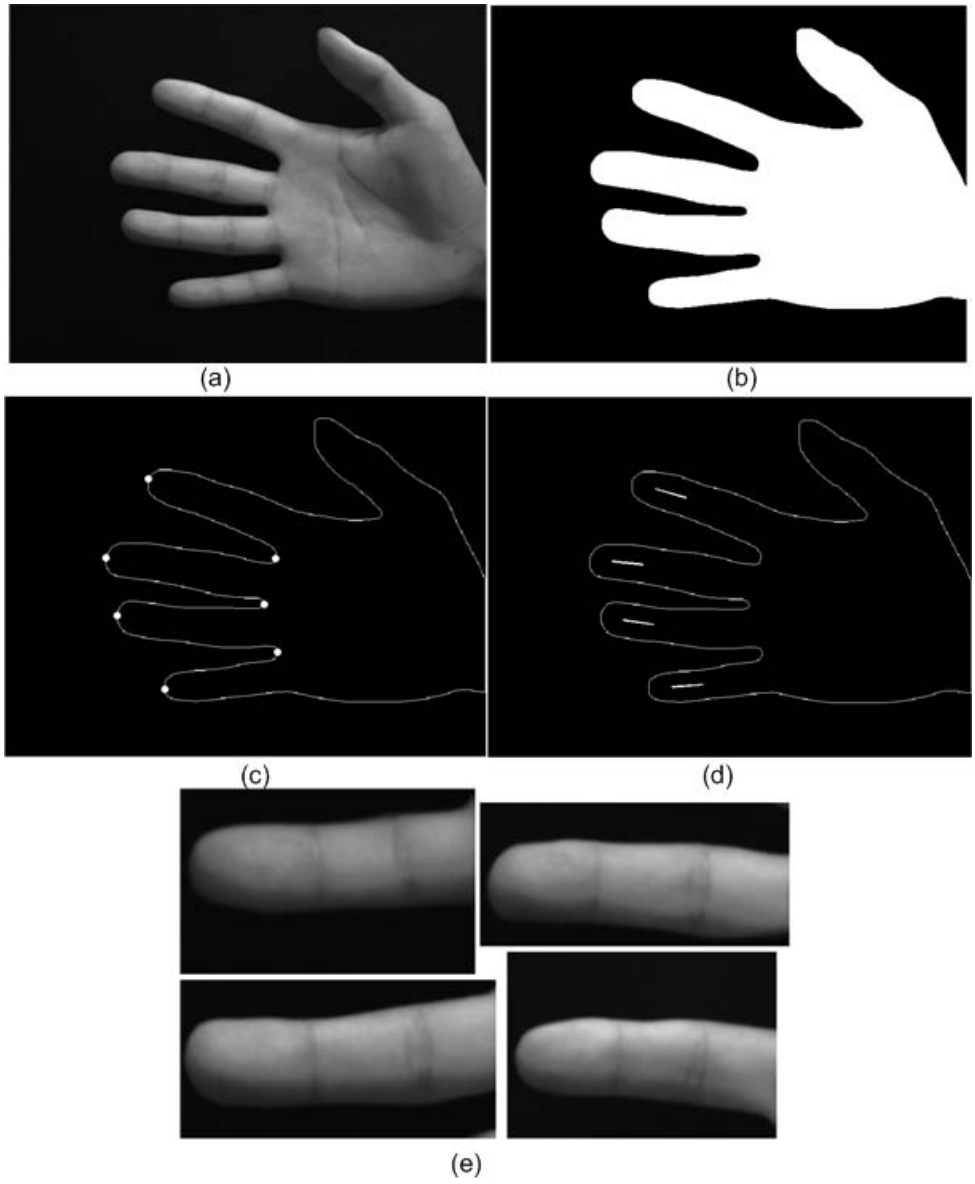

Figure 4.2: Pre processing and finger extraction. (a) Acquired intensity image. (b) Binary hand image after thresholding and morphological operations. (c) Finger tips and valleys located. (d) Detected finger orientations. (e) Extracted individual fingers.

The process of finger extraction discussed above can handle rotation and translation of the hand in the image plane, which are inevitable in a peg free data acquisition set up.

Region of interest (ROI) for finger texture features are extracted (from the individual fingers shown in figure 4.2(e)) as the largest rectangular regions around their centroids. These extracted images are then resized to obtain fixed size ROI images. Extracted individual fingers and corresponding finger texture images depicted in figure 4.3 demonstrate that the approach employed in this work for finger extraction can effectively handle transformations of the hand in the image plane.

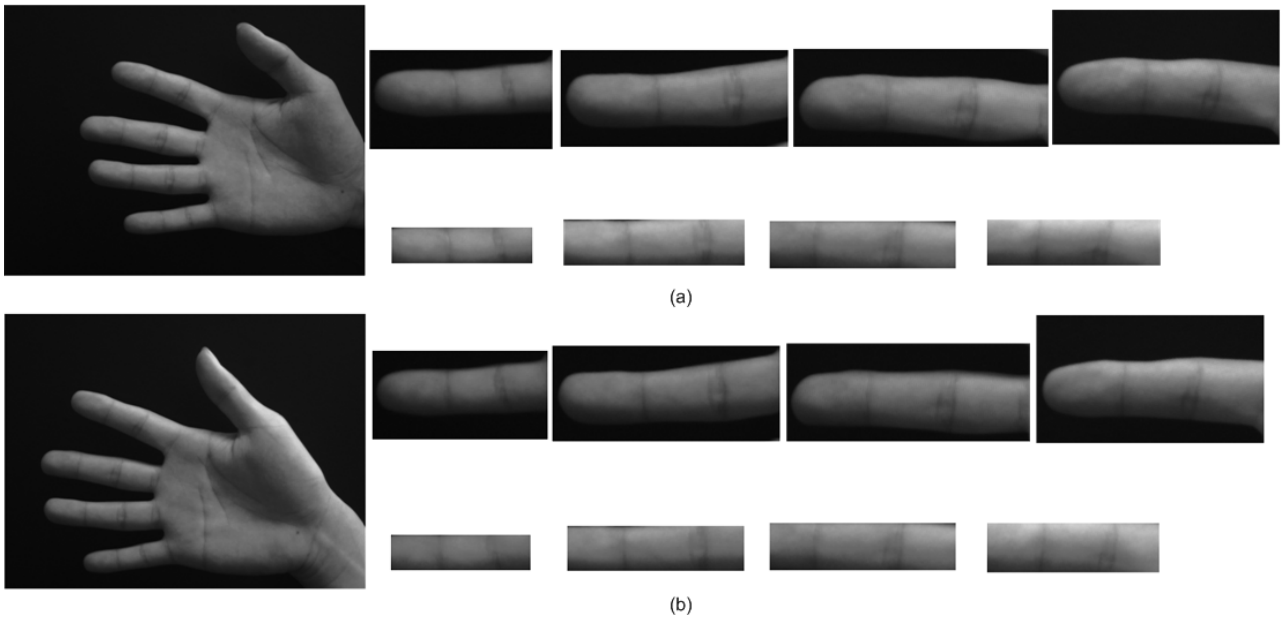

Figure 4.3: Robustness of the finger extraction approach to rotation and translation of the hands. Images in (a) and (b) show two samples of intensity images acquired from the same hand and the corresponding regions of interest.

4.4 3D Finger Geometry

4.4.1 Finger Modeling and Feature Extraction

The finger localization algorithm described in the previous section is employed to locate and extract individual fingers from the acquired range images. Figure 4.4 shows the 3D visualization for a typical finger extracted from the range image of a hand. Each of the

four finger range images is further processed for feature extraction. The 3D feature extraction approach adopted in this work is inspired by the conventional finger width features in the hand geometry verification. For each finger, a number of cross sectional segments are extracted at uniformly spaced distances along the finger length (refer to Figure 4.4(b)). The next step in the feature extraction process is to compute two representations, namely, mean curvature and unit normal vector, for every data point on the extracted 3D finger segments. In order to compute these features, we firstly experimented by fitting one dimensional polynomial to the data points on a segment and computing 1-D curvature of the fitted polynomial. A one dimensional polynomial of degree two has the following form:

$$f(x) = c_1 x^2 + c_2 x + c_3 \tag{4.1}$$

Where c_1, c_2 and c_3 are the coefficients of the polynomial. The curvature of the above polynomial, in terms of coefficients c_1 and c_2, can be expressed as follows:

$$\kappa_{1D} = \frac{2c_1}{\left(1+\left(2c_1 x + c_2\right)^2\right)^{3/2}} \tag{4.2}$$

Figure 4.5(a) shows one of the cross sectional segments extracted from the range image of the 3D finger shown in figure 4.4(a). The data points on the segment are fitted with a second degree polynomial as shown in figure 4.5(a). Figure 4.5(b) depicts the curvature value estimated at every data point on the segment.

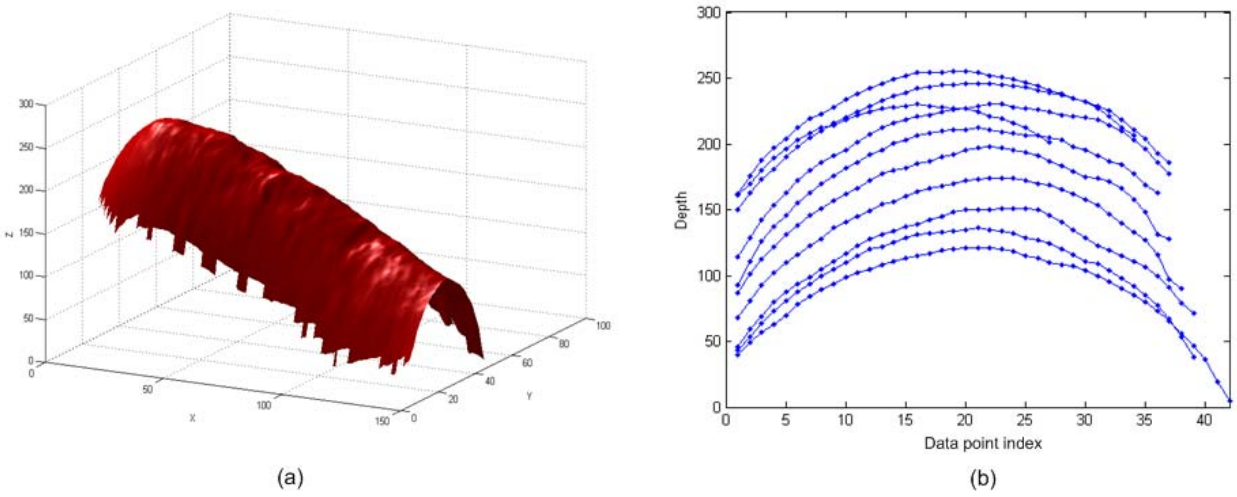

Figure 4.4: (a) Rendered view of a 3D finger and (b) the extracted cross sectional segments.

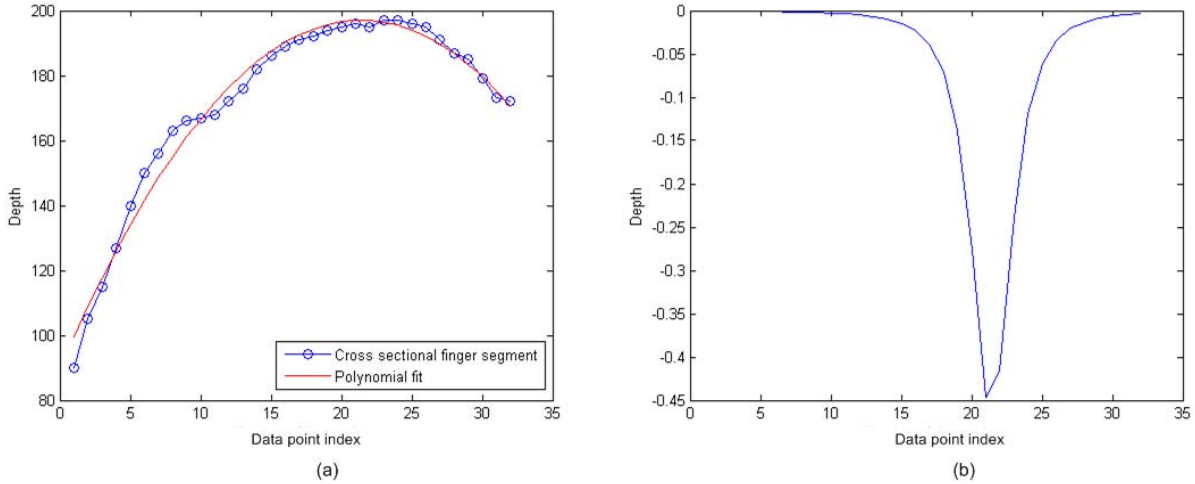

Figure 4.5: (a) Polynomial fit on a cross sectional finger segment. (b) Computed curvature features.

This approach, however, only considered the neighboring points in one direction while ignoring other surrounding points and the crucial finger surface detail in the cross sectional finger segments. As a result, the computed features lacked sufficient discriminatory information and the experiments yielded poor performance. Therefore, we further modified this approach and employed a two dimensional polynomial to model the

data point and its neighbors. The mean curvature and normal vector features can then be more effectively computed from the fitted 2D polynomial by estimating numerical partial derivates of the polynomial at each data point. Savitzky-Golay filters [114] are widely used to fit one dimensional polynomial and compute its numerical derivatives. The concept of one dimensional Savitzky-Golay filters can be easily extended to two dimensional polynomial fitting. In our experiments, we used the two dimensional Savitzky-Golay filters implementation available in [106]. The 2D polynomial $f(x, y)$ employed for modeling each of the fingers can be generalized as follows:

$$f(x, y) = c_{00} + c_{10}x + c_{01}y + c_{11}xy + c_{20}x^2 + c_{02}y^2 \tag{4.3}$$

where x and y are the two dimensional coordinates of a data point. The degree of the polynomial (two) in the above equation and the neighborhood size N (5×5) are determined empirically and was fixed. In order to model the data point and its neighbors represented by a vector $\mathrm{d} = [d(0)\ d(1)\ ...\ d(N)]^{\mathrm{T}}$, a matrix equation can be formulated as

$$\mathrm{M} \times \mathrm{c} = \mathrm{d} \tag{4.4}$$

where each of the N rows of the matrix M, takes the value $[1\ x_i\ y_i\ x_i y_i\ x_i^2\ y_i^2]$ with $i = 0,1,...,N-1$ and c is the column vector of polynomial coefficients. The above equation can be easily solved for finding polynomial coefficients using least squares approach. The next step in our approach is to extract the features from the fitted polynomial. The expression for mean curvature of a 2D polynomial in terms of its coefficients is given by

$$\kappa_{2D} = \frac{(1+c_{10}^2)c_{02} + (1+c_{01}^2)c_{20} - c_{10}c_{01}c_{11}}{(1+c_{10}^2+c_{01}^2)^{3/2}} \tag{4.5}$$

The mean curvature in the above equation is computed for every data point on the cross sectional finger segments and stored as feature templates. Figure 4.6(a) depicts a typical cross sectional finger segment extracted (same sample as in Figure 4.5(a)) from the 3D finger and the corresponding mean curvature plot. Note the presence of detailed information in this curvature plot (see Figure 4.6(b)), as compared to the one shown in figure 4.5(b). It can be observed from these figures that the feature extraction approach employed in this work effectively captures the local curvature information present on the cross sectional finger segments.

In addition to the curvature feature, we also compute surface normal vector at every data point on the extracted finger segment. In order to compute surface normal vectors, let us define a parametric surface as follows:

$$\mathrm{p}(x, y) = (x, y, z(x, y)) \tag{4.6}$$

Since the surface normal is parallel to the cross product of partial derivatives of this surface with respect to x and y, it can be obtained as follows:

$$\mathrm{n} = \frac{\partial \mathrm{p}}{\partial x} \times \frac{\partial \mathrm{p}}{\partial y} \tag{4.7}$$

Computing the above cross product, expression for unit normal vector n_u at each data point (in terms of the fitted polynomial coefficients) simplifies to

$$\mathrm{n}_u = \frac{1}{\sqrt{1 + c_{10}^2 + c_{01}^2}} (-c_{10}, -c_{01}, 1) \tag{4.8}$$

Figure 4.6(c) shows a typical 3D finger segment and the corresponding normal vectors. These computed normal vectors are also utilized as feature templates for computing the matching distance.

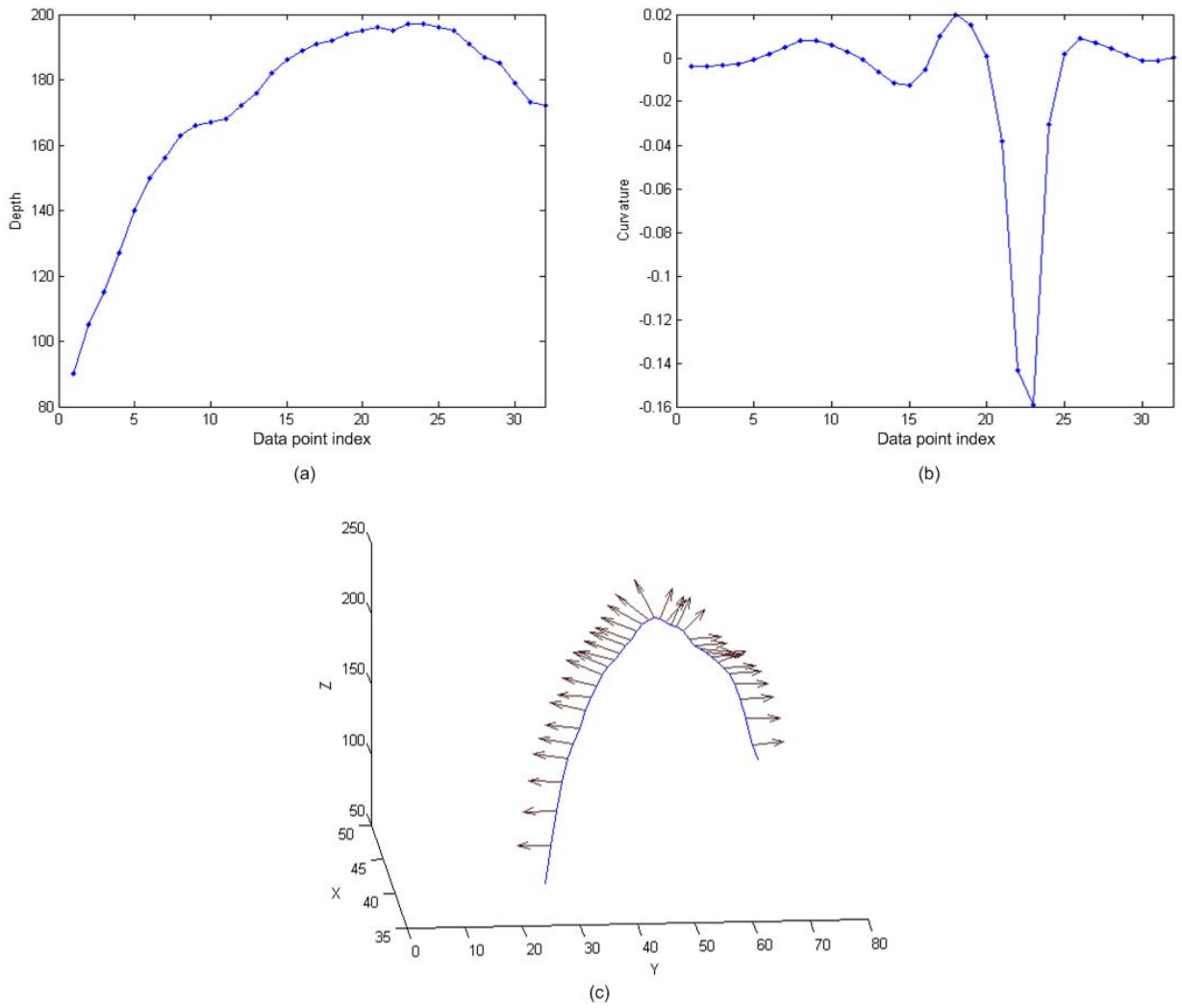

Figure 4.6: (a) A cross sectional finger segment and (b) its computed curvature features. (c) Normal features computed for a finger segment.

4.4.2 3D Finger Feature Matching

In order to match 3D finger surface features, two simple but efficient matching distance metrics are introduced. The proposed metrics can effectively deal with small changes resulting from hand pose variations during the imaging process. Features extracted from each of the four fingers are matched individually and then combined to obtain a consolidated match score.

Let the features extracted for N_s number of cross sectional segments from template and probe (query) fingers are represented by T_i and Q_i respectively, where the subscript i represents the index for fingers which can include the values from 1 to 4 for little, ring, middle and index finger respectively. The computation of matching distance (denoted as s_i^c) for the curvature features from a corresponding pair of fingers is based on the cosine similarity metric and is computed as follows:

$$s_i^c = \frac{1}{N_s}\sum_{j=1}^{N_s}\phi_i^j, \quad \text{where} \quad \phi_i^j = \begin{cases} \dfrac{T_i^j . Q_i^j(1:l_T^j)}{\left|T_i^j\right|\left|Q_i^j(1:l_T^j)\right|} & \text{if} \quad l_T^j < l_Q^j \\ \dfrac{T_i^j(1:l_Q^j).Q_i^j}{\left|T_i^j(1:l_Q^j)\right|\left|Q_i^j\right|} & \text{otherwise} \end{cases} \tag{4.9}$$

where l_T^j and l_Q^j are the number of feature points on the j^{th} cross sectional segment of the template (T_i^j) and query (Q_i^j) fingers respectively. The number of feature points l_T^j and l_Q^j cannot be guaranteed to be equal, even when they are from the corresponding fingers (from different samples) of the same user. This is because, the feature points are computed at every data point on the cross sectional segment and the number of these data points recorded during the 3D imaging process varies from one sample to another. Therefore we perform multiple matches by sliding the shorter feature vector over the longer one and considering the best score among them as the final matching distance. This approach can also effectively accommodate limited variations in the hand pose. However, in order to minimize the computational complexity, the number of sliding matches has been limited to four.

The computation of matching distance from the unit normal vector features is achieved in a manner similar to the one described for curvature features. Angle in radians

between two feature points is considered to be the degree of agreement (match) between them. Therefore we refer to this matching distance as *angular distance*. For the template and query feature vectors represented by T_i and Q_i respectively, the angular distance (match score) is computed as

$$s_i^n = \frac{1}{N_s}\sum_{j=1}^{N_s}\psi_i^j \text{ , where } \psi_i^j = \begin{cases} \frac{1}{l_T^j}\sum_{p=1}^{l_T^j}\cos^{-1}(T_i^j(p).Q_i^j(p)) & \text{if } l_T^j < l_Q^j \\ \frac{1}{l_Q^j}\sum_{p=1}^{l_Q^j}\cos^{-1}(T_i^j(p).Q_i^j(p)) & \text{otherwise} \end{cases} \quad (4.10)$$

where l_T^j and l_Q^j represents the length of template and query feature vectors respectively. In order to generate reliable matching distances in the presence of hand pose variations, multiple matches are performed between the unit normal feature vectors extracted from the cross sectional 3D finger segments. Match scores generated for four fingers by individually matching corresponding fingers are then averaged to obtain the final score for 3D normal feature. Finally, the weighted sum rule is employed to combine scores from the two matchers. Therefore, the consolidated 3D finger match score $S_{3DFinger}$ is given by

$$S_{3DFinger} = w_1 \times S_{curv} + (1 - w_1) \times S_{norm} \quad (4.11)$$

where S_{curv} $(= \frac{1}{4}\sum_{i=1}^{4} s_i^c)$,and S_{norm} $(= \frac{1}{4}\sum_{i=1}^{4} s_i^n)$ are the matching scores generated from curvature and normal features respectively. The weight parameter w_1 is empirically determined from the training samples acquired during the registration stage.

4.5 Other Hand Features

4.5.1 3D Palmprint

The Chapter 3 described the curvature map representation and the normalized local correlation based similarity metric for 3D palmprint matching. However, the utility of this approach for online usage is quite limited, mainly due to large feature size as well as the computationally intensive matching process required for the verification. This section presents a compact feature representation for 3D palmprints, namely SurfaceCode, and an efficient matching approach. Once the maximum ($k_{\max}$) and the minimum ($k_{\min}$) principal curvatures are computed (refer to Section 3.3), a quantitative measure of shape of the palm surface at every point, *i.e.*, shape index (SI) [28], is computed as follows:

$$SI(p) = \frac{1}{2} - \frac{1}{\pi}\tan^{-1}\left\{\frac{k_{\max}(p) + k_{\min}(p)}{k_{\max}(p) - k_{\min}(p)}\right\} \tag{4.12}$$

Based on the value of shape index (SI) in the above equation, every point on the palm surface can be classified in to one of the nine surface categories [28]. Therefore a four bit binary code is employed to encode the shape feature at every point on the 3D palm surface. Figure 4.7 shows sample 3D palmprints from our database and the corresponding SurfaceCode representations. For a 3D palmprint of size 128 × 128 pixels, the proposed SurfaceCode representation results in feature templates of 8K bytes, as against 16K bytes for the curvature map representation. The matching distance between two $N \times N$ SurfaceCode representations, *i.e.*, template (T) and a query (Q), is computed as follows:

$$S_{3DPalm} = \frac{1}{4 \times N^2} \sum_{y=1}^{N} \sum_{x=1}^{N} HD(T(x,y), Q(x,y)) \tag{4.13}$$

where HD denotes the Hamming distance between the two four bit codes. In order to take into account the possible translations in the extracted ROI (with respect to the one extracted during the enrolment), multiple matches are performed with one of the features translated in horizontal and vertical directions. Specifically, we perform two matches in steps of two pixels in each of the four different directions (left, right, up and down), resulting in a total of nine matches. Minimum of the resulting matching scores is considered to be the final score.

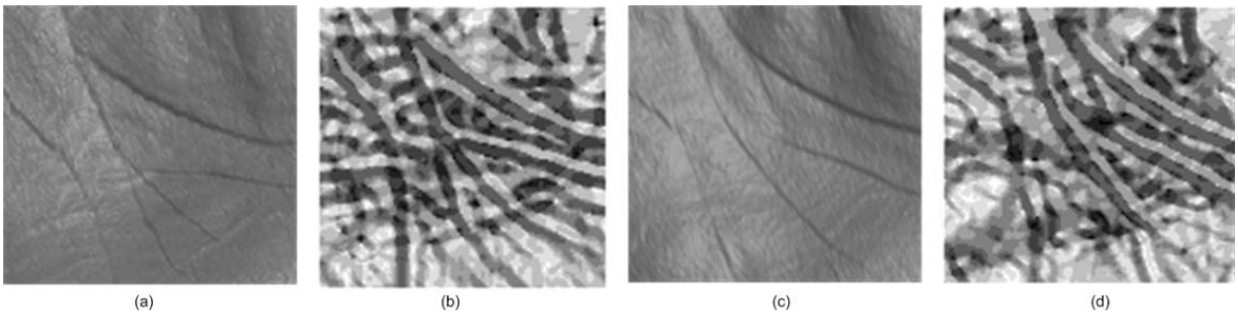

Figure 4.7: Sample 3D palmprints in (a) and (c), corresponding gray level *SurfaceCode* representations in (b) and (d) respectively.

4.5.2 2D Palmprint

The 2D palmprint matching employed in this work is based on the competitive coding scheme presented in [22] (refer to Section 3.4 for details). This approach uses a bank of six Gabor filters oriented in different directions to extract discriminatory information on the orientation of lines and creases on the palmprint. Six Gabor filtered images are used to compute the prominent orientation for every pixel in the palmprint image and the index of this orientation is binary encoded to form a feature representation (CompCode). The

similarity between two CompCodes is computed using the normalized Hamming distance.

4.5.3 2D Finger Texture

Besides 2D and 3D palmprints, we also utilize the discriminatory information contained in the 2D finger texture, extracted from the acquired intensity images of the hand. Ribaric and Fratic [104],[103] are perhaps the first researchers to utilize the discriminatory features extracted from finger images for biometric identification. They presented a simple and computationally efficient matching approach based on the principal component analysis (PCA). However, since the finger texture images contain line features such as finger creases and wrinkles, we employ the competitive coding approach (same as the one described for 2D palmprint feature extraction) to effectively extract and match these features. The three parameters of the Gabor filter $(filterSize, \sigma, \omega)$ are empirically determined to be $(15, 2.4, 0.7)$ respectively. Figure 4.8 shows two finger texture ROI images from the database and their corresponding CompCode representations.

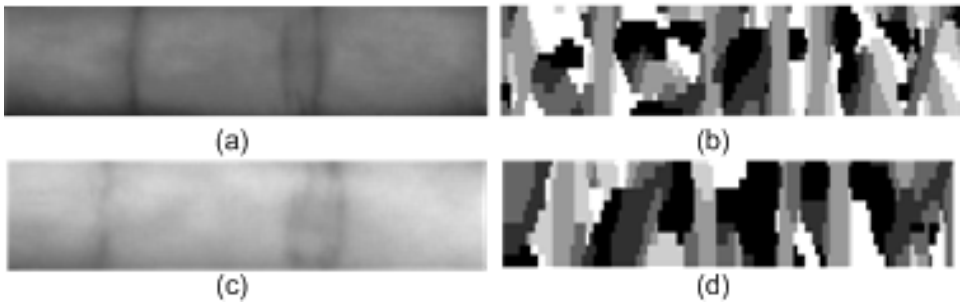

Figure 4.8: Finger surface features. (a,c) Sample 2D finger texture images. (b,d) CompCodes representations for images in (a) and (c)

4.5.4 2D Hand Geometry

2D hand geometry features are extracted from the binarized intensity images of the hand. The hand geometry features utilized in this work include – finger lengths and widths, finger perimeter, finger area and palm width. Measurements taken from each of the four fingers are concatenated to form a feature vector. The computation of matching score between two feature vectors from a pair of hands being matched is based on the Euclidean distance. A detailed description of the 2D hand geometry features is provided in Chapter 2.

4.6 Experiments

The performance of the proposed approach for hand authentication is evaluated on a database of 3,540 right hand images acquired from 177 subjects. Since there is no publicly available database of 3D and 2D (palm-side) hand images, we developed such a database in our university during October 2008 – March 2009. The details of our data collection process are described in the following section.

4.6.1 Dataset Description

The 3D hand images in the database were acquired using a commercially available 3D digitizer [81]. The data collection process spanned over 4 months and 177 subjects volunteered for the database. The participants were mainly the students and staff from our institute and were in the age range of 18 – 50 years, with multiple ethnic backgrounds. Each subject contributed 5 hand images (range and a registered intensity image acquired simultaneously) in the first session, followed by another 5 in the second session.

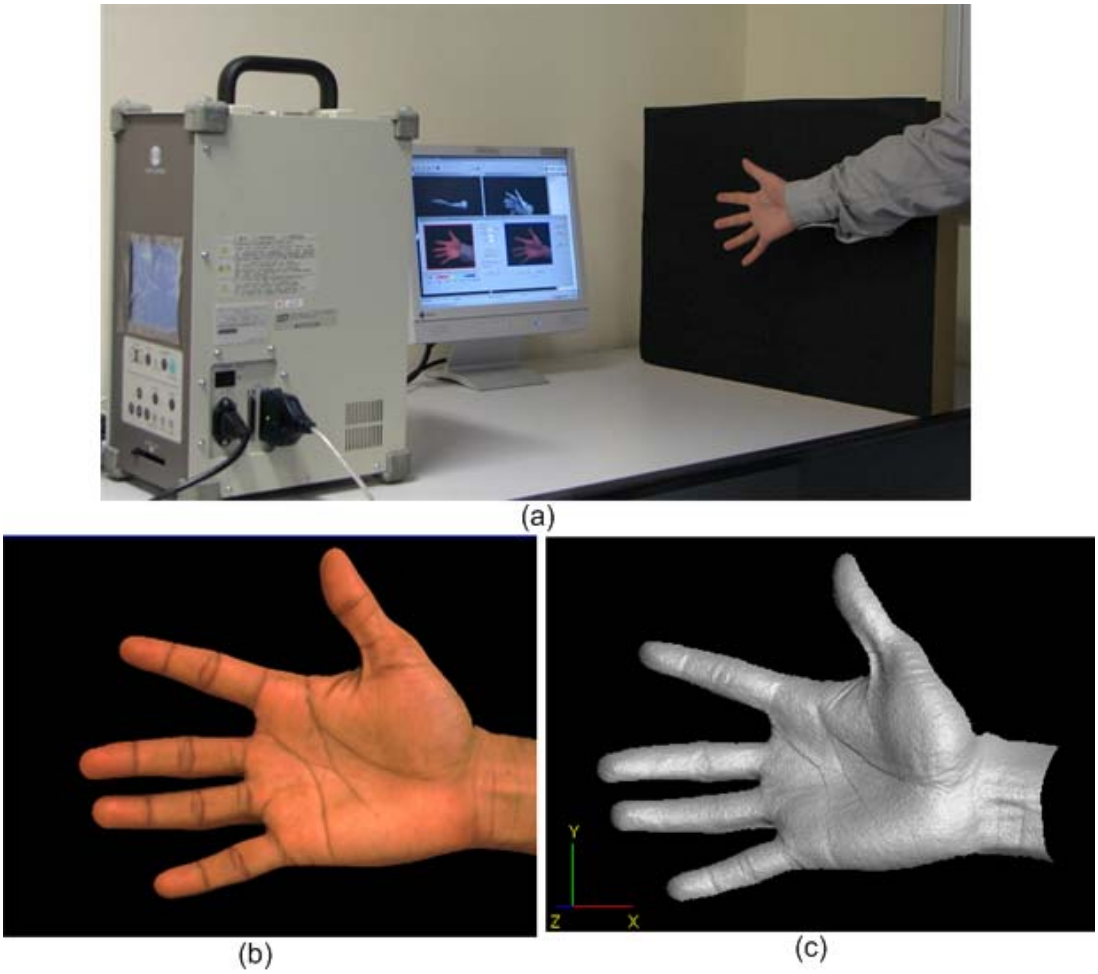

Figure 4.9: Hand image acquisition. (a) Contact-free image acquisition set up. (b) Acquired color image and (c) the rendered view of the acquired 3D data.

Therefore our database currently has 3,540 hand images (of 3D and corresponding 2D). Time lapse between two data collection sessions was not fixed for all subjects; instead it ranged from a minimum of one week (only for 27 subjects) to three months. All the hand images were collected in indoor environment, with no restrictions on the surrounding illumination. In fact, our data collection process was carried out at three different locations which had notable variations in surrounding illuminations. During the image acquisition, every user is expected to hold his/her right hand in front of the scanner at a distance of about 0.7 m, empirically chosen to maximize the relative size of the hand in

the acquired image frame. No constraints were employed to confine the position of the hand nor were the users instructed to remove any hand jewelry that they were wearing. However, in order to simplify the hand segmentation task, the background behind the user's hand was ensured to be of black color. Users were only requested to hold their hand with their palm approximately parallel to the image plane of the scanner and inside the imaging area. This task was facilitated by providing the users a live visual feedback for positioning of the hand. In order to introduce variations in the database, users were asked to change their hand position after the acquisition of every image. Figure 4.9 shows a picture of the data acquisition set up employed in this work. Representative hand images (color as well as range) of our database are shown in figure 4.10, which clearly shows variations (in hand pose, finger bending and illumination) present in the acquired database. Acquired data are stored in the raw format and later converted to range and color images of size 640 × 480 pixels.

4.6.2 Experimental Results

Two sets of experiments are carried out in the verification mode to obtain performance estimates for the proposed scheme. In the first set, we evaluate the individual performance of the proposed 3D hand geometry features, and investigate the performance improvement that can be achieved by combining 3D and 2D hand geometry features. In addition, in order to ascertain the performance improvement from the proposed unified framework, we combined all the hand based biometric features, *i.e.*, 3D hand geometry, 2D hand geometry, 3D palmprint, 2D palmprint and finger texture, which are extracted from a pair of range and intensity hand images.

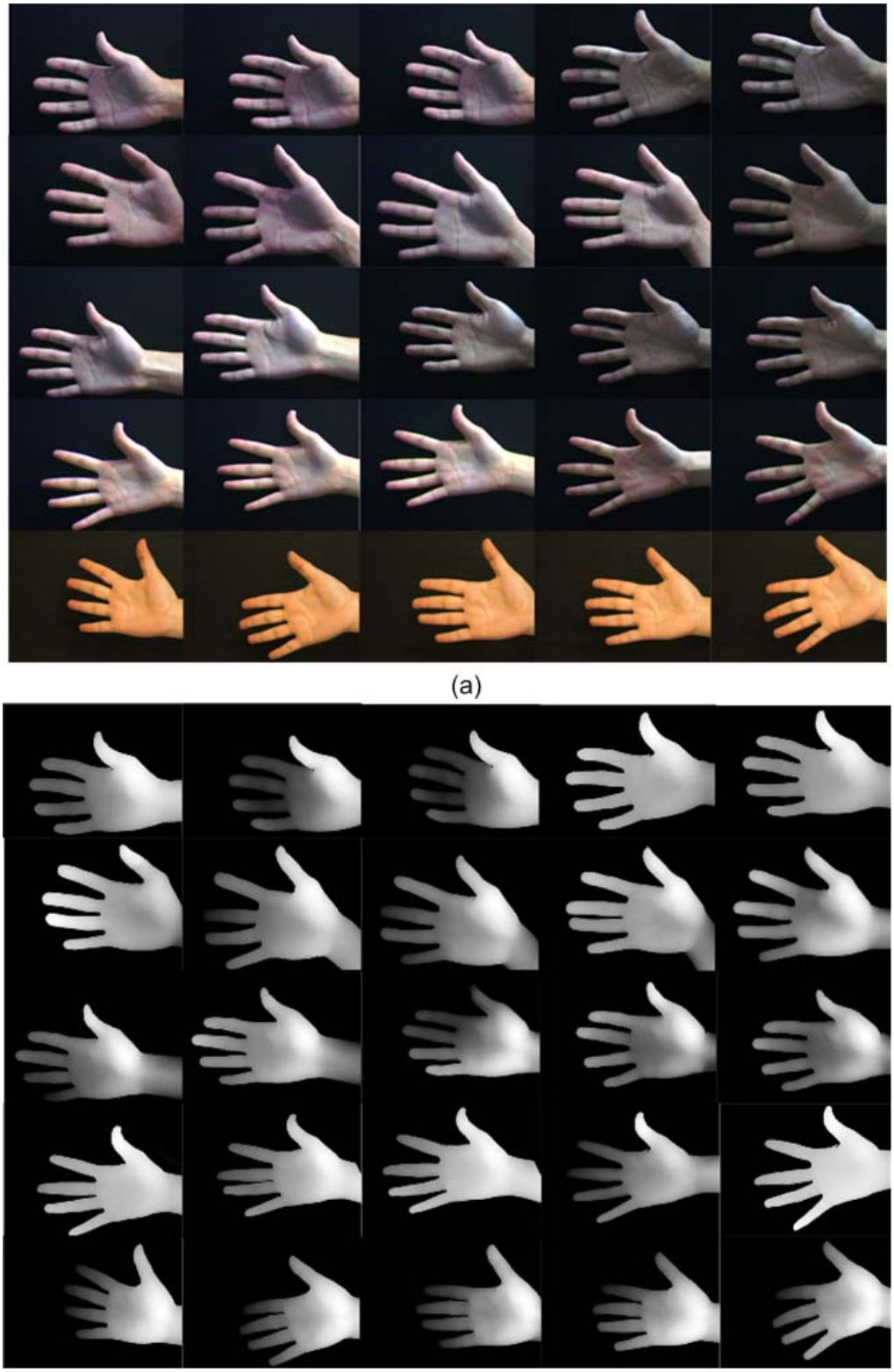

Figure 4.10: Representative samples for five users (row wise) in the database. (a) Sample color and (b) the corresponding range images.

4.6.2.1 Hand Geometry

In the first set of experiments, we evaluate the performance of the proposed hand geometry system that can simultaneously acquire and combine 3D and 2D hand geometry features. Five image samples collected from each user in the first session are used to generate feature templates, while another five hand images acquired in the second session constitute the query samples. A set of genuine matching scores are generated by matching features from each of the query samples with the user's feature templates and taking the best score among them as the final match score. The same approach is followed for generating impostor matching scores. Therefore, 885 (177 × 5) genuine and 77,880 (177 × 176 × 5/2) impostor matching scores are generated. The False Acceptance Rate (FAR) and False Reject Rate (FRR) are then computed using the generated matching scores (test data) and employed to generate the Receiver Operating Characteristics (ROC) curve. Genuine and impostor scores generated by matching 3D hand geometry features are firstly used to ascertain the matching performance from the individual fingers. Figure 4.11 depicts the ROC curves from the four different fingers – little, ring, middle and index. These experimental results suggest that there is a marked difference in discriminatory power of fingers, with the middle finger carrying the highest discriminatory information among all fingers. The noticeable difference in performance could be due to their inherent distinctiveness among the population considered in this study. Poor performance from the little finger (compared to that from others) may also be attributed to factors such the high degree of rotation (and the resulting image distortion) involved in the image normalization and finger extraction stage. Figure 4.12 shows the ROC curves for the proposed verification scheme using 3D hand geometry features.

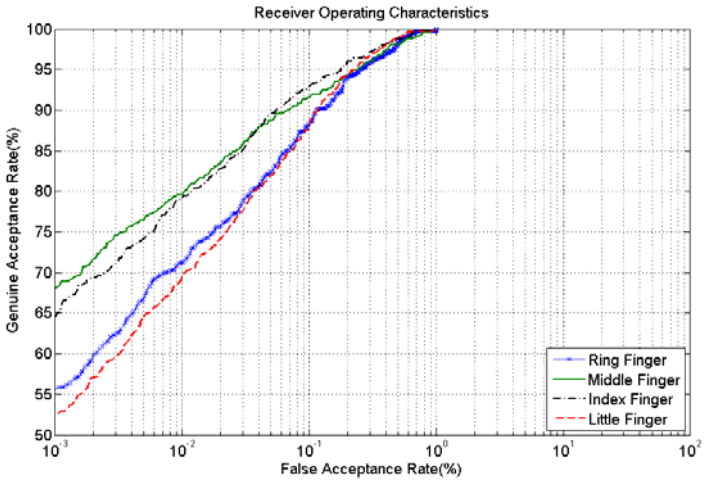

Figure 4.11: ROC curves from the individual 3D finger geometry representations.

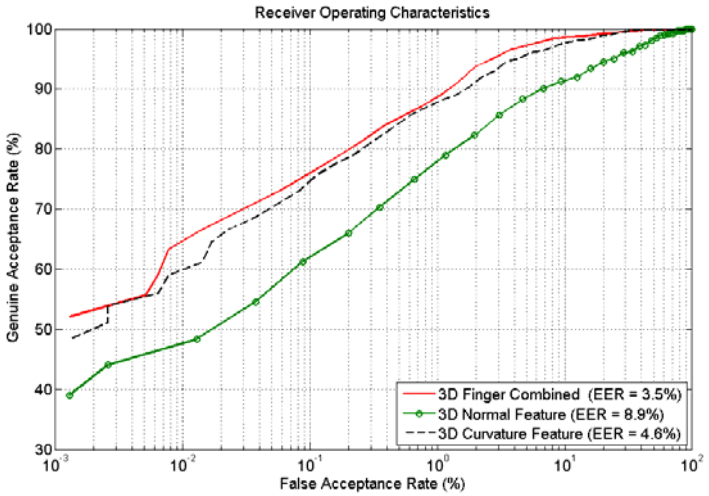

Figure 4.12: ROC curves from the individual 3D hand geometry representations and their combined performance.

It also depicts the overall 3D hand geometry performance resulting from the combination of curvature and normal features. These features are combined using weighted sum rule as in equation (4.11), with empirically selected weights 0.7 and 0.3 for curvature and normal features respectively. Empirical selection of weight parameters was based on the performance only on the training data set, with genuine and impostor scores generated using the five samples collected in the first session. As shown in figure 4.12, the

combination of the proposed 3D hand geometry features achieves an Equal Error Rate (EER) of 3.5%. This result clearly demonstrates that the 3D hand geometry features carry significant discriminatory information for personal authentication. Moreover, the proposed 3D hand geometry features can be efficiently combined with simultaneously extracted 2D hand geometry features to further improve the performance of the system.

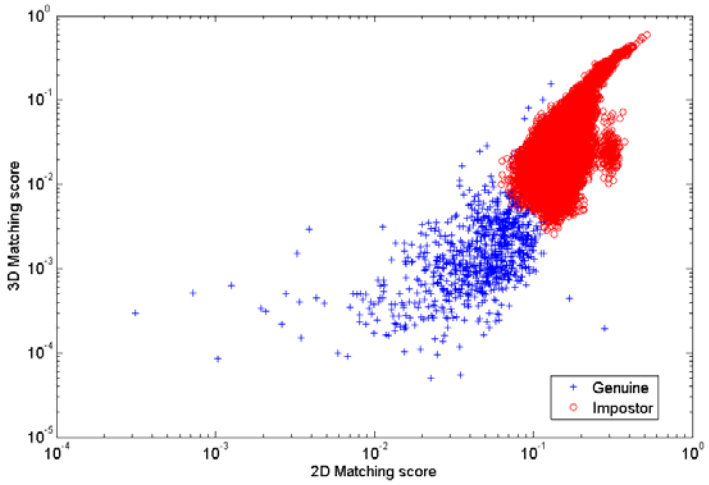

Figure 4.13: Distribution of genuine and impostor matching scores from the 2D and 3D hand geometry features.

We also performed experiments to ascertain the performance improvement resulting from the combination of the 3D and 2D hand geometry features, which are simultaneously acquired. The matching scores (from the test data) corresponding to 3D and 2D hand geometry features are combined using the weighted combinations (with empirically selected weights 0.6 and 0.4 for 2D and 3D hand geometry scores respectively). Genuine and impostor matching score distributions (in the two dimensional space) for 2D and 3D hand geometry features are shown in figure 4.13. The results from this set of experiments are summarized in figure 4.14, which depicts ROC curves for 2D,

3D as well as their combination. As can be observed from this figure, simultaneous combination of 2D hand geometry features with the proposed 3D features can significantly improve the performance (relative EER improvement of 34% over 3D hand geometry), which cannot be achieved by either 2D or 3D hand geometry features alone.

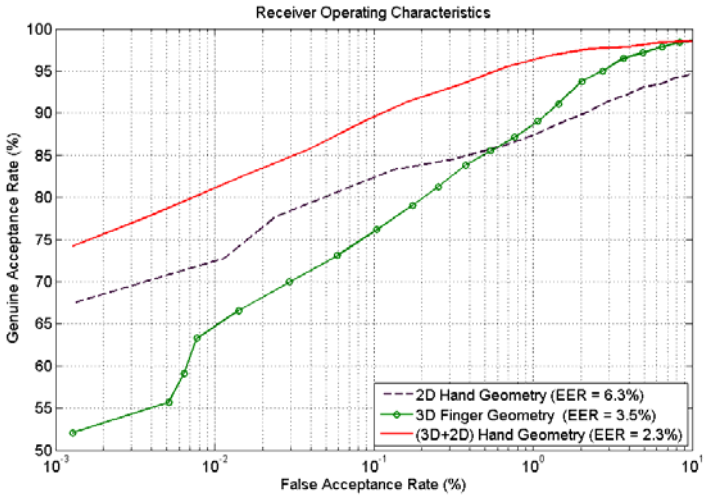

Figure 4.14: ROC curves from the proposed 3D hand geometry, 2D hand geometry features and their combination.

4.6.2.2 Unified Hand Verification

In this set of experiments, our objective was to ascertain the performance improvement that can be achieved from the unified fusion framework for hand authentication that can simultaneously extract and combine user's 2D and 3D hand features. The hand based biometric features considered in this framework include – 3D hand geometry, 2D hand geometry, 3D palmprint, 2D palmprint and 2D finger texture features.

Firstly, we compare the matching performance from the individual 2D and 3D palmprint representations, and their combination. Figure 4.15 shows the comparative ROC curves for 2D palmprint, 3D palmprint and their score level combination. As can be

observed from this figure, 2D palmprint representation consistently outperforms the 3D representation. This suggests that 2D palmprints carry are more discriminatory information than 3D palmprints [112]. Nevertheless, the combination of the two palmprint representations results in considerable performance improvement as shown in figure 4.15. More importantly, such a combination helps to increase the robustness of the palmprint verification to sensor level spoof attacks, since it is extremely difficult to fabricate 3D palm with fine surface details.

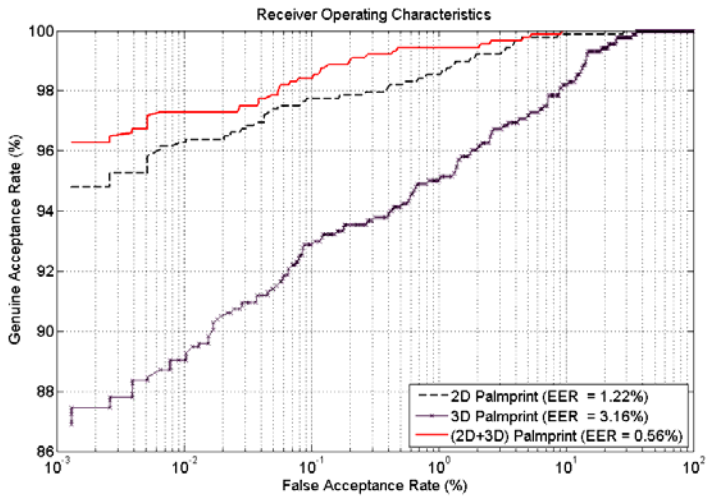

Figure 4.15: ROC curves for 2D, 3D palmprint representations and their combined performance.

Furthermore, we performed experiments to compare the performance of the proposed SurfaceCode representation with that of the 3D palmprint matching approach described in Chapter 3. As shown in figure 4.16, SurfaceCode representation for 3D palmprints achieves significantly better performance. The extraction of curvature as well as SurfaceCode features (based on shape index) involves the computation of second derivatives of the locally fitted polynomial. Therefore the computed features can be influenced by the noise present in the acquired 3D palm data. While the approach

described in Chapter 3 (refer to Section 3.3) directly employs the extracted curvature features for matching, the SurfaceCode representation is obtained by quantizing the shape index values into different categories and encoding the corresponding indices. The process of quantization and the subsequent encoding can reduce the influence of the noise in the feature extraction stage. This possibly explains why the proposed SurfaceCode representation outperforms the curvature map representation.

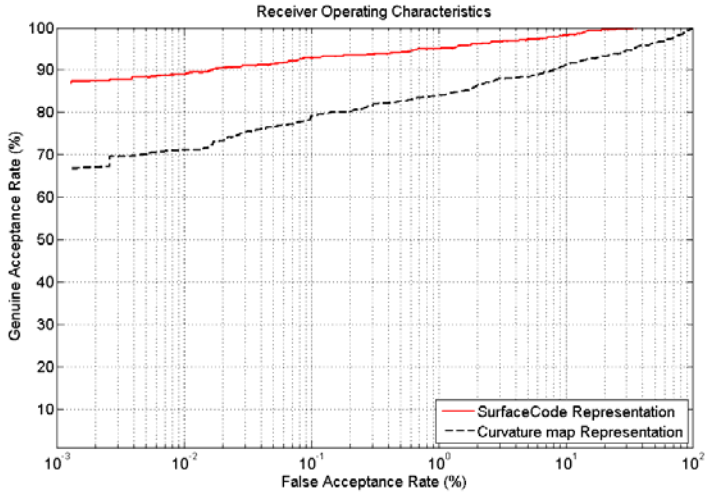

Figure 4.16: ROC curves for 3D palmprint matching using the SurfaceCode and the curvature map representation.

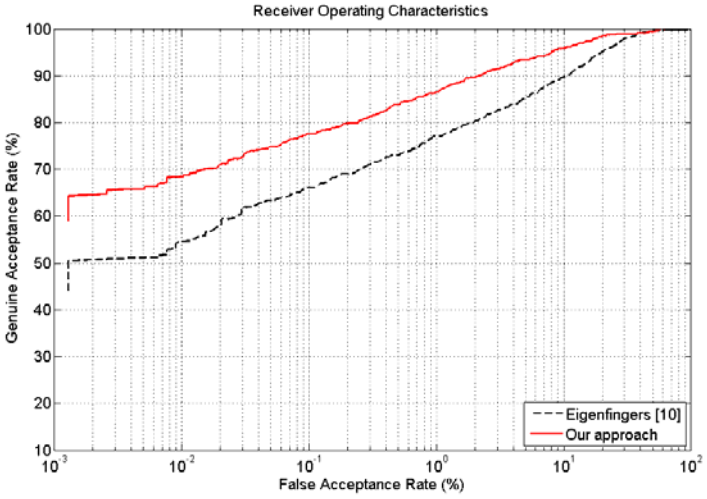

Figure 4.17: The ROC curves from the 2D finger texture details using eigenfingers and the CompCode representation.

The experimental results from the matching of finger texture (CompCode) features are shown in figure 4.17. For comparison purpose, this figure also depicts the performance from the eigenfingers approach proposed in [103]. It is evident from this figure that the CompCode feature representation outperforms eigenfingers for finger texture matching.

Finally, experimental results from combining 3D and 2D hand geometry (figure 4.14), 3D and 2D palmprint (figure 4.15) and finger texture (figure 4.17) features are presented in the form of ROC curve in figure 4.18. Table 4.1 provides a summary of our experimental results with EER as the performance index. It can be observed from this table that the combination of hand (3D shape and 2D texture) features results in the best performance and is significantly better than the performance obtained from any of the individual hand features considered in this study.

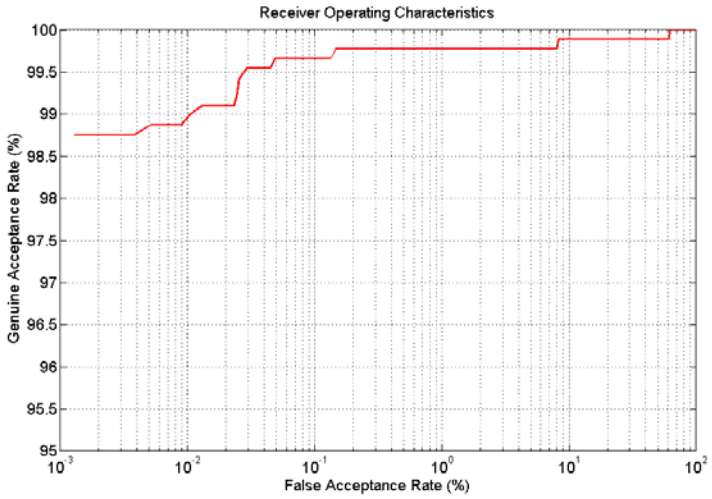

Figure 4.18: The ROC curve for the proposed system utilizing multiple hand features.

Table 4.1: Performance indices from the experiments.

Matcher	EER (%)
3D Hand Geometry	3.5
2D Hand Geometry	6.3
(2D+3D) Hand Geometry	2.3
2D Palmprint	1.22
3D Palmprint	3.16
(2D+3D) Palmprint	0.56
Finger Texture	6
(2D+3D) Hand Geometry + (2D+3D) Palmprint + Finger Texture	0.22

Table 4.2: Time requirements of individual matchers

Matcher	Processing time (seconds)	
	Feature Extraction	Matching
2D Hand Geometry	0.08	0.05
3D Hand Geometry	0.84	0.08
2D Palmprint	0.09	0.14
3D Palmprint	1.20	0.23
Finger Texture	0.24	0.10

Table 4.2 provides the typical time required by the individual matchers for processing a sample range or the intensity image. All of these approaches are implemented in MATLAB and run on a computer with 1 GB of RAM and a 1.66GHz Intel Pentium 4 CPU. It can be observed from this table that the typical time required for 3D feature extraction (Hand geometry and palmprint) is considerably higher than that for 2D features. On the other hand, the processing times for feature matching of the two modalities (2D and 3D) are quite comparable. This is due to the computationally simple 3D matching metrics employed in this work. The use of parallel fusion strategy (such as

the weighted sum rule employed in this work) to combine 2D and 3D matchers may considerably increase the computational requirements of the resulting system. However, the processing time can be reduced by employing multithreading scheme for its implementation.

4.7 Discussion

This chapter has presented a unified approach for hand based authentication that utilizes simultaneously extracted 3D and 2D hand features. The experimental results presented in the previous section demonstrate that significant performance improvement can be achieved when matching scores from the 3D and the 2D hand geometry features are consolidated. It is important to note that the performance from the proposed 3D hand geometry features alone is comparable with those from the identification approaches proposed in [102] and [36].

The major difference between the approach presented in this chapter and previous studies [102], [36], [131], [21] involving 3D hand features is that we acquire images from the *palm-side* of the user's hand. This enables us to utilize much of the discriminatory features on the hand including the palmprint information. Moreover, the proposed approach for 3D hand geometry based verification takes into account limited variations in hand pose (rotation of the hand in the 3D space). While image plane rotations (around z-axis) are normalized by the finger extraction algorithm, out-of-plane rotations (only around x-axis) are handled by the *sliding* approach employed in the 3D finger matching stage. However, the current approach may fail in the presence large out-of-plane rotations of the hand and also in the case of considerable finger bending. In this context, the

approach makes the assumption that the user is cooperative while presenting his/her hand to avoid out-of-plane rotations. One way, to explicitly handle hand pose variations and to reduce subsequent erroneous matches, is to detect and normalize the 3D hand pose (by bringing it to the frontal pose). The problem of pose variation (between a pair of 3D hands being matched) may also be handled by registering the acquired 3D hands using geometric alignment algorithms such as Iterative Closest Point (ICP). ICP algorithm has found successful applications in identification systems utilizing 3D biometric traits such as 3D face or 3D ear, which contain significant amount of global (structural) information. Mean squared error (MSE) between the aligned 3D models is often considered as the match score. However, such approaches are not suitable for matching a pair of 3D fingers. This is because the global information from 3D finger surface is quite limited and generates poor performance due to large overlapping of genuine and impostor matching scores.

The 3D palmprint feature representation presented in this chapter, SurfaceCode, has been shown to be highly compact and generates more reliable (refer to figure 4.16) performance as compared to the curvature map representation presented in Chapter 3 and thereby making it more suitable for online applications. The experimental results (refer to figure 4.17) from our comparison study demonstrated that CompCode representation outperforms eigenfingers approach [103] for finger texture matching. Possible reason for the significantly better performance from CompCode features could be that the small inaccuracies in localization and extraction of the ROI, which are inevitable in a contact free image acquisition system, can be easily accommodated in the matching phase of CompCode features. On the other hand, the appearance based approaches like

eigenfingers assume perfect alignment of the pair of ROI being matched. In addition, being a Gabor filter based approach, CompCode may be able to better characterize the local texture information present on the extracted 2D finger images.

The experiments to ascertain the performance from the unified hand verification framework yielded promising results that demonstrate that a highly reliable authentication system can be developed by combining multiple features from the hand. The motivation for such a combination arises from the fact that all the hand features considered in this work have been simultaneously extracted from a pair of 3D and 2D hand images, acquired from the presented hand. It may be noted that our approach does not utilize fingerprint features on the hand since the extraction of fingerprint features requires higher resolution (500 dpi or more) images. The system developed by Rowe *et al*. [97] acquires images of the hand placed on a platen and combines multiple hand features including hand geometry, fingerprint and palmprint. However, since we acquire hand images in a contact free manner, the fingerprint modality is not suitable to be integrated in to the framework of touchless hand authentication. The development of 3D fingerprint and touch less fingerprint systems has been recently investigated and therefore these features can be possibly integrated in to the framework in the further extension of this work.

One of the major drawbacks of the hand geometry systems has been the high degree of vulnerability of these systems to spoof attacks. Researchers [57] have demonstrated how easily a commercial hand geometry system can be circumvented. One of the simplest ways to overcome this problem is to utilize multiple (available) features on the hand (such as the one presented in this chapter). Such an approach invariably leads to

increased robustness against various kinds of attacks directed at circumventing the system. In fact, even the hand geometry system (utilizing 3D hand geometry features) presented here is more robust to sensor level attacks (with fake hands) than a traditional 2D image based hand geometry system. This is because, the approach explicitly captures finger surface information and therefore it is highly unlikely that an attacker can fabricate fake hands good enough to circumvent the system, without user's cooperation.

4.8 Summary

This chapter presented a new approach to achieve reliable personal authentication based on simultaneous extraction and combination of multiple biometric features extracted from 3D and 2D images of the human hand. The key advantage of the proposed approach is that it simultaneously acquires range and gray-level images from the *palm side* of user's hand and thereby offers range of features (2D and 3D hand geometry, 2D and 3D palm-print and finger texture) that can be simultaneously extracted and combined to achieve reliable and secure multimodal biometric authentication. The approach acquires hand images in a contact-free manner to ensure high user friendliness and also to avoid the hygienic concerns. Simultaneously captured range and intensity images of the hand are processed for feature extraction and matching. In order to extract discriminatory information for 3D hand geometry based biometric authentication, two representations, namely, finger surface curvature and unit normal vector are introduced. The proposed 3D hand geometry features explicitly capture curvature variation by computing the local features for every data point on cross sectional segments extracted from the individual fingers. Simple and efficient metrics, capable of handling limited variations in the hand

pose, are presented for matching a pair of 3D hands. The experimental results on a database of 177 subjects demonstrate that the 3D hand geometry features have high discriminatory information for biometric verification. In addition, the experimental results presented in this chapter further demonstrate that performance improvement can be achieved by combining the 3D hand geometry information with the 2D hand geometry features extracted from user's 2D hand images.

Besides hand geometry information, other hand biometric features such as 2D palmprint, 3D palmprint and 2D finger texture can also be simultaneously extracted from the acquired images. Therefore we investigated the potential of integrating these hand based features in to our unified framework and obtained the best performance when all of the features are combined. Although combining these hand features is a straight-forward task, there is actual need to quantify the performance improvement that can be achieved by such combinations, especially in the touchless imaging set up. Moreover, all hand biometric features considered in this work can be simultaneously extracted from the acquired images with little additional cost for imaging. Therefore it is prudent to combine all available biometric features.

The work presented here can be expanded in many ways. Slow acquisition speed of 3D imaging device, such as the Vivid 910 3D digitizer employed in this work, limits the online usage of the proposed system for the civilian applications. This limitation can be potentially overcome by acquiring 3D data with alternative imaging technologies, such as stereo imaging. Also the 3D digitizer employed in this work is quite expensive and large in size. However, customized low cost and compact 3D scanners can be developed (similar to the one developed for 3D fingers in [102] or for 3D palm in [24]) to overcome

this problem. Another area for future work is to explore the possibility of combining the proposed 3D finger feature representations at the feature level. It would also be interesting to assess the vulnerability of the proposed 3D hand geometry approach to sensor level attacks using fabricated hand models.

Chapter 5
Pose Invariant textured 3D Hand Identification

The 3D hand identification approach presented in Chapter 4 acquires 3D scans of the user's hand in a contact-free manner. However, this approach does not address the highly challenging problem of variations in 3D pose of the hand resulting due to the increased freedom offered to the users. The variation in the hand pose can be considerably high when the image acquisition process is unsupervised or when the users are not properly trained to provide their frontal scans. Large hand pose variations often lead to erroneous matches and subsequent deterioration in matching performance. Therefore, if the problem of changes in hand pose is not addressed, it can severely limit the performance and applicability of hand identification approaches.

This chapter presents a novel approach that can achieve improved performance even in the presence of large hand pose variations. The proposed method utilizes a 3D digitizer to simultaneously acquire intensity and range images of the user's hand presented to the system in an arbitrary pose. The approach involves determination of the orientation of the hand in 3D space followed by pose normalization of the acquired 3D and 2D hand images. Multimodal (2D as well as 3D) palmprint and hand geometry features, which are simultaneously extracted from the user's pose normalized textured 3D hand, are used for matching. Individual matching scores are then combined using a new dynamic fusion strategy. Consistent (across various hand features considered)

performance improvement achieved with the pose correction demonstrates the usefulness of the proposed approach for hand based biometric systems with unconstrained and contact-free imaging. It is also shown that the dynamic fusion approach employed in this work helps to achieve performance improvement of 60 percent (in terms of EER) over the case when matching scores are combined using the weighted sum rule. The database for experiments includes 3D hand scans acquired from 114 subjects with large pose variations.

5.1 Background

Hand based biometric systems, especially hand/finger geometry based verification systems are amongst the highest in terms of user acceptability for biometric traits. Despite the commercial success, several issues remain to be addressed in order to make these systems more user friendly. Major problems include, inconvenience caused by the constrained imaging set up, especially to elderly and people suffering from limited dexterity [5], and hygienic concerns among users due to the placement of the hand on the imaging platform. Moreover, shape features (hand/finger geometry or silhouette) extracted from the hand carry limited discriminatory information and therefore are not known to be highly distinctive. Over the years, researchers have proposed various approaches to overcome these problems. Several research systems have been developed to simultaneously acquire and combine hand shape and palmprint features and thereby achieving significant performance improvement. Furthermore, a lot of researchers have focused on eliminating the use of pegs used for guiding the placement of the hand.

Recent advances in hand biometrics literature is towards developing systems that acquire hand images in a contact free manner.

Malassiotis *et al.* [102] have developed a system that authenticates users based on 3D finger geometry information. Their system acquires range and color images of the hand held against the users' face. Kumar [17] has presented promising results for touch less palmprint authentication on a large database of 235 users. The Work presented in [19] utilizes hand geometry features extracted from infra red images of the hand. Users need to place their hand freely in the 3D space in front of the camera at a fixed distance, in order to get authenticated. Authors in [111] proposed an approach to authenticate individuals based on the features extracted from range and intensity images of the hand held freely and approximately parallel to the image plane of a 3D scanner. Authors achieved encouraging results on a relatively large database. All of the above described approaches acquire hand images of the user in a contact free manner and perform identification using various features extracted from it. However, none of these approaches explicitly perform 3D pose normalization nor do they extract any pose invariant features. In other words, these approaches assume that the user's hand is being held parallel to the image plane of the camera during image acquisition, which may not always be the case, especially with such unconstrained imaging set up. Therefore these approaches may face serious challenges when employed for real world applications.

Zheng *et al.* [54] are perhaps the first researchers to examine a hand identification approach based on extracting distinctive features that are invariant to projective transformations. Cross ratios formed by a set of landmark feature points on the finger creases constitute their feature vector. Authors have achieved promising results on a

rather small database of 23 subjects. However, the performance of their approach heavily relies on the accuracy of feature point detection on the hand images, which may deteriorate especially under large pose variations. Another drawback of their approach is that authors have not been able to utilize the palmprint information available in the acquired hand images, and therefore the lack such highly discriminatory information may pose limitations on the scalability of their approach.

The work presented by Methani *et al.* [30] is based on the alignment of a pair of intensity images of the hand using the homographic transformation between them. Two out of four corresponding points required for the estimation of homographic transformation matrix are located on the edge map of the palmprint region. However, it should be noted that the palmprint region on the human hand lacks well defined features points and therefore it may not be possible to robustly estimate the homographic transformation. Moreover, even the more stable points, i.e., interfinger points used for estimating the homographic transformation cannot not always be accurately located, especially under hand large pose variations, as we show later in this chapter.

Approaches proposed in the literature for 3D ear recognition [56],[94],[93] employ Iterative Closest Point (ICP) algorithm in order to align a pair of 3D ears. These approaches can handle pose variation since the ICP computes a rigid transformation that aligns a pair of point clouds being matched. However, ICP based approaches are not suitable for matching 3D hands as movement of one finger can introduce significant deformation that may lead to erroneous matches. ICP based matching may not be able to exploit the rich local surface details present in the palmprint region of a 3D hand [112]. Moreover, ICP based approaches do not explicitly perform pose normalization and

therefore cannot be employed to correct the pose of the corresponding intensity/color image. On the other hand, 3D face recognition algorithm proposed by Chang *et al.* [67] performs explicit 3D pose normalization using landmark points located on the face. As discussed earlier, the approaches based on detection multiple landmark points may not be reliable for hand identification.

As one can find in the literature, the problem of 3D pose variation has been well addressed in the context of 3D face and 3D ear recognition. However, little work has been done in this area for hand identification, despite it being one of the highly acceptable biometric traits. The approaches proposed for 3D face or ear recognition cannot be adopted directly as the hand identification poses its own challenges such as lack of well defined landmark points. This has motivated us to explore this area and develop an approach for pose invariant hand identification using textured 3D hands acquired in an unconstrained and contact-free manner.

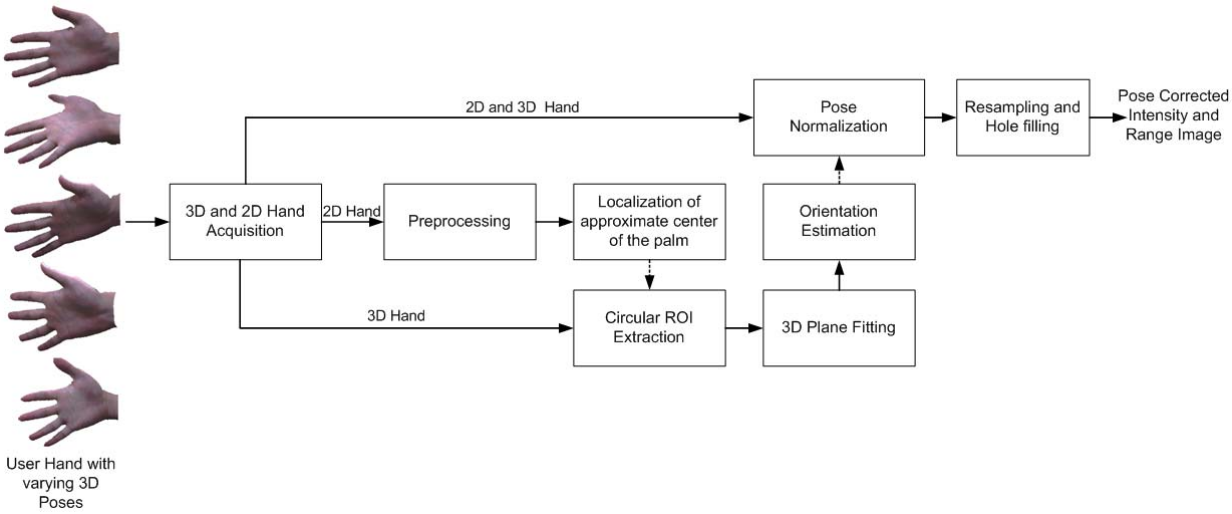

Figure 5.1: Block diagram of the hand pose normalization approach.

5.2 3D and 2D Hand Pose Normalization

Figure 5.1 depicts the block diagram of the proposed 3D and 2D hand pose normalization approach. The key idea of the approach is to robustly fit a plane to a set of 3D data points extracted from the region around the center of the palm. The orientation of the plane (normal vector) in 3D space is then computed and used to estimate and correct the pose of the acquired 3D and 2D hand.

The first preprocessing step is to localize the hand in the acquired hand images. Since the intensity and range images of the hand are acquired near simultaneously, these images are registered and have pixel to pixel correspondence. Moreover, the hand images in our database are acquired using a uniform black background. Therefore we simply localize the hand by binarizing the intensity image using Otsu's threshold [85]. These binary images are further refined by morphological open operators, which remove isolated noisy regions. Finally, the largest connected component in the resulting binary image is considered to be the set of pixels corresponding to the hand. In order to locate the palm center, we initially experimented with an approach based on inter finger (valley) points, commonly employed in the literature to extract the region of interest for palmprint identification [116],[88]. This approach traverses the foreground boundary pixels (hand contour) to detect local minima points corresponding to finger valleys between little-ring and middle-index fingers. Center of the palm is then located at a fixed distance along a line that is perpendicular to the line joining the two finger valley points. Finally, a set of 3D data points inside a circular region around the center of the palm is extracted for further processing. Radius of this circular region of interest is empirically set to 60 pixels

(in the range image). Figure 5.2 pictorially illustrates the above approach on a sample hand image in the database. This approach, however, fails to accurately detect the two inter finger points when the degree of rotation of the hand around the x- axis is considerably high. This is due to the overlapping of the fingers and subsequently leads to erroneous localization of the center of the palm. Therefore, a much simpler but robust method based on distance transform to locate the center of the palm is employed in this work. Distance transform computes the Euclidean distance between each foreground pixel (part of the hand) and its nearest pixel on the hand contour. The point that has the maximum value for the distance transform is considered to be the center of the palm. Figure 5.3(a) shows a sample hand image in the database. It can be noticed that there is an overlap between fingers due to high degree of rotation. Figures 5.3(b) and 5.3(c) depict the located region of interest using the above described approaches. Please note (in figure 5.3(c)) that the first approach based on landmark points locates a point which is far off the actual center of the palm. We also observed that the approach based on distance transform may not always locate the same palm center for different images from the same hand with varying poses. However, it still locates a point in the close vicinity of the actual center and such small error is permissible as we utilize a set of data points inside the extracted region, rather than a single feature point, for further processing.

Figure 5.2: Localization of circular palmar region using interfinger valley points.

(a)

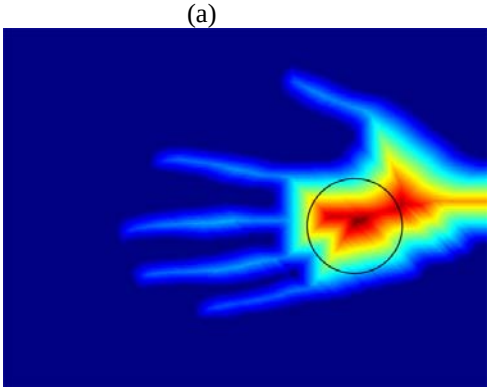

(b)

Figure 5.3: (a) Incorrect localization of interfinger finger points and subsequently the center of the palm due to considerable pose variation of the hand and the resulting overlap between little and ring fingers. (b) Localization of circular palmar region using the distance transform approach.

Once a set of 3D data points (represented by $[x_i, y_i, z_i]^T, i = 1...m,$ where m is the number of points) is extracted from the region of interest, a 3D plane is fit using the Iterative reweighted least squares (IRLS) approach. This approach solves a weighted least

squares formulation at every iteration until convergence. The weighted least squares optimization at iteration p can be formulated as follows

$$\alpha^{p} = \arg\min_{\alpha} \sum_{i=1}^{m} w_i^{(p-1)} (z_i - X_i \alpha^{(p-1)})^2 \tag{5.1}$$

where $\alpha = [\alpha_1, \alpha_2, \alpha_3]^{\mathrm{T}}$ are the three parameters of the plane and $X_i = [1, x_i, y_i]$. The w_i is the weight given to each data point, the value of which depends on how far the point is from the fitted plane (in the previous iteration). A bisquare weighting function is employed to assign the weights when the least squares residual (r_i) is less than a certain threshold and is defined as

$$w_i = (1 - (r_i)^2)^2 \tag{5.2}$$

where $r_i = (z_i - X_i \alpha)$. For points farther than the threshold, its weight is set to zero. Once the plane approximating the region around the center of the palm is computed, it is straightforward task to compute its normal vector, which gives an estimation of the orientation of the hand in 3D space (refer to figure 5.4). Here we make an assumption that the human hand is a rigid plane, which may not always be true, especially in the case of inherent bend or skin deformations. Nevertheless, the IRLS approach employed here is robust and is less influenced by the outliers in the data, which in our case arise from the bend or the deformations of the hand.

Let H_{3D} be a $3 \times n$ matrix representing the point cloud data of the acquired 3D hand

$$H_{3D} = \begin{bmatrix} x_1 & x_2 & \dots x_n \\ y_1 & y_2 & \dots y_n \\ z_1 & z_2 & \dots z_n \end{bmatrix} \tag{5.3}$$

where x, y and z are the three coordinates of the data points. Given this point cloud data and its orientation (in terms of the normal vector to the plane and represented by $\mathrm{n} = [n_x, n_y, n_z]$), the pose corrected point cloud H'_{3D} is given by

$$H'_{3D} = R\, H_{3D} \tag{5.4}$$

where R is the transformation matrix and can be expressed as follows

$$R = \begin{pmatrix} \cos\theta_y & 0 & \sin\theta_y \\ \sin\theta_x \sin\theta_y & \cos\theta_x & -\sin\theta_x \cos\theta_y \\ -\cos\theta_x \sin\theta_y & \sin\theta_x & \cos\theta_x \cos\theta_y \end{pmatrix} \tag{5.5}$$

where $\theta_x = -\arctan(n_y / n_x)$ and $\theta_y = \arctan(n_x / n_z)$ are the rotation angles about x and y axis respectively. The rotation matrix R is also used to correct the pose of the intensity image of the hand. For this purpose, the original data can be represented as

$$H_{2D} = \begin{bmatrix} x_1 & x_2 & \ldots x_n \\ y_1 & y_2 & \ldots y_n \\ I_1 & I_2 & \ldots I_n \end{bmatrix} \tag{5.6}$$

where x, y are the two coordinates and $I_1, I_2, \ldots, I_n$ are the intensity values corresponding to the hand in the acquired intensity image. The pose corrected data is given by

$$H'_{2D} = R\, H_{2D} \tag{5.7}$$

The pose corrected 3D and 2D data are a set of three dimensional points (point cloud) and need to be converted to range and intensity images respectively for further processing. This is achieved by re-sampling the pose corrected data on a uniform grid on the $x - y$ plane. In our experiments, the grid spacing (resolution) is set to $0.45\,mm$, as the x and y axes resolution of the originally scanned data is found to be around this value. The process of pose correction and re-sampling introduces several holes in the pose corrected range and intensity images. This is due to some regions, which are originally

not visible or occluded to the scanner, getting exposed after pose correction. Therefore, besides re-sampling, the post processing after pose correction involves hole filling using bicubic interpolation. Figure 5.5 shows the shaded view of a sample 3D hand and the corresponding pose normalized point cloud.

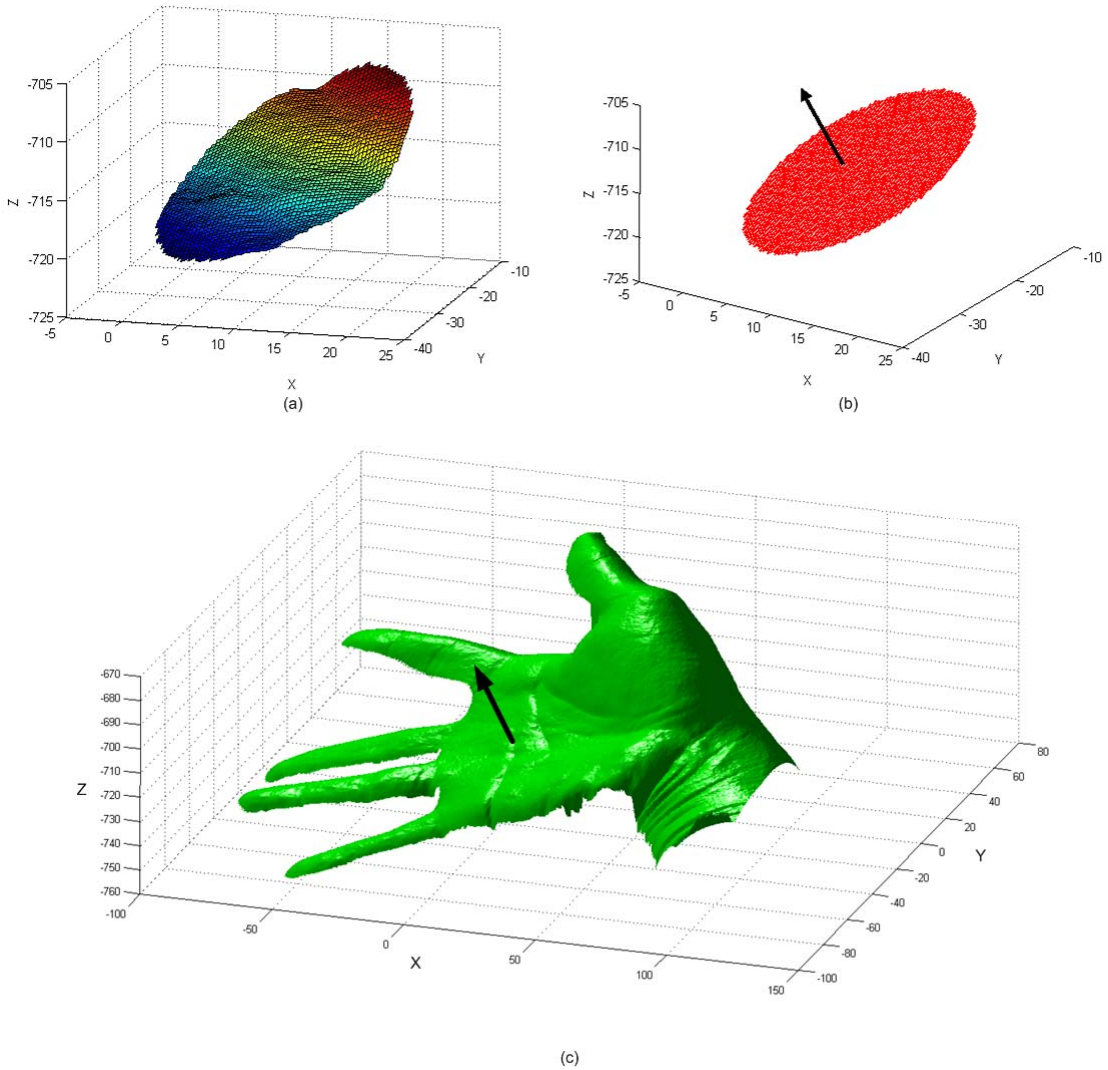

Figure 5.4: Estimation of orientation of the hand. (a) Circular region of interest extracted from the region around the center of the palm. (b) The fitted 3D plane and the corresponding normal vector. (c) Rendered view of the 3D hand with the normal vector indicating its orientation.

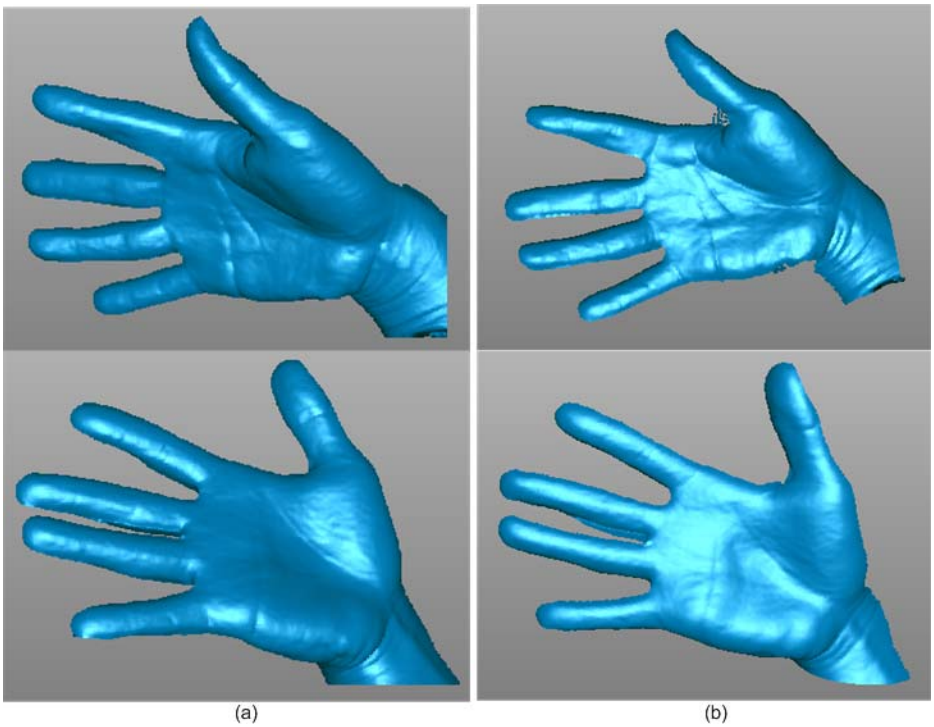

Figure 5.5: (a) Shaded view of sample 3D hand point clouds before and (b) after pose correction.

Figure 5.6 shows sample intensity hand images with varying pose in our database. The corresponding pose corrected and re-sampled images and the pose corrected images after hole filling are also shown in figure 5.6. As can be seen in figure 5.6(a), the hand in the third sample (refer to third row in figure 5.6) has a high degree of rotation about the x- axis. The pose correction on this image leads to large number of holes in the resampled image, and loss of significant information, especially around the finger edges. It should be noted that the 3D and 2D hands shown in figure 5.5(b) and 5.6(c) have not been corrected for their pose variations about the z- axis, since this process is a part of our subsequent feature extraction method.

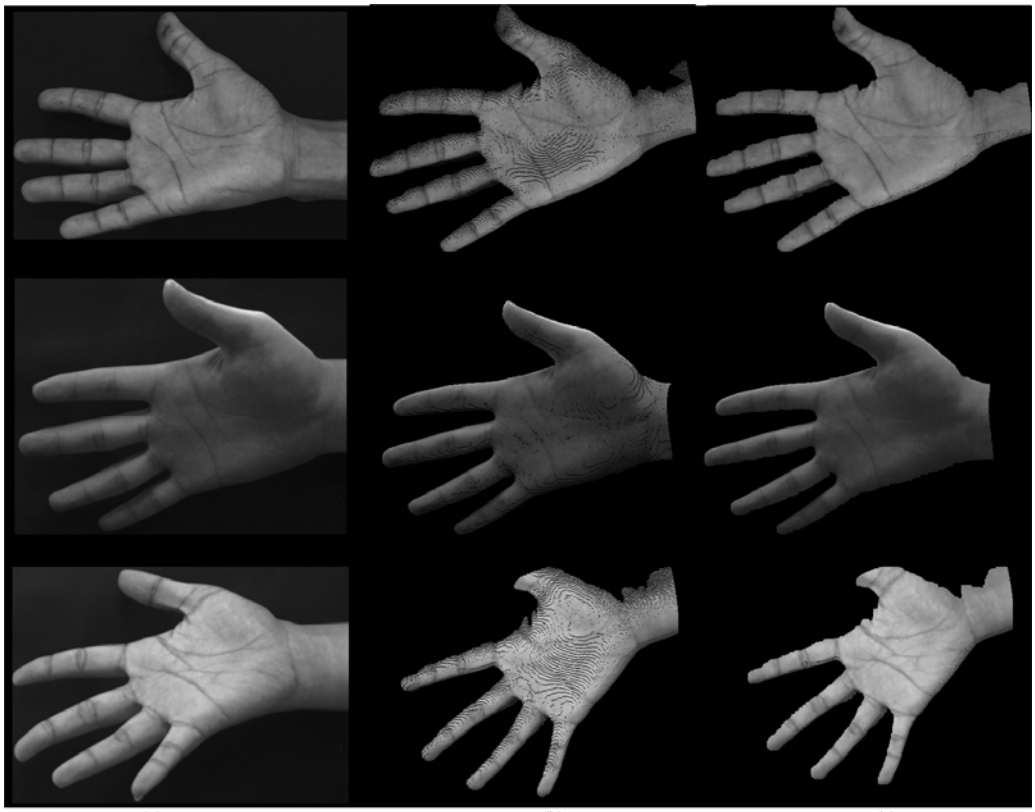

Figure 5.6: (a) Sample intensity images with varying pose in the database. (b) The corresponding pose corrected and resampled images. (c) Pose corrected images after hole filling.

5.3 Hand Feature Extraction

The pose corrected range and intensity images are processed to locate regions of interest (ROI) for hand geometry and palmprint feature extraction. The detailed description of this method, which is based on the detection of inter finger points, can be found in Chapter 4. It may be noted that the inter finger points can be reliably located as there can be no overlap between fingers in the pose corrected hand images. The regions of interest extracted from the range and intensity images undergo further processing in order to extract discriminatory palmprint and hand geometry features. Details of the feature

extraction and matching methods (for hand geometry as well as palmprint) are provided in Chapter 4.

5.4 Dynamic Fusion

Weighted sum rule based fusion is widely employed in the Multibiometrics to combine individual match scores. The major drawback of such a fusion framework is that poor quality samples can have adverse influence on the consolidated score since fixed weights are given for all samples. In order to overcome this problem, researchers have come up with fusion approaches that can dynamically weight a match score based on the quality of the corresponding modality [68]. However, accurately computing the quality of a biometric feature can be very challenging. Therefore we develop a simple but efficient approach for combining palmprint and hand geometry scores that are simultaneously extracted from the pose corrected range and intensity images. For every probe hand, the orientation information estimated in the pose normalization step is utilized to selectively combine palmprint and hand geometry features. The motivation for such an approach arises from our observation that pose correction leads to loss of information around the finger edges and therefore results in incomplete (partial) region of interest for finger geometry feature extraction. The loss of crucial information in fingers is prominent when the hand is rotated about x- axis. The process of matching finger/hand geometry features extracted from the pose corrected images generates poor match scores for such cases. We found from our observation that in such cases it is judicious to ignore the hand geometry information and rely only on the palmprint match scores to make a more effective decision.

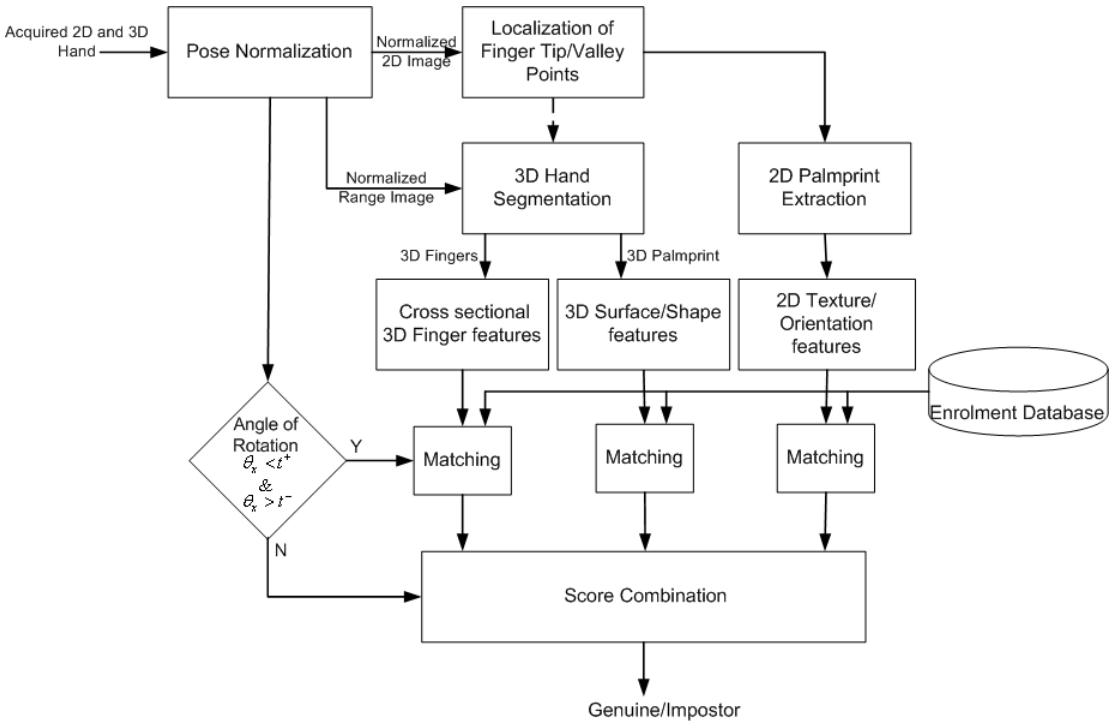

Figure 5.7: Block diagram of the hand identification approach with dynamic framework for combination of palmprint and hand geometry match scores.

The proposed dynamic combination approach attempts to identify and ignore those poor hand geometry match scores using the estimated orientation of the hand. The expression for consolidated score can be given as

$$S_{Final} = \begin{cases} w_1 s_{3DPalm} + w_2 s_{2DPalm} + w_3 s_{3DHG} & if\ (\theta_x < t^+)\ \&\ (\theta_x > t^-) \\ (s_{2DPalm} + s_{3DPalm})/2 & otherwise \end{cases} \tag{5.8}$$

where s_{2DPalm}, s_{3DPalm} and s_{3DHG} are the matching scores from 2D palmprint, 3D palmprint and 3D hand geometry matchers respectively. θ_x is the estimated angle of rotation of the hand about x axis; t^+ and t^- are the two thresholds for clockwise and counter-clockwise rotation respectively. The weights w_1, w_2 and w_3 are empirically set to 0.4, 0.4 and 0.2 respectively. Figure 5.7 shows the block diagram of the proposed pose invariant hand identification approach with dynamic fusion framework.

5.5 Experimental Results

5.5.1 Dataset Description

Since there is no publicly available 3D hand database where hand images are acquired in a contact-free manner, we developed our own database using a commercially available 3D digitizer [81]. The image acquisition system employed in this work is the same as the one described in Chapter 4. Participants in the data collection process conducted at our institute included mainly students who volunteered to give their biometric data. The database contains 1140 right hand images (2D and 3D) acquired from 114 subjects. In order to introduce considerable pose variations in the database, subjects were instructed to present their hand in five different poses (refer to figure 5.8). Specifically, for every user, five images are acquired in the following scenario:

1. Pose I: Frontal pose where hand is held approximately parallel to the image plane.
2. Pose II: Hand is rotated in the clockwise direction about x - axis
3. Pose III: Hand is rotated in the counter-clockwise direction about x - axis
4. Pose IV: Hand is rotated in the clockwise direction about y - axis
5. Pose V: Hand is rotated in the counter-clockwise direction about y - axis

The amount of out-of-plane rotation (in Pose II through V) is normally not restricted and is left to the user's discretion. Users are given the freedom to pose at any angle as long as the hand is inside the imaging volume of the scanner and there is no significant overlap of fingers in the acquired images that would make it impossible to locate and separate fingers before pose correction. This is done in order to perform experiments and evaluate the performance prior to pose normalization. Table 5.1 provides the absolute

mean and standard deviation of angles of rotation for each of the five poses in the database. It should be noted that the figures provided in this table are not accurate measurements (since the ground truth is not available), but are the angles of rotation estimated using the proposed approach. Nevertheless, the table gives an idea about the amount of pose variations present in our database. It can be observed that, the mean of angles about y - axis (Pose IV and V) is much lower compared to the case when the hand is rotated about the x - axis (Pose II and III). This is due to the limitation posed by the scanner's imaging volume. During image acquisition, we observed that a user's hand cannot be scanned completely for larger angles of rotation around y - axis and therefore we restricted the angle of rotation to ensure that the hand is held well inside the imaging volume. We also observed that the users are more comfortable while rotating their hand about the x - axis. This might be the reason for higher angles of rotation about x - axis (refer to Pose IV and V in Table 5.1), when user were only instructed to rotate their hand about y - axis.

Table 5.1: Statistics of the 3D hand database.

Pose	**Angle of rotation about x - axis (in degree)**		**Angle of rotation about y - axis (in degree)**	
	Mean	**Std**	**Mean**	**Std**
Pose I	6.48	4.51	5.01	3.67
Pose II	28.91	8.93	8.16	5.42
Pose III	25.99	8.88	5.42	4.798
Pose IV	13.71	8.05	15.17	10.93
Pose V	8.81	7.67	18.50	8.08

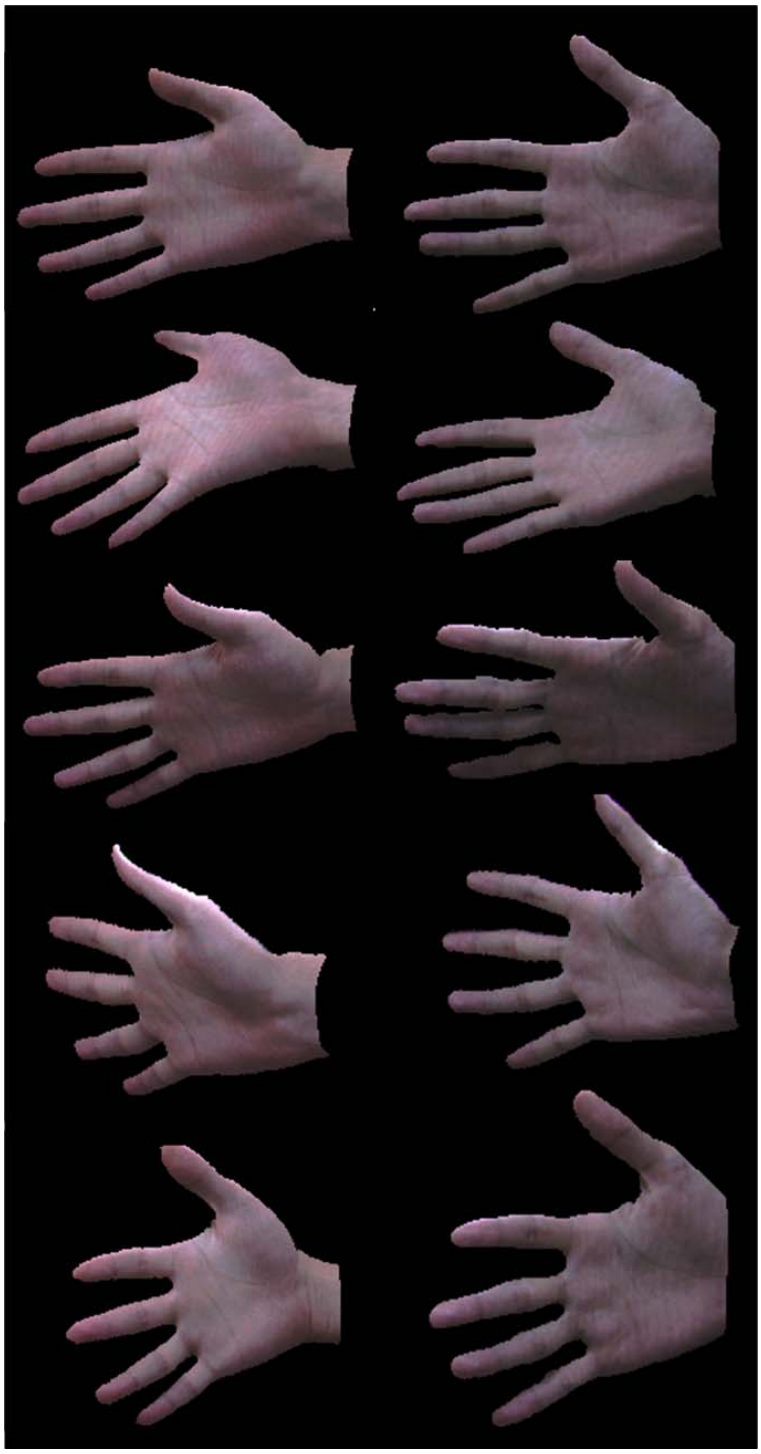

Figure 5.8: Textured 3D hands showing five different hand poses (Pose I through V) for two users (column-wise) in the database.

5.5.2 Verification Experiments

In order to ascertain the usefulness of the proposed pose correction and dynamic fusion approaches, we performed verification experiments on the acquired database. In the first set of experiments, we evaluate the performance improvement that can be achieved by employing the pose correction approach for the individual hand features. In the second set, experiments are performed to evaluate and compare the performance of the dynamic approach and weighted sum rule based fusion for hand features that are extracted from the pose corrected intensity and range images. All experiments reported in this chapter follow leave-one-out strategy. In other words, in order to generate genuine match scores, a sample is matched to all the remaining samples of the user (considering them as training data) and the best match score is considered as the final score. This process is repeated for all the five samples of the user. Therefore the number of genuine and impostor matching scores in the experiments are 570 and 32,205 respectively. Figure 5.9(a) shows the match score distribution for 2D palmprint features extracted directly from the acquired intensity images. It can be observed that there is a large overlap of genuine and impostor match scores due to the considerable variations in pose present in the database. Genuine and impostor score distribution for 2D palmprint features extracted from pose corrected intensity images is shown figure 5.9(b). It is quite clear from this figure that the process of pose normalization has greatly reduced the overlap of genuine and impostor match scores. Further, in order to ascertain this performance improvement, we computed FAR and FRR from the matching scores for the above two cases. The corresponding ROC curves are shown in figure 5.10. The consistent improvement in

performance (with pose correction) seen in this figure demonstrates the usefulness of the pose normalization approach for 2D palmprint features. We also performed experiments to investigate whether similar performance improvement can be achieved for 3D palmprint features. Match score distribution and ROC curves for 3D palmprint matcher with and without pose correction are shown figure 5.11 and figure 5.12 respectively. Two dimensional matching score distribution for 2D and 3D palmprint matchers shown in figure 5.13 shows significant reduction in overlap of genuine and impostor scores after pose correction. This indicates that a simple linear classifier such as weighted sum rule can be used to combine these matching scores. In the case of hand geometry features, 3D features perform slightly better than 2D features. (refer to ROC curves in figure 5.14(a) and 5.14(b)). Table 5.2 provides a summary of this set of experiments with EER as the performance index.

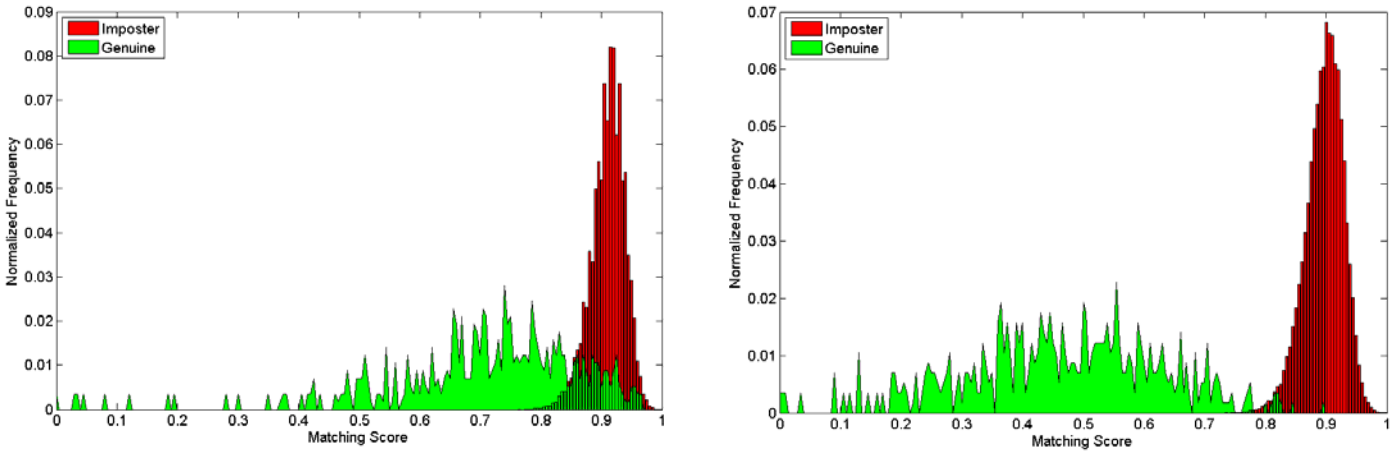

(a) (b)

Figure 5.9: (a) Genuine – Impostor score distribution for 2D palmprint matching before and (b) after pose correction.

Finally, we evaluate the performance from the combination of palmprint and hand geometry features using weighted sum rule and the proposed dynamic fusion approach.

As shown figure 5.15, the dynamic approach consistently outperforms the simple combination of match scores using the sum rule. Table 5.3 provides equal error rates from our experiments on combination of palmprint and hand geometry match scores.

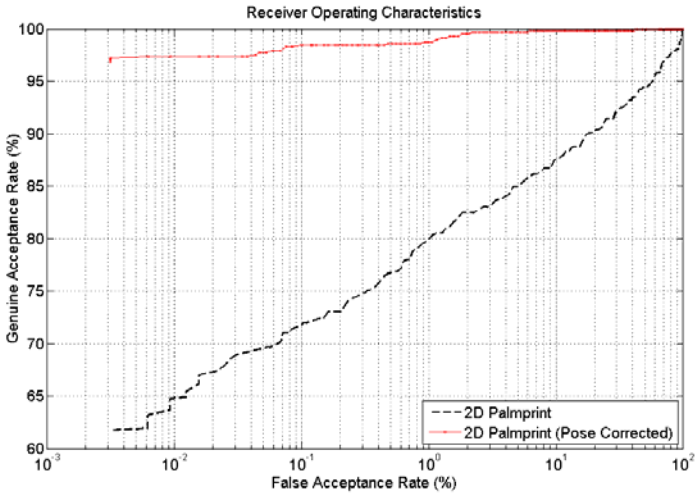

Figure 5.10: ROC curves for the 2D palmprint matching before and after pose correction.

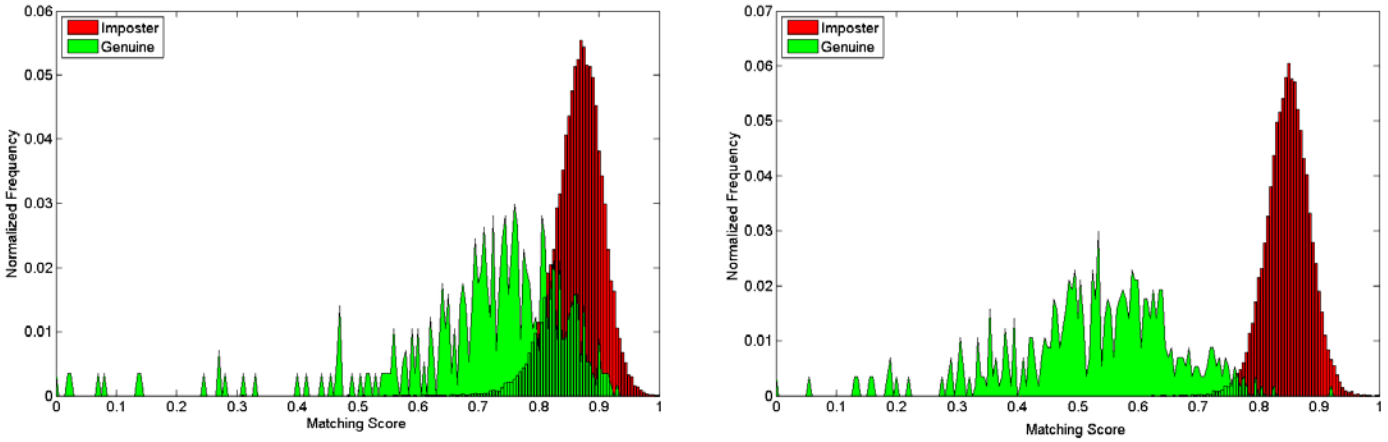

(a) (b)

Figure 5.11: (a) Genuine – Impostor score distribution for 3D palmprint matching before and (b) after pose correction.

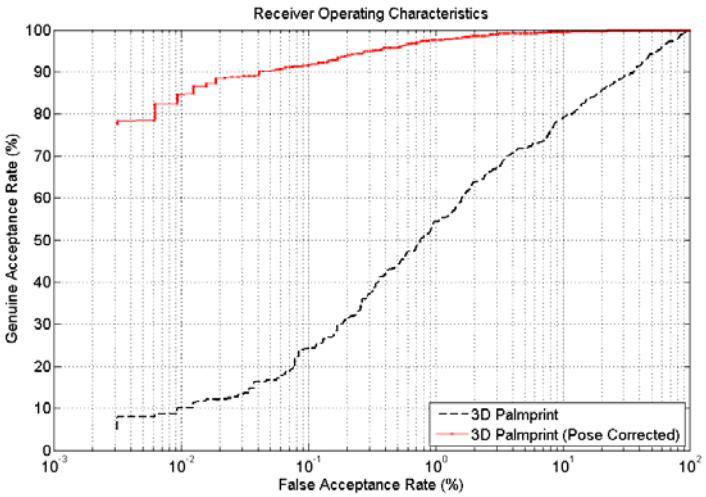

Figure 5.12: ROC curves for the 3D palmprint matching before and after pose correction.

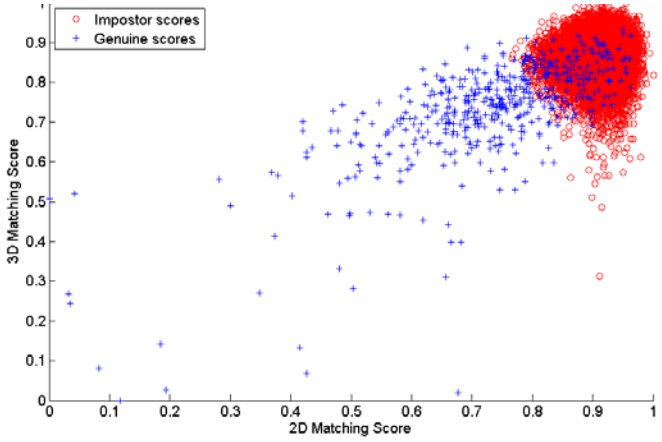

(a)

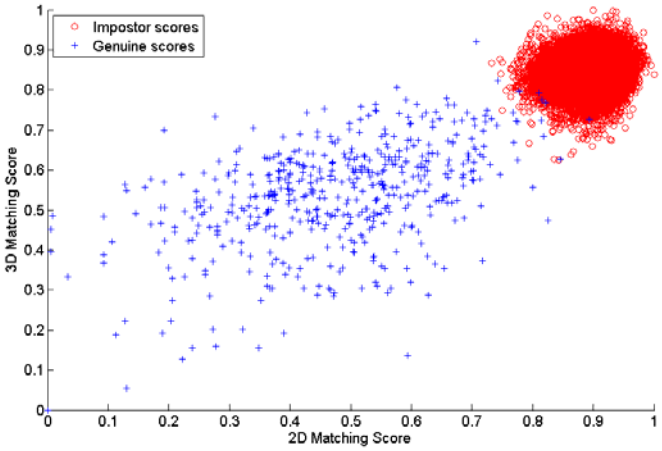

(b)

Figure 5.13: (a) Two dimensional score distribution for 2D and 3D palmprint matchers before and (b) after pose correction.

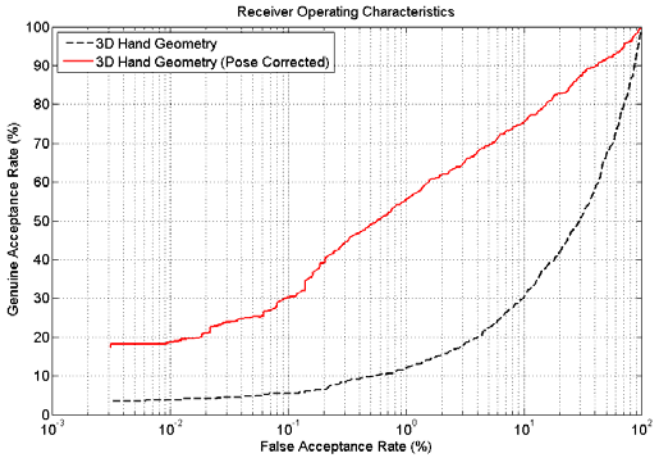

(a)

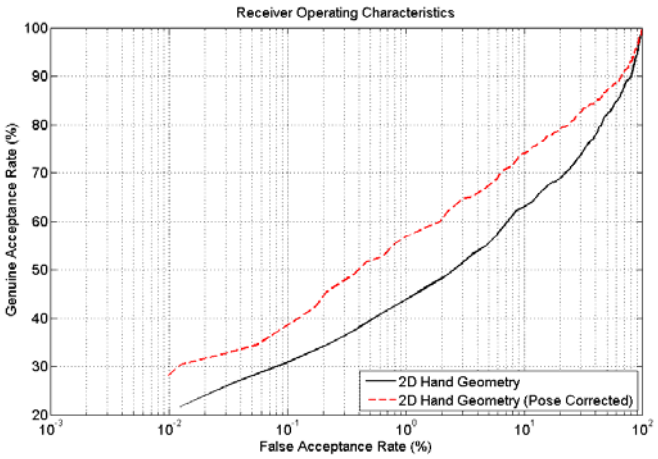

(b)

Figure 5.14: (a) ROC curves for the 3D hand/finger geometry and (b) 2D hand geometry matching before and after pose correction.

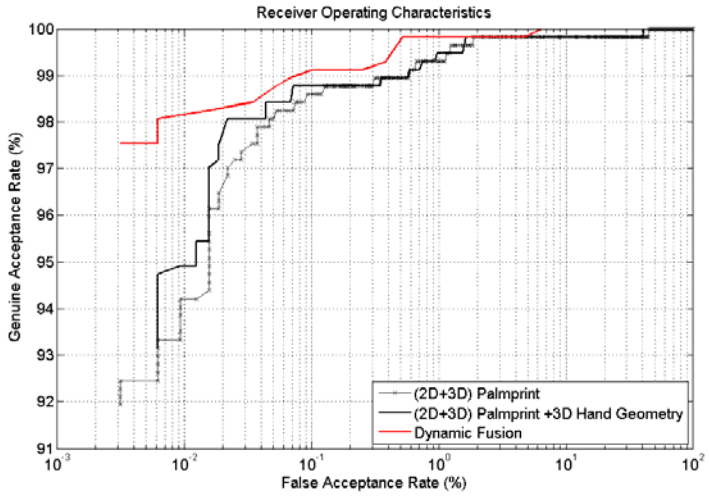

Figure 5.15: ROC curves for the combination of 2D, 3D palmprint and 3D hand geometry matching scores using weighted sum rule and the proposed dynamic approach.

Table 5.2: Equal error rates of palmprint and hand geometry matchers before and after pose correction.

Matcher	EER (%) (Without Pose Correction)	EER (%) (Pose Corrected)
2D Palmprint	11.80	1.10
3D Palmprint	16.32	1.61
3D Hand Geometry	40.9	17.2
2D Hand Geometry	28.69	22.15

Table 5.3: Equal error rates for combination of palmprint and hand geometry features.

Matcher	EER (%)
(2D+3D) Palmprint	0.72
(2D+3D) Palmprint + 3D Hand Geometry	0.71
Dynamic Fusion	0.28

5.6 Discussion

The experimental results presented in this previous section assume significance in the context of contact-free hand identification as it has been demonstrated that reliable identification can be performed even in the presence of significant pose variations. Most of the previous studies on unconstrained and contact-free hand identification do not deal with pose variations of the user hand. Instead these approaches implicitly make an assumption that the user is cooperative enough to acquire the frontal view of his/her hand. However in practice such approaches may require supervision in order to ensure that frontal views of the hand are acquired, especially for users who are not trained to use

the system. More recently, researchers have developed pose invariant hand identification approaches that yield promising performance even when the hand images are acquired under large pose variations. However, these approaches are based on multiple land mark points located on the hand and therefore their performance largely relies on the accuracy of feature point detection. The approach presented in this chapter exploits the acquired 3D hand data to estimate the pose of the user's hand. The advantage of the 3D data is that the orientation of the hand can be robustly estimated using a single point detected on the palm. In addition, discriminatory 3D features extracted from the pose corrected range images help to improve the performance of the system when used in combination with 2D hand features.

Experimental results from our investigation on individual hand features indicated that the palmprint features (2D as well as 3D) are more suitable to be utilized, especially when the degree of rotation of the hand is considerably high. This is mainly because the palmprint features are less affected by occlusion. In other words, the major part of the palmprint region is visible to the scanner (even at higher angles of rotation) and therefore the complete palmprint can be extracted from the pose corrected range images. On the other hand, performance of the hand geometry features has been disappointing. Although there is significant improvement in performance with the proposed pose normalization approach, the hand (finger) geometry features suffer from loss of crucial information due to occlusion around the finger edges. The occlusion is noticeably severe when the hand is rotated about the x- axis as major part of finger around its edges is not visible to the scanner, resulting in significant loss of information during pose correction. Therefore only a partial region of interest for fingers can be recovered from the pose corrected

intensity and range images. Moreover, the assumption that the palm and fingers lie on a plane (coplanar) does not strictly hold good in most cases due to finger movement and bending. This also might have played a role in the poor performance of the hand geometry features.

The experimental results also show that 3D hand geometry features performed slightly better than 2D features. This is because the computation of matching distance for 3D finger features involves a sliding approach that performs multiple matches between the cross sectional finger features. This approach can effectively handle the partial matching of fingers to certain extent. On the other hand, two dimensional finger width features extracted from the pose corrected intensity images suffer the most when only partial finger is available for matching.

Figure 5.15 shows the ROC curves for combination of palmprint and hand geometry features. As can be observed from this figure, a simple weighted combination of palmprint (2D as well as 3D) and 3D hand/finger geometry fails to achieve the desired results. In fact, the combination achieves only marginal improvement in EER (refer to Table 5.3) over the case when only 2D and 3D palmprint matching scores are combined. On the other hand, the new dynamic combination approach achieves a relative performance improvement of about 60 percent in terms of EER over the case when features are combined using weighted sum rule. As discussed earlier, the dynamic fusion approach can lessen the influence of the poor hand geometry match scores on the consolidated match score and thereby it helps to improve the verification accuracy.

5.7 Summary

In this chapter, a fully automatic hand identification approach that can reliably authenticate individuals even in the presence of significant hand pose variations (in 3D space) is presented. The orientation (or the 3D pose) of the hand is estimated based on the acquired 3D hand. The 3D orientation information is then used to correct pose of the acquired 3D as well as 2D hand. The Pose corrected intensity and range images of the hand are further processed for extraction of multimodal (2D and 3D) palmprint and hand geometry features. The major advantage of using 3D hand data is that the pose of the hand can be robustly estimated using only a single point (approximate palm center), unlike the existing approaches for 2D hand [54],[30] that require detection of multiple landmark points on the hand.

A novel dynamic approach to efficiently combine these simultaneously extracted hand features has also been presented. This approach selectively combines palmprint and hand geometry features, while ignoring some of the poor hand geometry matching scores resulting from high degree of rotation of the user's hand, especially about the x- axis. The motivation behind such an approach emerges from the observation (with the pose corrected hand data) that there is significant loss of hand/finger geometry information whenever the degree of rotation of the hand is considerably high. Therefore in such cases it is judicious to ignore hand geometry information and rely only on the palmprint match scores to make a more effective decision. The experimental results demonstrate that an explicit pose normalization step prior to matching significantly improves identification accuracy. It has also been shown that the dynamic approach to combining palmprint and

hand geometry matching scores consistently outperforms their straightforward fusion using weighted sum rule.

Chapter 6
Adaptive Framework for Score Level Fusion

Earlier chapters in this thesis introduced methods for personal identification using 3D hand scans. Matching scores from multiple features, namely, 3D palmprint, 3D hand geometry, 2D palmprint and 2D hand geometry are consolidated prior to decision making. The combination approach employed a single fusion rule (i.e., weighted sum rule) and a fixed set of parameters. The weight parameters of the fusion rule are selected based on the performance on a training dataset with EER as the performance measure. Although this score combination approach is simple, the resulting multibiometric system operates at a fixed operating point offering a fixed performance. In other words, the performance of such a system cannot be made adaptive to the varying security level requirement. This chapter addresses the problem of combining multiple matching scores that are generated based on the matching techniques (for hand features) described in previous chapters and presents a fusion framework that is adaptive to the security level requirement.

Most of the multimodal biometric systems employ a single fixed fusion rule to achieve the desired performance. The parameters of the fusion rule employed are tuned to provide the desired performance for a fixed security level. Therefore the performance of these systems is not adaptive to the security level requirement. However, there are applications where a biometric system with multiple levels of security is desirable. Figure

6.1 shows the Receiver Operating Characteristics (ROC) of a biometric system. The highlighted points on the curve indicate the desired operating points for different applications. There are also times when security levels of a biometric system should be set depending on the perceived threat.

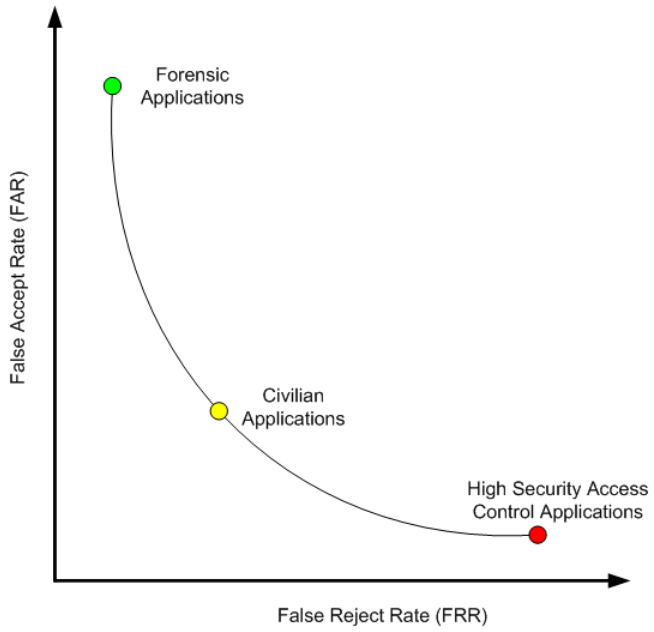

Figure 6.1: ROC curve for a typical biometric system.

This chapter presents a framework for adaptive combination of match scores from multiple biometric systems. The matching scores from individual matchers are combined at the score level, which is expected to result in better performance than the decision level fusion approach. Four different score level fusion rules have been considered in this work. However, any number of new combination rules can be added to the proposed framework. A Particle Swarm Optimizer is employed to select the optimal fusion rule and the optimal decision threshold that minimizes a weighted error rate objective function. The experiments are performed on a set of simulated matching scores in order to

ascertain the usefulness of the proposed approach. Further, the proposed system is evaluated on the real biometric database of 3D hand scans. 2D palmprint, 3D palmprint and 3D hand geometry matching scores are generated based on the feature extraction and matching approaches described in the chapters 3 and 4. Experimental results on these two datasets demonstrate that the proposed method based on fusion at the score level consistently outperforms a similar approach based on the decision level fusion of individual biometric systems.

6.1 Background

Biometrics has emerged as the best access control solution for applications where resources or information need to be protected from unauthorized access. Biometric traits such as fingerprint, face, palmprint, iris and hand-geometry have been well explored and matured approaches are available in order to perform personal identification. Yet, biometric systems that employ single biometric trait (unimodal biometric systems) suffer from inherent short comings such as limited discriminability, intra-class variations and vulnerability to spoof attacks. A multimodal biometric system, on the other hand, provides enhanced security and has been shown to overcome some of these limitations. Although the multibiometrics has been extensively studied in the literature [20],[37],[47],[64],[110] there has been little work directed towards developing multimodal systems that can adapt to the varying security requirements.

As indicated earlier, the design of reliable multimodal fusion algorithms that are adaptive to the variable security requirement and the traffic flow has received little

attention in the literature. The significance of an adaptive multibiometric system can be visualized in the following scenario: Consider a multimodal biometric system deployed to control access to a room. At any given point of time, based on the perceived threat, the proposed system tunes its parameters to achieve the desired performance. For example, if low security level is desired, the proposed system minimizes false rejection and thereby minimizing inconvenience caused to the users. This also helps to increase the traffic flow rate in to the room, by reducing the number of attempts required by genuine users to get authenticated. On the other hand, if high level of security is desired, the system can be made to tune its parameters to achieve it. This parameter setting can also be used when a decreased traffic flow is required. The scenario described above only considers two extreme levels of security. An adaptive system, however, should be able to provide multiple levels of security between the two extremes.

The BioID system developed by Frischholz *et al.* [100] offers multiple security levels by employing different decision strategies on the biometric modalities (face, lip motion and voice) being fused. When the required security level is low, it may well be enough to make a decision based on the agreement of two out of three modalities. On the other hand, for high security applications, this system demands agreement of all the three modalities. However, BioID system does not provide a systematic way to vary the level of security. Instead, a system administrator makes a decision on the decision strategies to be adopted to achieve the desired performance. On the other hand, the adaptive multimodal biometric management algorithm (AMBM) proposed by Veeramachaneni *et al.* [69] employs a particle swarm optimizer to choose the optimal fusion rule and decision thresholds depending on the level of security required. AMBM considers all

possible fusion rules and selects the one that optimizes the system performance in terms of accuracy. However their approach combines multiple biometric decisions and therefore suffers from the inherent problems associated with any decision level fusion strategy. In addition, experimental results reported are based only on simulated distributions of match scores that follow Gaussian distribution.

The adaptive fusion approach presented in this chapter employs a particle swarm optimizer to tune the system parameters by minimizing an objective function that reflects desired level of security (or level of perceived security threat). The following section provides a brief review of the particle swarm optimization algorithm.

6.2 Particle Swarm Optimization

Particle swarm optimization is an evolutionary search algorithm developed based on the social behavior of a flock of birds trying to fly to a favorable environment. The PSO is employed to find the solution for the adaptive selection of combination of individual points which are referred as the particles in multidimensional search space. Each particle (representing a bird the flock), characterized by its position and velocity, represents the possible solution in search space. Behavior of the particles in the PSO imitates the way in which birds communicate with each other, while flying. During this communication, each bird reviews its new position in the space with respect to the best position it has covered so far. The birds in the flock also identify the bird that has reached the best position/environment. Upon knowing this information, others in the flock update their

velocity (that depends on a bird's local best position as well as the position of the best bird in the flock) and fly towards the best bird. The process of regular communication and updating the velocity repeats until the flock finds a favorable position. In a similar manner, the particle in the PSO moves to a new position in multidimensional solution space depending upon the particle's best position (also referred to as local best position) (p_{ak}) and global best position (p_{gk}). The p_{ak} and p_{gk} are updated after each iteration whenever a suitable, *i.e.* lower cost, solution is located by the particle. The velocity vector of each particle represents/determines the forthcoming motion details. The velocity update equation of particle a of the PSO, for instance (t +1), can be represented as follows [77]:

$$v_{ak}(t+1) = \omega v_{ak}(t) + c_1 r_1\left(\rho_{ak}(t) - x_{ak}(t)\right) + c_2 r_2\left(\rho_{gk}(t) - x_{ak}(t)\right) \tag{6.1}$$

where ω is the inertia weight between 0-1 and provide a balance between global and local search abilities of the algorithm. The accelerator coefficients c_1 and c_2 are positive constants, and r_1 and r_2 are two random numbers in 0-1 range. The corresponding position vector is updated by

$$x_{ak}(t+1) = x_{ak}(t) + v_{ak}(t+1) \tag{6.2}$$

The equation (6.1) indicates that the new velocity of a particle in each of its dimensions is dependent on the previous velocity and the distances from previously observed best solutions (positions of the particle).

The particle swarm optimization approach detailed above operates on continuous space. However, there exists optimization problems where the particles are better

represented as discrete binary variables. Such problems require that these binary particles be evolved to obtain an optimal solution. A binary version of the particle swarm optimization algorithm is also described in reference [95]. The position vector for each particle in binary PSO can have a value of either zero or one on each dimension. The formula for calculating the velocity update in binary PSO remains the same as real valued version, except that ρ_{ak} , x_{ak} and ρ_{gk} in equation (6.1) are binary valued. The velocity v_{ak} for binary PSO represents the probability of bit x_{ak} taking the value 1. A sigmoid function *S* is employed to limit the value of the probability v_{ak} to the range [0, 1]. Therefore the position vector of a particle in binary PSO is updated as follows:

$$x_{ak}(t+1) = \begin{cases} 1 & \text{for } r_3 < S(v_{ak}(t+1)) \\ 0 & \text{Otherwise} \end{cases} \tag{6.3}$$

where $S(v_{ak}(t+1)) = \dfrac{1}{1+\exp(-v_{ak}(t+1))}$ and r_3 is a random number in the interval [0, 1] with uniform distribution.

6.3 Observations on the Adaptive Decision Level Fusion

We observe that there are some discrepancies in the results reported in the paper [69] that originally presented an adaptive fusion approach for multimodal biometrics. Our experiments indicate that the authors have considered only a subset of all possible fusion rules, contradicting the statement that all possible rules have been considered. Moreover, the authors state that only monotonic rules can be optimal [91], and therefore all other

rules can be ignored. However, our experimental results examining all possible rules demonstrate that a non monotonic rule can also be an optimum fusion rule.

In the paper [69], the authors propose an algorithm based on Particle Swarm Optimization (PSO) to optimally combine the individual biometric sensor decisions. The proposed algorithm selects the fusion rule and sensor operating points that minimize a given cost function. The cost function, formulated in terms of global false acceptance and rejection rates, is defined as:

$$E = C_{FA}(F_{AR_a} - F_{AR_d}) + (2 - C_{FA})(F_{RR_a} - F_{RR_d}) \tag{6.4}$$

where C_{FA} is the cost of falsely accepting an impostor. F_{AR_a} (F_{RR_a}) and F_{AR_d} (F_{RR_d}) are the achieved and desired global false acceptance (rejection) rates. Enforcing the most stringent condition to achieve false acceptance rate of zero while ensuring zero false rejection ($F_{AR_d} = 0$ and $F_{RR_d} = 0$), the cost function (Equation 6.4) reduces to:

$$E = C_{FA}(F_{AR_a}) + (2 - C_{FA})(F_{RR_a}) \tag{6.5}$$

An optimization problem, employing PSO is formulated to minimize the cost function given in equation (6.4). Each particle of PSO algorithm is defined as,

$$X_m = \{F_{AR_{1m}}, F_{AR_{2m}}, f_m\} \tag{6.6}$$

where the first two dimensions are false acceptance rates of individual unimodal biometric systems and the last dimension is the four bit fusion rule.

The authors in [69] claim that the proposed adaptive multimodal biometric algorithm (AMBM) comprehensively considers all fusion rules and all possible operating points of the individual sensors. However, we find that there are some discrepancies in the reported results. Our observations are summarized as follows:

1. The experimental results presented in [69] show that the AMBM algorithm considers only the monotonic rules. The results are quite contradictory to the claims in [69], *i.e.*, 'algorithm considers all fusion rules'.
2. We find that some of the non monotonic rules perform as good as monotonic rules and therefore these rules cannot be ignored by the algorithm.

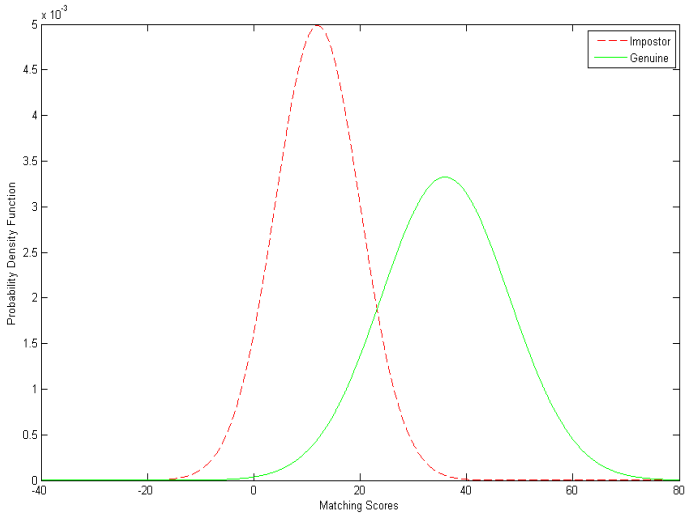

Figure 6.2: Score distribution for sensor 1.

6.3.1 Experimental Results

We carried out the experiments under the same conditions, using the same parameter values and data reported in the paper [69]. Figure 6.2 and figure 6.3 show the genuine and impostor score distributions for individual biometric systems. These distributions are assumed to be Gaussian, with parameters described in the paper ([69], pp. 352, Table VI). For every cost of false acceptance (C_{FA}) from 0 to 2, in steps of 0.1, the AMBM algorithm is run 100 times to select an optimal operating point and a fusion rule.

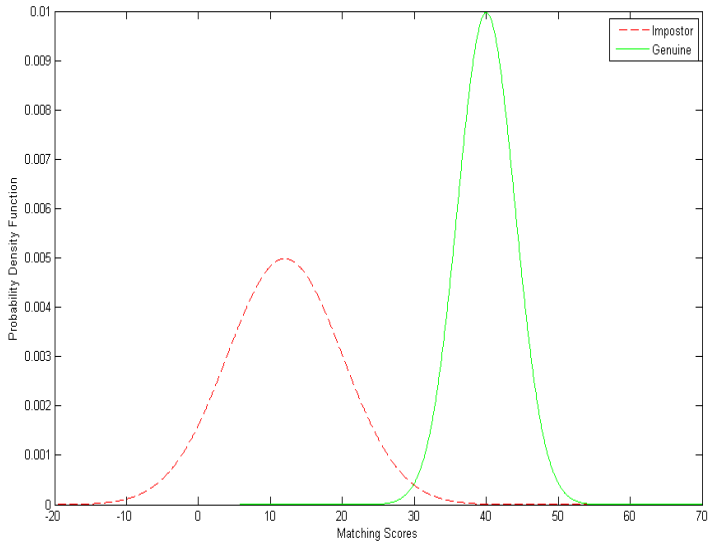

Figure 6.3: Score distribution for sensor 2.

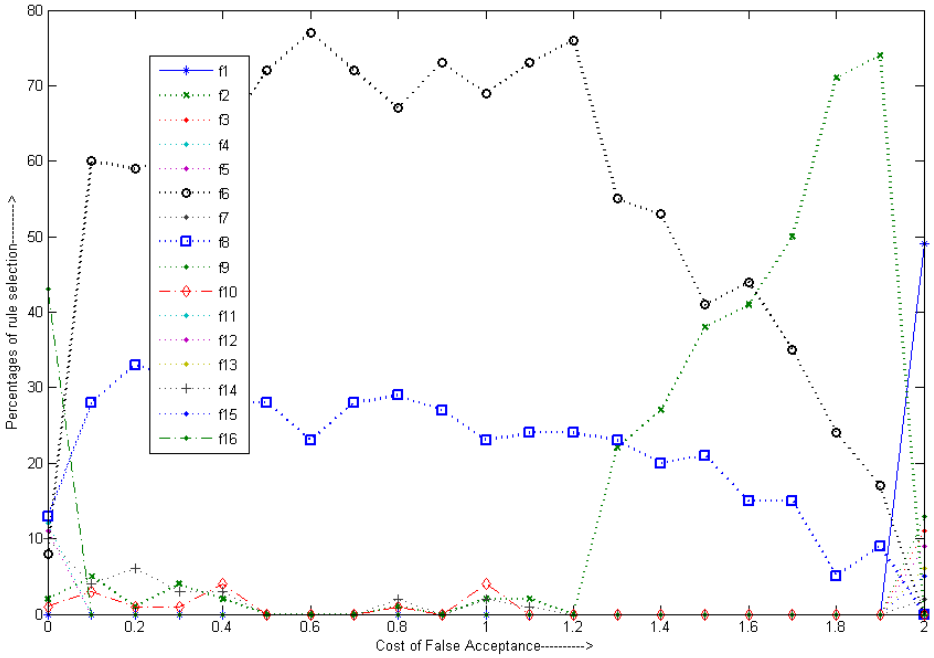

Figure 6.4: Probability of selection of fusion rules versus the cost of false acceptance.

Figure 6.4 shows the number of times a rule has been actually selected versus the cost of false acceptance. It can be observed from Figure 6.4 that in the range of C_{FA} from 0 to 1.2, the five different rules, namely f_8, f_6, f_{14}, f_2 and f_{10} are selected. However, rules

f_{10} and f_{14} have never been selected in the reported experimental results in ([69], pp. 354, Figure 14). This is unlikely as the rules f_6, f_{14} and f_{10} are equally good and can give the same minimum cost for a particular set of operating points. This is illustrated below:

For rule f_6:

global $F_{AR} = F_{AR_2}$, and global $F_{RR} = F_{RR_2}$

For rule f_{14}:

global $F_{AR} = 1 - F_{AR_1}(1 - F_{AR_2})$, and global $F_{RR} = F_{RR_2}(1 - F_{RR_1})$

For rule f_{10}:

global $F_{AR} = (1 - F_{AR_1})(1 - F_{AR_2}) + F_{AR_1}F_{AR_2}$, and global $F_{RR} = F_{RR_2}(1 - F_{RR_1}) + F_{RR_1}(1 - F_{RR_2})$

Therefore, when $F_{AR_1} = 1$ and $F_{RR_1} = 0$, rules f_{14} and f_{10} result in global error rates $F_{AR} = F_{AR_2}$, $F_{RR} = F_{RR_2}$ and as a result, all of the above rules give the same cost under these operating conditions.

In addition, the results reported in [69] show that rules f_6 and f_8 are the optimal solutions when C_{FA} is 0. Under these conditions, for rules f_6 and f_8 to selected, the individual biometric systems must be operating at $F_{AR_2} = 1, F_{RR_2} = 0$ and F_{AR_1} (or F_{AR_2}) $= 1$, F_{RR_1} (or F_{RR_2}) $= 0$ respectively. However, we find through the experiments that, for $C_{FA} = 0$, rules f_6 and f_8 are not the only optimal solutions and there are a number of other rules (including non monotonic ones) that result in the same minimum PSO cost and therefore they should have appeared in the results reported by the authors. Optimal rules selected (for $C_{FA} = 0$) in our experiments are summarized in Table 6.1.

Table 6.1: Selection of optimal rules for $C_{FA} = 0$.

Rule	Monotonic/Non monotonic	Global FRR (F_{RR})	Operating Point	Cost(Eq.1) at operating point	Number of times selected
f_2	Monotonic	$F_{RR_1} + F_{RR_2} - F_{RR_1}F_{RR_2}$	$F_{RR_1}, F_{RR_2} = 0$	0	2
f_4	Monotonic	F_{RR_1}	$F_{RR_1} = 0$	0	12
f_6	Monotonic	F_{RR_2}	$F_{RR_2} = 0$	0	8
f_8	Monotonic	$F_{RR_1}F_{RR_2}$	F_{RR_1} (or F_{RR_2}) $= 0$	0	13
f_{10}	Non monotonic	$F_{RR_1} + F_{RR_2} - 2F_{RR_1}F_{RR_2}$	$F_{RR_1}, F_{RR_2} = 0$	0	1
f_{12}	Non monotonic	$F_{RR_1}(1 - F_{RR2})$	$F_{RR_1} = 0$	0	12
f_{14}	Non monotonic	$F_{RR_2}(1 - F_{RR_1})$	$F_{RR_2} = 0$	0	10
f_{16}	Monotonic	0	NA	0	43

Similarly, for $C_{FA} = 2$, we obtain a number of optimal rules satisfying the performance criteria, where as there is only one rule, f_1 appearing in the authors' results. These rules are summarized in Table 6.2.

Table 6.2: Selection of optimal rules for $C_{FA} = 2$.

Rule	Monotonic/Non monotonic	Global FAR (F_{AR})	Operating Point	Cost(Eq.1) at operating point	Number of times selected
f_1	Monotonic	0	NA	0	49
f_3	Non monotonic	$F_{AR_1}(1 - F_{AR_2})$	$F_{AR_2} = 1$	0	11
f_5	Non monotonic	$F_{AR_2}(1 - F_{AR_1})$	$F_{AR_1} = 1$	0	9
f_7	Non monotonic	$F_{AR_1} + F_{AR_2} - 2F_{AR_1}F_{AR_2}$	$F_{AR_1}, F_{AR_2} = 1$	0	2
f_9	Non monotonic	$1 - F_{AR_1} - F_{AR_2} + F_{AR_1}F_{AR_2}$	F_{AR_1} (or F_{AR_2}) $= 1$	0	13
f_{11}	Non monotonic	$1 - F_{AR_2}$	$F_{AR_2} = 1$	0	5
f_{13}	Non monotonic	$1 - F_{AR_1}$	$F_{AR_1} = 1$	0	6
f_{15}	Non monotonic	$1 - F_{AR_1}F_{AR_2}$	$F_{AR_1}, F_{AR_2} = 1$	0	5

While selection of all the rules in Table 6.1 and Table 6.2 cannot be guaranteed (especially the ones with very low number of selections, due to stringent conditions on

operating points) on repeated runs of the simulation, complete absence of these rules as in [69] cannot be justified. Most of them did appear consistently in our experiments.

6.4 Score Level Adaptive Fusion

The block diagram in figure 6.5 shows the framework for combining match scores from multiple biometric traits. In this work, we considered four score level combinations, namely, weighted sum or average, product, exponential and tan-hyperbolic rules. In fact any number of score level combination rules can be incorporated by expanding the proposed framework.

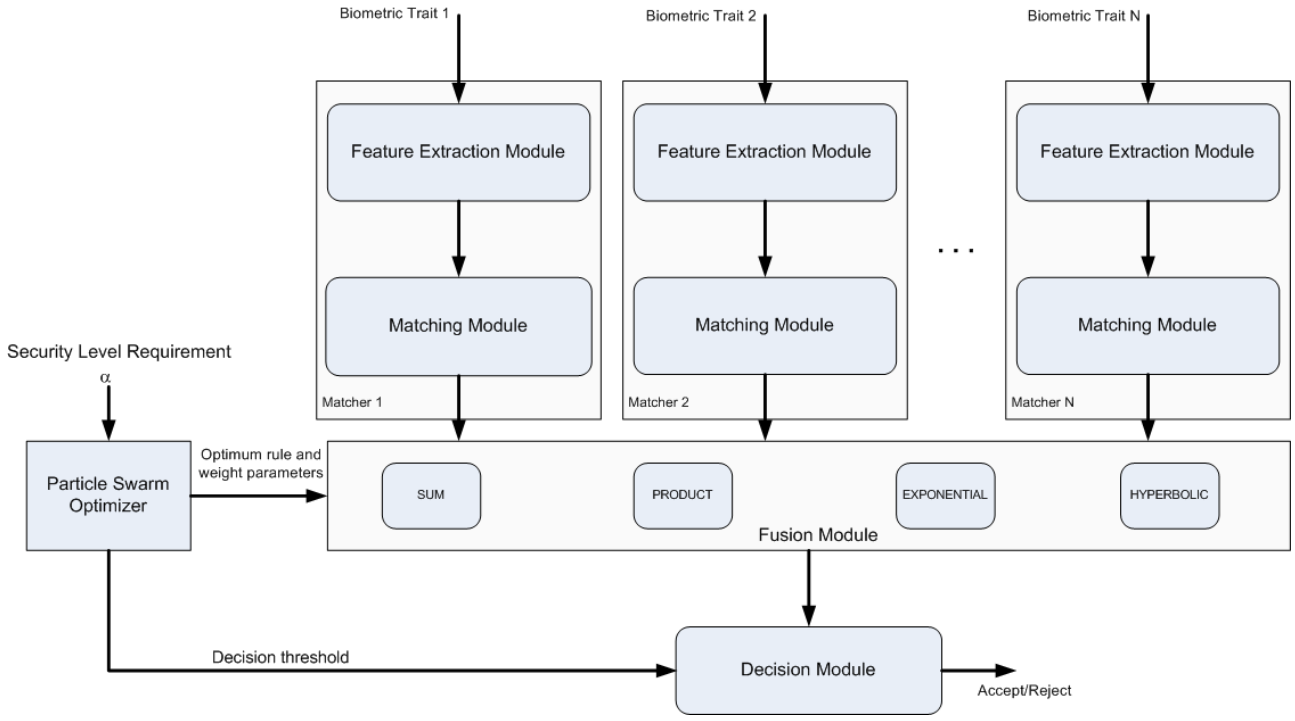

Figure 6.5: Block diagram of the proposed adaptive multimodal system based on score level fusion.

The consolidated match score S from each of these combinations is computed as follows:

$$\text{Sum rule: } S = \sum_{j=1}^{m} s_j w_j \tag{6.7}$$

$$\text{Product rule: } S = \prod_{j=1}^{m} s_j^{w_j} \tag{6.8}$$

$$\text{Exponential rule: } S = \sum_{j=1}^{m} \exp(s_j) w_j \tag{6.9}$$

$$\text{Tan Hyperbolic rule: } S = \sum_{j=1}^{m} \tanh(s_j) w_j \tag{6.10}$$

The Particle Swarm Optimizer (PSO) dynamically selects the optimum fusion rule and weight parameters to minimize the following weighted error rate (WER) function:

$$WER(\alpha, \lambda) = \alpha FAR(\lambda) + (1-\alpha) FRR(\lambda) \tag{6.11}$$

where the parameter $\alpha \in [0,1]$ offers the balance between FAR and FRR and determines the desired level of security. The parameter λ represents the decision threshold and an optimal value for this parameter is selected by the PSO. Therefore PSO selects optimal fusion rule, weight parameters and decision threshold for a fixed value of input α. The value of α is input to the system depending on the level of security desired. The homeland security advisory [33] system represents a typical example of the qualitative assessment of the adaptive security requirement. Depending on the perceived threat or risk of attack, this system recommends citizens a set of appropriate actions. In a similar way, the risk of attack on a biometric system can be varying and therefore it is critical for it to provide multiple levels of security. By varying the parameter α, different levels of

security can be achieved for the proposed multimodal biometric system. The higher the value of α, the higher the cost of false acceptance in equation (6.11), and therefore PSO selects suitable operating points to achieve a low rate of false acceptance (FAR). The four fusion rules in equations (6.7) through (6.10) and the corresponding parameters are optimally chosen by the particle swarm optimizer. In our implementation for combining 3 biometric sensors, each particle of the PSO is characterized by four continuous variables; the parameters of score level fusion rule w_1, w_2, w_3 and the decision threshold *thr* and a two bit discrete binary variable representing four different score level fusion rules. Therefore we employ a hybrid PSO with real valued and binary versions of the algorithm to determine the optimal fusion strategy and the corresponding fusion parameters. The search process in PSO is initialized with a number of particles at random positions in the search space. Each particle is characterized by its position and velocity. Position, represented by $x_{ak}(t)$, is the multidimensional vector (6 dimensions, as described above) and the velocity ($v_{ak}(t)$) determines the direction and speed with which a particles moves from one position to another in the search space. At each iteration, the position and velocity vector of particles are updated (according to the equations (6.1) through (6.3)) in a way that drives the particles to converge at the global minima of the objective function given in equation (6.11).

6.4.1 Experimental Results

6.4.1.1 Synthetic Dataset

The proposed adaptive score level fusion approach is rigorously evaluated using synthetic as well as real biometric matching scores. The distribution of matching scores from biometric traits such as iris [60] has been shown to closely follow binomial distribution and the Poisson distribution can be considered as an approximation to the binomial distribution when the number of trials is large. Therefore, in our experiments, synthetic matching scores corresponding to genuine and impostor matches for two modalities are generated using the Poisson distribution. Figure 6.6 shows the distribution of these synthetically generated matching scores. There are 1000 genuine and 100,000 impostor scores for each of the two biometric modalities. Since the particle swarm optimizer finds multiple optimal operating points (generating varying results in each run), we ran the algorithm 100 times for every value of α from 0 to 1, insteps of 0.1 and the experimental results are presented in terms of average and standard deviation of the minimum cost achieved over the 100 runs. Figure 6.7(a) shows the average of the minimum WER achieved by the proposed adaptive score level approach and the one presented in [69]. It can be observed from this figure that the proposed approach consistently outperforms (with significantly lower WER) the AMBM algorithm for the complete range of the security level α (0 through 1). In order to get an idea of how much the values of minimum WER vary (over 100 runs of the algorithms, for a fixed α), we examined the standard deviation of minimum WER achieved. Figure 6.7(b) shows the comparative plot for the two algorithms. The lower values of standard deviation for the proposed algorithm

clearly suggests that every run of the algorithm achieved almost the same minimum WER, where as AMBM algorithm, though converged to a minimum on every run, exhibits higher instability and does not achieve the same (or nearly the same) minimum value for WER.

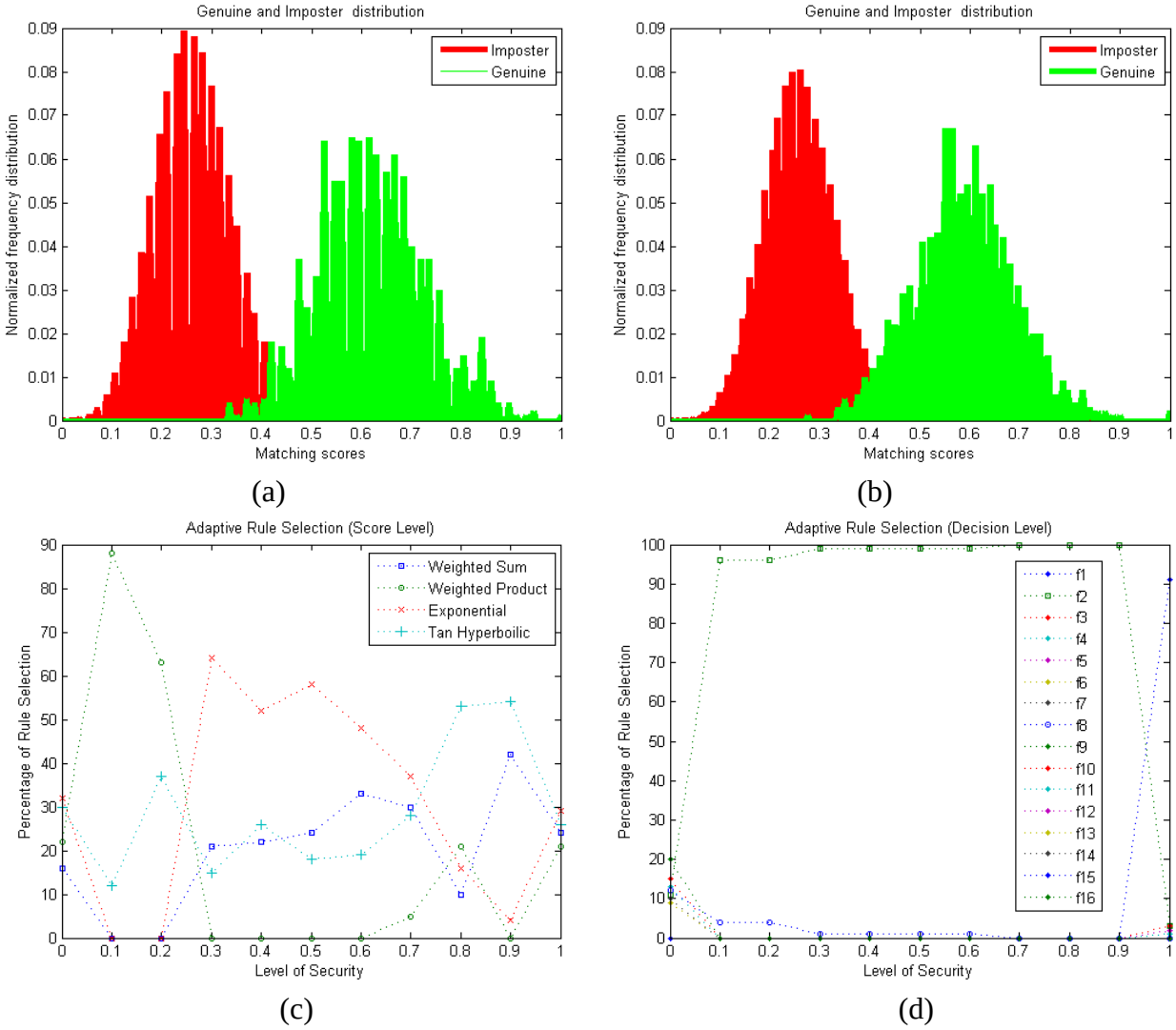

Figure 6.6: (a)-(b) Genuine-Impostor match score distributions that follow Poisson distribution for two modalities. (c)-(d) Adaptive selection of fusion rules for score and decision level approaches.

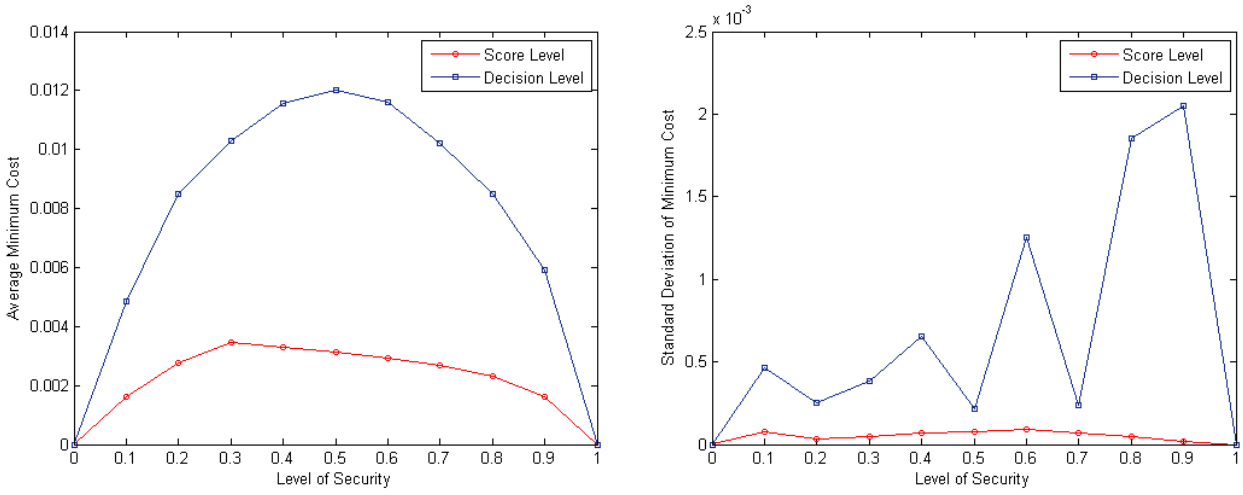

(a) (b)

Figure 6.7: Performance curves for combination of synthetic matching scores. Comparative plots of (a) average and (b) standard deviation of minimum cost for adaptive score and decision level combinations.

6.4.1.2 3D Hand Dataset

In order to further ascertain the superior performance of the proposed algorithm, we performed two sets of experiments using the real biometric matching scores. In the first set of experiments, 3D Palmprint database is employed to generate the genuine and impostor matching scores for the 2D and 3D palmprint matchers. Details of the database and the matching algorithms are provided in Chapter 3. The database consists of 6 palmprint (2D as well as 3D) images for each of the 108 users, resulting in a total of 648 images for 2D and 3D palmprint. Exhaustive matching results in 1,620 genuine and 208,008 impostors matching scores for each of the two modalities. Figure 6.8(a) and 6.8(b) show the score distributions for 2D and 3D palmprint matchers.

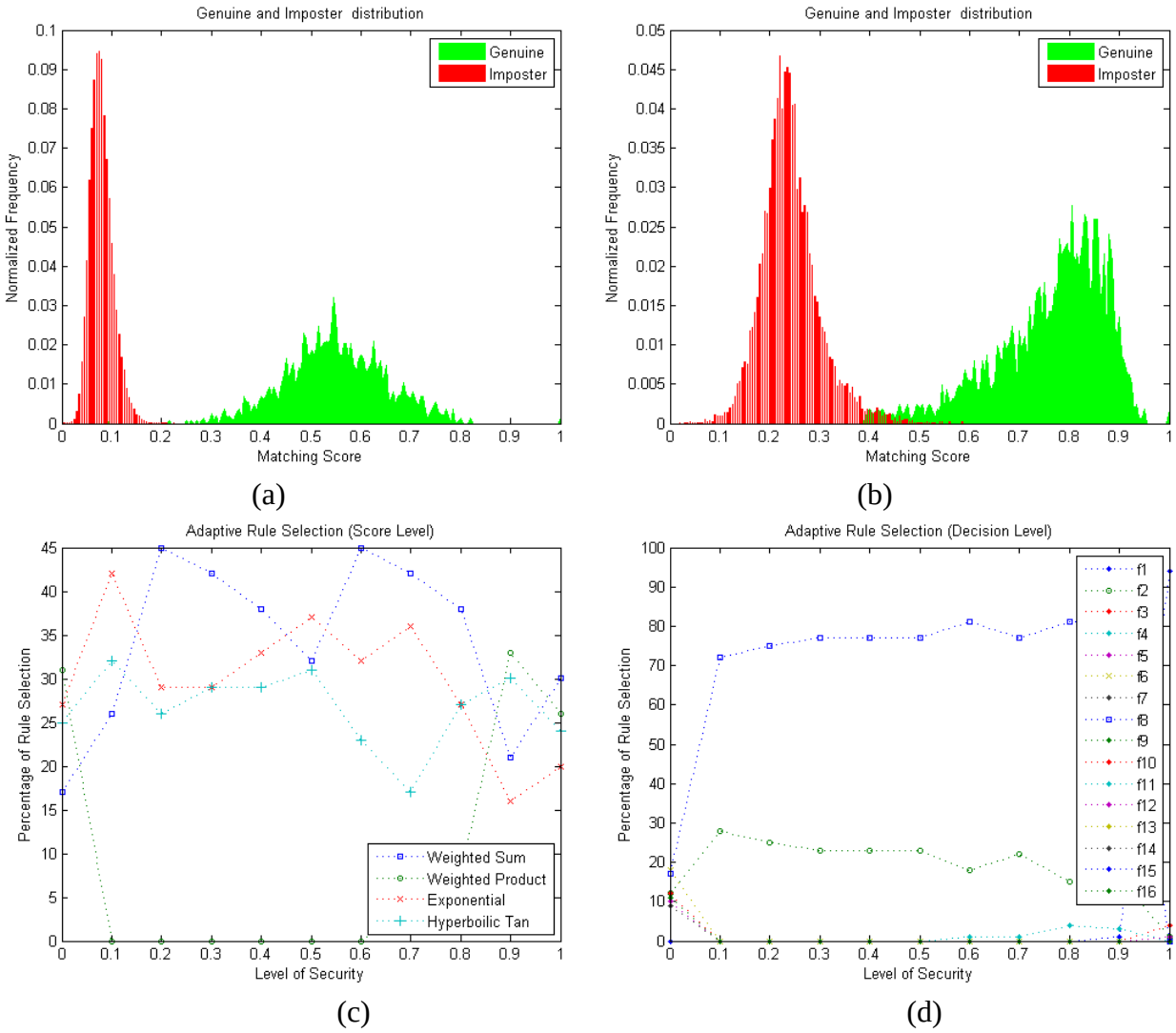

Figure 6.8: Genuine-Impostor match score distributions for (a) 2D palmprint and (b) 3D palmprint matchers. Adaptive selection of fusion rules for (c) score level and (d) decision level approaches.

The performance curves from the adaptive combination of 3D and 2D palmprint biometrics is shown in figure 6.9 (a)-(b), while the adaptive selection of rules is shown in figure 6.8 (c)-(d). It can be observed from the figure 6.9 that the performance from the score level adaptive combination is significantly better as compared to the decision level combination, both in terms of the minimum and the standard deviation of the error (cost).

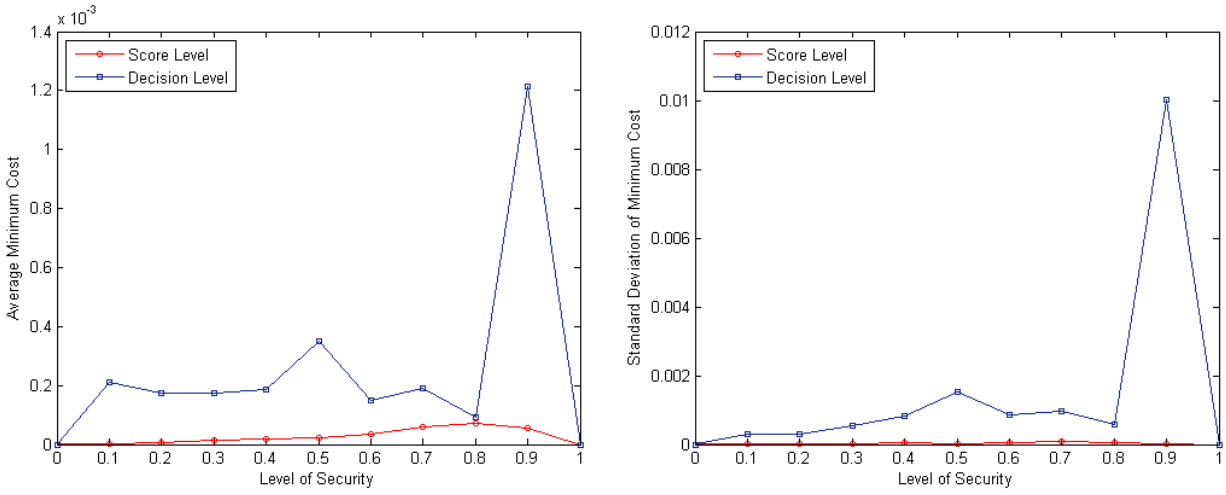

(a) (b)

Figure 6.9: Performance curves for adaptive combination of two palmprint matchers. Comparative plots of (a) average and (b) standard deviation of minimum cost for the adaptive score and decision level combinations.

In the second set of experiments on the real biometric samples, we combine three biometric modalities. The 3D hand database is employed to generate the genuine and impostor matching scores for the 2D palmprint, 3D palmprint and 3D hand geometry matchers. Figures 6.10(a), 6.10(b) and 6.10(c) depict the distributions of matching scores for the three modalities considered in this work. Adaptive selection of fusion rules for score level as well as decision level is shown figures 6.11(a) and 6.11(b), while the comparative plots for performance in terms of the average and the standard deviation of the minimum error is shown in figures 6.11(c) and 6.11(d) respectively. These results once again confirm the superiority of the adaptive score level approach over the decision level approach. The extremely low values of the standard deviation (nearly zero for all values of the security level α) suggests that the adaptive score level approach is highly stable and converges to the true optimal operating point on every run of the algorithm. Therefore the proposed approach requires significantly less number of runs to select the

optimal fusion rule and the corresponding parameters as compared to the decision level approach, which is highly instable and results in varying optimal operating pints on each run of the algorithm (refer to figure 6.11(d).

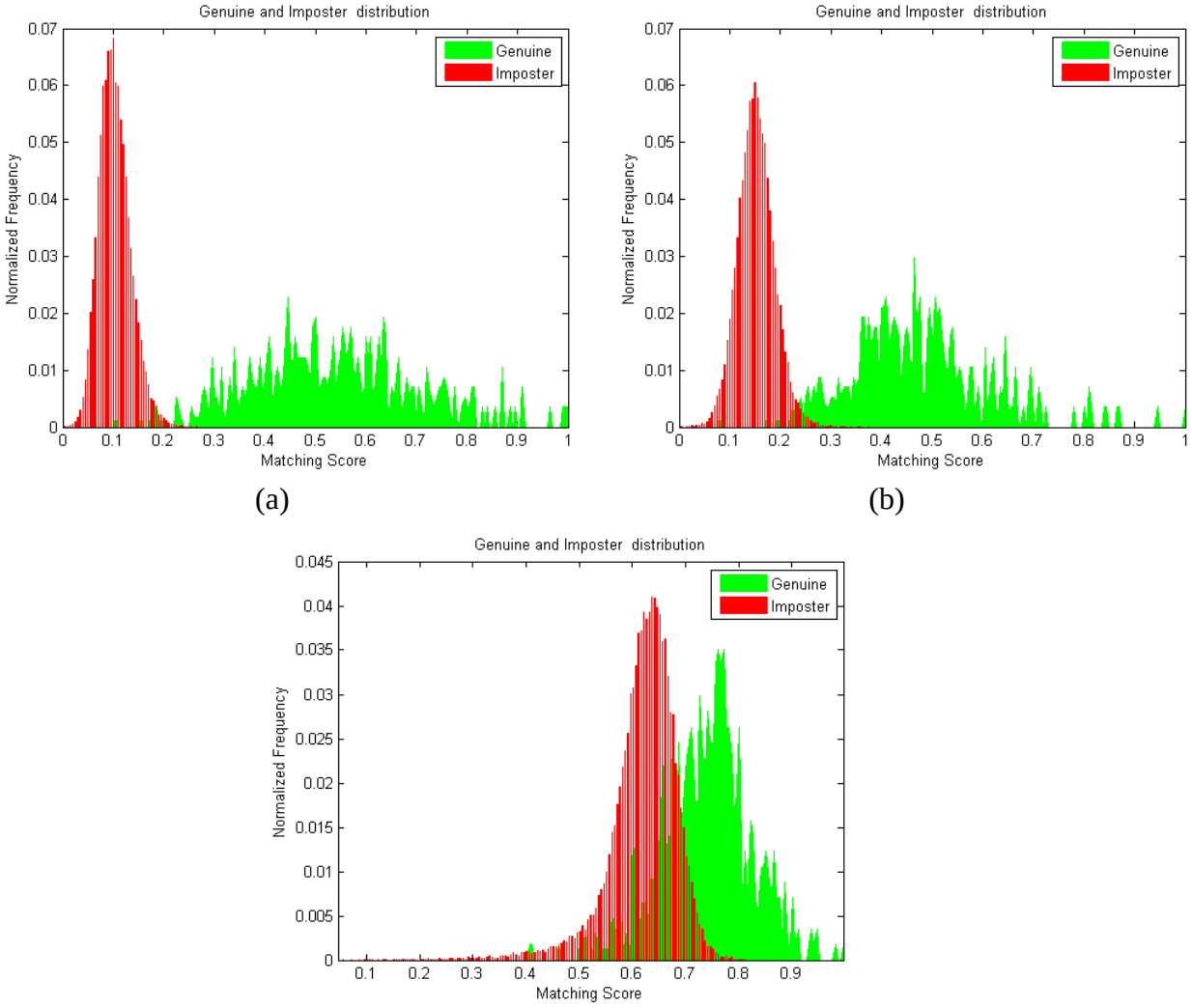

Figure 6.10: Genuine-Impostor match score distributions for (a) 2D palmprint, (b) 3D palmprint and (c) 3D hand geometry matchers.

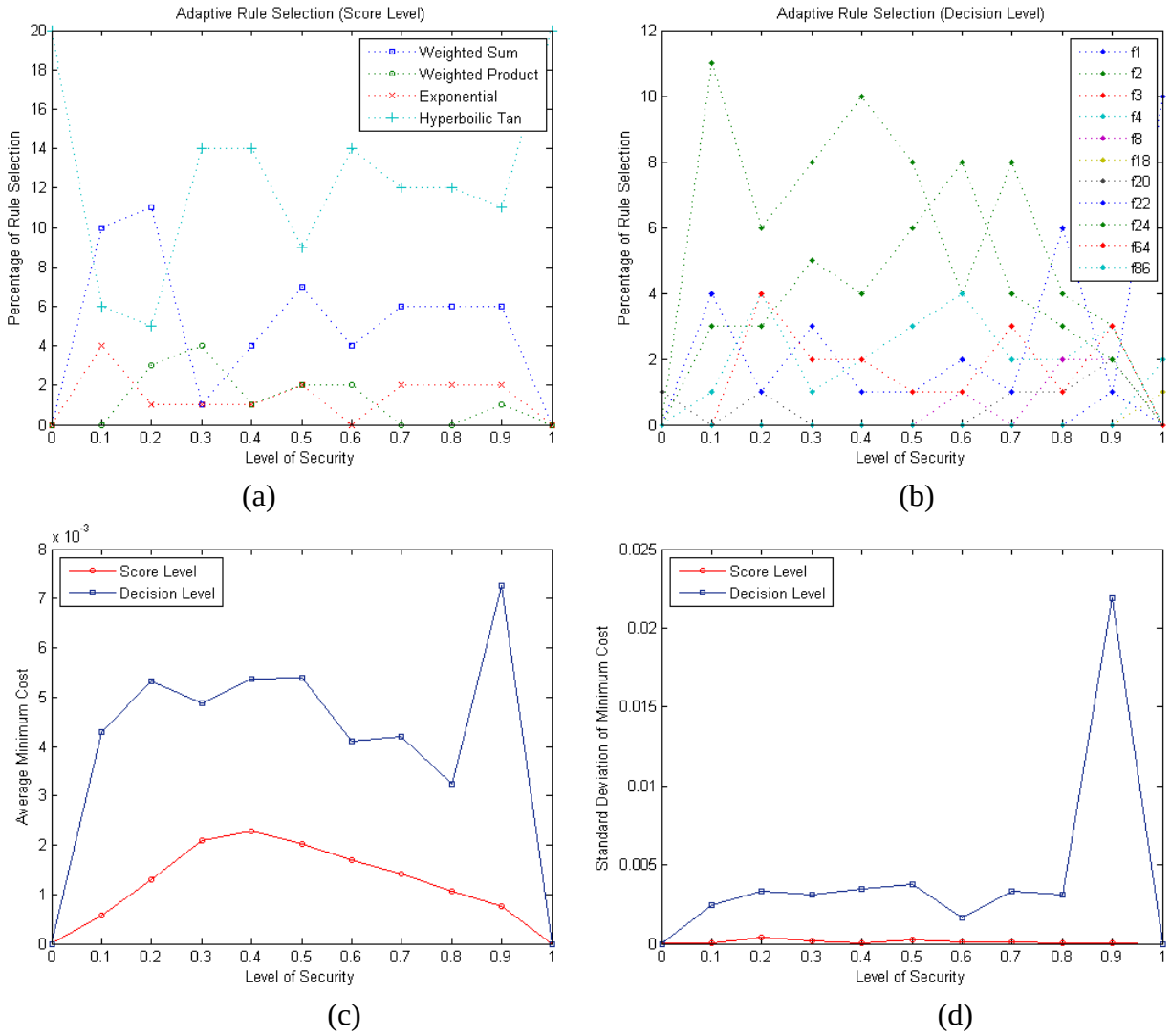

Figure 6.11: Adaptive selection of fusion rules and performance curves for combination three biometric matchers. (a)-(b) Adaptive selection of fusion rules for score and decision level approaches.(c)-(d) Comparative plots of average and standard deviation of minimum cost for adaptive score and decision level combinations.

6.4.2 Discussion

The experimental results presented in the previous section clearly demonstrate that the proposed adaptive approach to score level fusion consistently outperforms the decision level approach presented in [69]. The proposed approach not only yields lower error

rates, but also exhibits significantly lower variation in minimum cost achieved (low standard deviation) over 100 runs of the algorithm. This experimental finding assumes significance in the context of adaptive multimodal fusion as it provides more stable solutions than the decision level approach proposed in [69].

The major drawback of the technique presented in [69] is the large standard deviation of the minimum cost. The variation of minimum cost (achieved by the PSO) over 100 runs arises due to the fact that not all solutions given by the PSO are truly optimal, instead some are suboptimal solutions with a minimum cost very close to the global (true) minimum cost. Since the number of fusion rules in a decision level fusion framework is extremely high (2^{2^N} rules for fusion of N modalities), the search space for potential optimal solutions becomes very large. This results in increased possibility of PSO converging to sub optimal solutions and thus causing higher standard deviation of minimum cost achieved. This is clear from the experimental results presented in [69] where authors run their PSO algorithm 100 times and then choose the solution (as optimal) that appears the most number of times. Extensive experimental results presented in this chapter on real as well synthetic matching scores clearly indicate that the PSO formulization in the proposed method generates fairly stable solutions, as compared to the decision level approach in [69]. Unlike the decision level fusion, number of rules in the proposed fusion framework does not depend on the number of modalities and is quite limited (4 rules considered in this work). This explains why the PSO in the proposed framework exhibits less variation in the minimum cost achieved. Therefore the proposed approach requires significantly lower number of iterations to choose an optimal solution.

Observing the experimental results, we believe that the formulation of optimization problem using hybrid PSO and the score level fusion rules have contributed to the superior performance of the proposed methodology. In multibiometrics, a well designed fusion of match scores of individual classifiers/matchers is expected to yield better performance than combining abstract class labels (decision level fusion). This is because; match scores have higher information content (about the input biometric data and the matching) and therefore they often provide better representation than the class labels. Disagreement (by the individual classifiers) in the output of the matching process often deteriorates the performance of a multibiometric system. However, it is intuitive to think that these conflicting decisions by the matchers can have more adverse effect on the performance of decision level fusion than that of score level combination.

Verification time of the proposed algorithm is comparable with that of any other score level fusion rules. PSO in the proposed framework takes up the major share of computational time. However, parameter tuning by the PSO can be performed offline by computing the optimal parameters (fusion rules, weights and decision threshold) for every value of input security level in the range 0 to 1(in steps of , say, 0.1) and storing it in a look up table. Therefore whenever there is a new value for security level at the input, optimal parameters for that particular security level can be retrieved from the look up table and used for performing authentication/verification tasks. That way the verification time the proposed methodology can be made equivalent to (or comparable with) any other non adaptive multimodal biometric system. Therefore the issue of verification time never arises in the implementation and deployment of the proposed system for real world applications.

6.5 Summary

In the first part of this chapter, it has been experimentally demonstrated that a non monotonic rule can also be an optimum fusion rule, under certain operating conditions as illustrated in Table 6.1 and 6.2. This is in contrast to the statement in the original paper [69] - “an optimum fusion rule for any set of Bayesian costs is monotonic”. The results reported in [69] also indicate that the search space has been limited to only few monotonic rules which can inherently prevent other optimum rules from being selected. Therefore the experimental results reported in [69] (figure 14, pp. 354) should be replaced/read as illustrated in figure 6.4 in this dissertation.

In the second part of this chapter, a novel framework for adaptive fusion of multiple biometric traits is presented. The proposed method employed a hybrid particle swarm optimization to achieve the adaptive combination of multiple matching scores by selecting the optimal fusion rule and the corresponding fusion parameters. The experiments performed on real as well as synthetic datasets suggest that significant performance improvement can be achieved using the adaptive score level fusion approach. The experimental results also confirm that the proposed approach generates fairly stable performance and therefore requires smaller number of iterations to generate better performance as compared to the decision level approach.

Chapter 7
Conclusions and Future Directions

7.1 Conclusions

Hand geometry and palmprint biometrics have attracted tremendous interest from researchers and over the past decade, considerable research effort has been focused on developing hand identification approaches and systems. Nevertheless, there are still a few major issues that remain to be resolved. Traditional approaches utilizing 2D hand images and constrained image acquisition modules are plagued by various problems such as hygienic concerns, high degree of vulnerability to impostor attacks. On the other hand, very little research has been done to develop contact-free hand identification approaches and the existing methods do not address some of the key issues such as hand pose variations.

This dissertation has investigated the use of contact-free 3D hand scans and the possibility of combining shape and texture information in order to improve the performance of hand matching. A multilevel matching framework that utilizes 2D and 3D features extracted from the palmprint region of the hand is presented in Chapter 3. The proposed matching framework helps to combine the robustness (against spoof attacks) and the high discriminating power of the 3D and 2D palmprint features. A novel representation, namely, curvature map that captures the local palm surface details is also presented. The normalized local correlation is used to compute the matching distance

between a pair of curvature maps being matched. The multimodal (2D and 3D palmprint) matching approach presented in Chapter 3 is evaluated on the database of 108 users and shown to enhance the matching performance of the palmprint system. Apart from the performance improvement, the key advantage of combining 2D and 3D palmprint information is the increased robustness of the resulting system against spoof attacks. Our experiments with fake palmprints have shown how effortlessly a 2D image based palmprint matcher can be circumvented by presenting palmprint images printed on paper. On the other hand, the proposed system utilizing 3D palmprint features is shown to be more robust against attacks at the sensor level.

A new approach for contact-free 3D hand matching using the 3D geometry features is investigated and presented in Chapter 4. In order to extract discriminatory features from the range images of the hand, two new representations that characterize the finger surface are presented. The extracted features are then matched using two simple matching metrics (refer to equation 4.9 and 4.10) that can handle limited variations in the hand pose. The performance evaluation of this approach performed on a relatively large database of 177 users suggested that the 3D finger geometry features carry sufficient discriminatory information and therefore ascertained their usefulness for personal verification based on 3D hand matching. Further, our experiments on combination of multiple hand features (palmprint, hand geometry and finger texture), which are extracted simultaneously from a single hand image, achieved promising results (0.22% equal error rate on the database of 177 subjects). One limitation of this work is the assumption that the user presents his/her hands parallel to the image plane, which would facilitate the acquisition of frontal scans.

The large variation in 3D pose of the hand (presented for identification) is one of the major challenges in matching hand images acquired in a contact-free scenario. In order to address this problem, a pose normalization approach that is tailored for the acquired 2D and 3D hand images is investigated and detailed in Chapter 5. This approach involves estimating the orientation of the hand in 3D space followed by a pose correction step in which the 3D hand is rotated to its frontal pose. The approach is robust to large variations in pose as it only requires detection of a single landmark point (approximate center of the palm) on the hand. The estimated orientation information is also utilized to correct the pose of the acquired intensity image. Our experimental results on a database with considerably large hand pose variations (refer to Table 5.1 for statistics of the database) shows that the pose correction for 3D and 2D hand images leads to significant improvement in matching performance (refer to Table 5.2). We also observed that 3D hand geometry matcher do not benefit significantly (marginal improvement in EER as reported in Table 5.2) from the pose normalization process, since there is significant loss of discriminatory information around the finger edges. In order to tackle this problem, a dynamic fusion approach, which selectively combines palmprint and hand geometry matching scores, is developed. The experimental results show that the dynamic fusion approach can achieve better performance (60% improvement in EER) than the straightforward fusion of matching scores using sum rule.

Finally, our observations on the discrepancies in the experimental results in [69] are discussed in Chapter 6. We also demonstrated through the experiments that a non monotonic rule can also be an optimal fusion rule, which is contrary to the findings in [69]. Further, we developed an adaptive score level fusion framework to combine

multiple features that are simultaneously extracted from a single image of the hand. The approach is based on the hybrid particle swarm optimizer (PSO) to choose an optimal fusion rule and the corresponding weight parameters while minimizing the weighted error rate objective function. The proposed fusion framework is adaptive to the security level requirement, which is provided as an input to the system. The experiments are performed on a synthetic dataset with artificially generated matching scores to ascertain the usefulness of this approach. Our experimental results on the contact-free hand images further confirm the superiority (in terms of accuracy as well as stability) of this approach over the existing decision level fusion framework.

The hand based biometric systems enjoy high user acceptance and are extensively deployed for applications such as access control, time and attendance monitoring etc. The personal verification approaches (namely, the 3D palmprint and 3D hand geometry) developed in this research can be utilized to enhance the performance of the traditional hand based biometric systems. The 3D hand pose normalization approaches introduced in this thesis can be utilized to significantly improve the matching performance, especially when the hand images are acquired in an unconstrained manner.

7.2 Future Directions

Finally, we conclude this dissertation with our remarks on the ways in which the current research can be advanced. The following paragraphs discuss some of the areas that can be further explored to develop robust and reliable hand biometric systems:

1. The approaches presented in this dissertation for 3D and 2D palmprint identification do not take in to account scale variations in the acquired hand

images. Users were instructed to hold their hand at a fixed distance in front of the scanner during data collection. Therefore there is little scale variations in the datasets used for experiments in this dissertation. However, it is possible to acquire hand scans using different lenses in order to introduce considerable scale variations that may more closely represent a real world application scenario. A scale invariant ROI (palmprint) from the pose corrected 3D hand can be extracted based on the detection of a landmark feature point on the hand (inside the palm region). Once the landmark point (for example, the center of the palm) is located, all points in the data that are inside a predetermined distance (in 3D space) from this point can be extracted as belonging to ROI. Regions of interest of varying sizes thus extracted can be resampled to generated fixed size range and intensity palmprint images. However, the localization of landmark point can be very challenging, especially in the absence of any well defined feature point on the hand. Therefore further efforts are required to develop a robust hand identification approach that can accommodate considerable scale variations in the acquired hand scans.

2. The estimation of orientation of the hand is based on fitting a plane to a set of 3D data points extracted from the palmar region. Therefore this approach makes an assumption that the hand (including the fingers) is a rigid plane. This assumption holds good for palmar region of the hand since this region is not prone to large skin deformations and is relatively flat. On the other hand, fingers are more prone to deformation arising from their movement or bending, especially towards the inner surface of the hand. The deformation in fingers leads to large differences in

their orientation with that of the palmprint region. The current approach may not be able to reliably estimate the orientation and correct the pose of the fingers under these circumstances. Therefore it needs to be investigated if the performance can be improved by estimating the 3D orientation of the individual fingers and then normalizing their pose. The challenging task, however, will be to localize individual fingers and estimate their 3D orientation.

3. The current 3D hand identification approach employs a single scan (2.5D) of the inner surface of the hand. A complete model of the hand can be built during enrolment phase by acquiring and registering multiple 2.5D scans. Although the automatic generation of a complete model can be very challenging in the absence of well defined landmark points, a few landmark points can be manually identified during enrolment phase and multiple range images can be stitched together to build a model. If one could develop a method to match the 2.5D scans acquired during the verification stage with the complete model of the hand in the database, such an approach will be able to effectively handle large variations in the hand pose. It also needs to be investigated if a direct matching approach can be developed since the pose correction process leads to loss of crucial information around the finger edges.
4. The experimental results presented in this dissertation demonstrated that integrating three dimensional shape information with texture leads to performance improvement for hand identification. However, the major limitation of this approach is the use of 3D scanner to acquire hand shape information. Scanning time, size and cost of this 3D scanner can be prohibitive for real world civilian

applications such as access control where real-time authentication is desirable. Therefore alternative imaging techniques need to be explored in order to develop a customized 3D hand scanner that can operate in real-time. Such a 3D scanner would be desirable for a practical 3D hand identification system.

5. In this dissertation, the problem of variations in the hand pose is handled by normalizing the pose (by bring it to frontal pose) of the acquired 3D hand scan. However, a more efficient approach would be to extract features that are intrinsically invariant to hand pose changes. Although developing such an approach is challenging, it is more desirable as it may obviate the need for rotation of 3D hand and lead to concomitant reduction in the computational time.
6. This dissertation has examined the vulnerability of 2D palmprint identification systems to spoof attacks using palmprint images printed on paper. It may seem intuitive that three dimensional features are more robust against such attacks, since it may be extremely difficult to fabricate 3D hand models that are good enough to circumvent the system. However, there is no scientific evidence to ascertain that three dimensional features are more robust against spoof attacks. Therefore there is an urgent need for an experimental assessment of the susceptibility of the proposed 3D hand identification approach to sensor level attacks using fabricated hand models.

BIBLIOGRAPHY

Bibliography

[1] A. Antonelli, R. Cappelli, D. Maio and D. Maltoni, "Fake finger detection by skin distortion analysis", *IEEE Trans. Inf. Forensics Security*, vol. 1, no. 3, pp. 360-373, Sep. 2006.

[2] A. K. Jain and J. Feng, "Latent palmprint matching," to appear in *IEEE Trans. Pattern Anal. Mach. Intell*., 2009.(Available online)

[3] A. K. Jain and N. Duta, "Deformable matching of hand shapes for verification", *Proc. International Conf. Image Processing*, pp. 857-861, Oct.1999.

[4] A. K. Jain, A. Ross and S. Pankanti, "A Prototype hand geometry-based verification system", *Proc. AVBPA*, Washington DC, pp. 166-171, Mar.1999.

[5] A. K. Jain, A. Ross and S. Prabhakar, "An introduction to biometric recognition", *IEEE Trans. Circuits and Systems for Video Technology, Special Issue on Image- and Video-Based Biometrics*, vol. 14, no. 1, pp. 4-20, Jan. 2004.

[6] A. K. Jain, K. Nandakumar and A. Ross, "Score normalization in multimodal biometricsystems", *Pattern Recognition*, vol. 38, pp. 2270-2285, Dec. 2005.

[7] A. K. Jain, Y. Chen and M. Demirkus, "Pores and ridges: high-resolution fingerprint matching using level 3 features", *IEEE Trans. Pattern Anal. Mach. Intell.*, vol. 29, no. 1, pp. 15–27, 2007.

[8] A. Kong and D. Zhang, "Feature-level fusion for effective palmprint authentication", *Proc. International Conference on Biometric Authentication*, vol. 1, 2004, pp. 520–523.

[9] A. Kong and D. Zhang, "Palmprint identification using feature-level fusion", *Pattern Recognition*, vol. 39, no. 3, pp. 478–487, 2006.

[10] A. Kong, D. Zhang and M. Kamel, "A survey of palmprint recognition", *Pattern Recognition*, vol. 42, no. 7, pp. 1408-1418, 2009.

[11] A. Kumar and Ch. Ravikanth, “Personal authentication using finger knuckle surface”, *IEEE Trans. Info. Forensics & Security*, vol. 4, no. 1, pp. 98-110, Mar. 2009.

[12] A. Kumar and D. Zhang, “Hand geometry recognition using entropy-based discretization”, *IEEE Trans. Info. Forensics & Security*, vol. 2, no. 2, pp. 181-187, Jun. 2007.

[13] A. Kumar and D. Zhang, “Personal authentication using multiple palmprint representation”, *Pattern Recognition*, vol. 38, no. 10, pp. 1695-1704, Oct. 2005.

[14] A. Kumar and D. Zhang, “Personal recognition using hand-shape and texture”, *IEEE Trans. Image Processing*, vol. 15, no. 8, pp. 2454-2461, Aug. 2006.

[15] A. Kumar and H. C. Shen, “Palmprint identification using PalmCodes”, *Proc. 3rd International Conference on Image and Graphics*, pp. 258–261, 2004.

[16] A. Kumar and K. V. Prathyusha, “Personal authentication using hand vein triangulation and knuckle shape”, *IEEE Trans. Image Procesing.*, vol. 18, no. 9, pp. 2127-2136, Sep. 2009.

[17] A. Kumar, “Incorporating cohort information for reliable palmprint authentication”, *Proc. ICVGIP 2008*, pp. 583-590, 2008.

[18] A. Kumar, D. C. M. Wong, H. C. Shen and A. K. Jain, “Personal verification using palmprint and hand geometry biometric”, *Proc. 4th AVBPA*, Guildford, U.K., pp. 668-675, 2003.

[19] A. Morales, M. Ferrer, F. Díaz, J. Alonso and C. Travieso, “Contact-free hand biometric system for real environments”, *Proc. 16th Euopean Signal Processing Conference (EUSIPCO)*, Laussane, Switzerland, Sep. 2008.

[20] A. Ross, K. Nandakumar and A. K. Jain, *Handbook of multibiometrics*, Springer Publishers, 2006.

[21] A. Sharma, N. Shobhit and A. M. Namboodiri, “Projected texture for hand geometry based authentication”, *Proc. CVPR 2008*, Anchorage, Alaska, Jun. 2008.

[22] A. W. K. Kong and D. Zhang, “Competitive coding scheme for palmprint verification”, *Proc. 17th ICPR*, Washington, DC, pp. 1051-4651, 2004.

[23] Accu-Time Systems. <http://www.accu-time.com/cyber_bio-fg.htm>.

[24] B. O’Neill, *Elementary Differential Geometry*. New York: Academic, 1966.

[25] Biomet Partners Inc. <http://www.biomet.ch/vf.htm>.

[26] C. C. Han, “A hand-based personal authentication using a coarse-to-fine strategy”, *Image and Vision Computing*, vol. 22, no. 11, pp. 909–918, 2004.

[27] C. C. Han, H. L. Cheng, C. L. Lin and K. C. Fan, “Personal authentication using palm-print features”, *Pattern Recognition*, vol. 36, no. 2, pp. 371–381, 2003.

[28] C. Dorai and A. K. Jain, “COSMOS - A representation scheme for 3D free-form objects”, *IEEE Trans. Pattern Anal. Mach. Intell*., vol.19, no.10, pp. 1115-1130, Oct. 1997.

[29] C. L. Lin and K.-C. Fan, “Biometric verification using thermal images of palm-dorsa vein patterns”, *IEEE Trans. Circuits and Systems for Video Technology*, vol. 14, no. 2, pp. 199–213, 2004.

[30] C. Methani and A. M. Namboodiri, “Pose invariant palmprint recognition”, *Proc. ICB 2009*, pp. 577-586, Jun. 2009.

[31] C. Oden, A. Ercil and B. Buke, “Hand recognition using implicit polynomials and geometric features,” *Pattern Recognition Letters*, vol. 24, no. 13, pp. 2145–2152, 2003.

[32] C. Poon, D. C. M. Wong and H. C. Shen, “A new method in locating and segmenting palmprint into region-of-interest”, *Proc. 17th International Conference on Pattern Recognition*, vol. 4, 2004, pp. 533–536.

[33] Citizen guidance on the homeland security advisory system. <http://www.dhs.gov/xlibrary/assets/CitizenGuidanceHSAS2.pdf>.

[34] D. G. Joshi, Y. V. Rao, S. Kar and V. Kumar, “Computer vision based approach to personal identification using finger crease pattern”, *Pattern Recognition*, vol. 31, no. 1, pp. 15-22, 1998.

[35] D. Gafurov, E. Snekkenes and P. Bours, “Spoof attacks on gait authentication system”, *IEEE Trans. Inf. Forensics Security*, vol. 2, no. 3, pp. 491-502, Sep. 2007.

[36] D. L. Woodard and P. J. Flynn, “Finger surface as a biometric identifier”, *Computer Vision and Image Understanding*, vol. 100, no. 3, pp. 357-384, Dec. 2005.

[37] D. M. J. Tax, M. V. Breukelen, R. P. W. Duin and J. Kittler, “Combining multiple classifiers by averaging or multiplying”, *Pattern Recognition*, vol. 33, pp. 1475-1485, 2000.

[38] D. Osten, H. M. Carim, M. R. Arneson and B. L. Blan, “Biometric personal authentication system”, U.S. Patent No.5,719,950, Feb. 17, 1998.

[39] D. P. Sidlauskas and S. Tamer, “Hand geometry recognition”, *Handbook of Biometrics*, A. K. Jain, P. Flynn and A. Ross (eds.), Springer, 2008.

[40] D. P. Sidlauskas, “3D hand profile identification apparatus”, U.S. Patent 4736203, 1988.

[41] D. S. Huang, W. Jia and D. Zhang, “Palmprint verification based on principal lines”, *Pattern Recognition*, vol. 41, no. 4, pp. 1316–1328, 2008.

[42] D. Zhang and W. Shu, “Two novel characteristics in palm-print verification: datum point invariance and line feature matching,” *Pattern Recognition*, vol. 32 , pp. 691–702, 1999.

[43] D. Zhang, G. Lu, W. Li, L. Zhang and L. Nan, “Three dimensional palmprint recognition using structured light imaging”, *Proc. BTAS 2008*, pp. 1-6, Sep. 2008.

[44] D. Zhang, W. K. Kong, J. You and M. Wong, “Online palmprint identification”, *IEEE Trans. Pattern Anal. Mach. Intell.*, vol. 25, no. 9, pp. 1041–1050, Sep. 2003.

[45] E. Yörük, E. Konukoglu, B. Sankur and J. Darbon, “Shape-based hand recognition”, *IEEE Trans. Image Processing*, vol.15, no.7, pp.1803-1815,2006.

[46] F. Chen, “3D Fingerprint and palm print data model and capture devices using multi structured lights and cameras”, U. S. Patent No. 20060120576, 2006.

[47] F. Roli, S. Raudys and G. L. Marcialis, “An experimental comparison of fixed and trained fusion rules for crisp classifier outputs”, *Proc. 3rd Intl. Workshop on Multiple Classifier Systems (MCS 2002)*, Cagliari (Italy), Springer-Verlag, LNCS, Jun. 2002.

[48] Fujitsu PalmSecure. <http://www.fujitsu.com/us/services/biometrics/palm-vein>.

[49] G. Amayeh, G. Bebis, A. Erol and M. Nicolescu, “Peg-free hand shape verification using high order zernike moments”, *Proc. CVPR 2006*, New York, USA, 2006.

[50] G. Feng, D. Hu, D. Zhang and Z. Zhou, “An alternative formulation of kernel LPP with application to image recognition”, *Neurocomputing*, vol. 67, pp. 1733–1738, 2006.

[51] G. Guo, M. Jones and P. Beardsley, “A system for automatic iris capturing”, <http://www.merl.com/publications/TR2005-044/> , TR2005-044, MERL, 2005.

[52] G. Lu, D. Zhang and K. Wang, “Palmprint recognition using eigenpalms features”, *Pattern Recognition Letters*, vol. 24, no. 9, pp. 1463–1467, 2003.

[53] G. M. Lu, K. Q. Wang and D. Zhang, “Wavelet based independent component analysis for palmprint identification”, *Proc. International Conference on Machine Learning and Cybernetics*, vol. 6, pp. 3547–3550, 2004.

[54] G. Zheng, C. J. Wang and T. E. Boult, "Application of projective invariants in hand geometry biometrics", *IEEE Trans. Info. Forensics Security*, vol. 2, no. 4, pp. 758-768, 2007.

[55] H. Cantzler and R. Fisher, "Comparison of HK and SC curvature description methods", *Proc. 3 rd Int. Conf. on 3-D Digital Imaging and Modeling*, pp. 285 – 291, 2001.

[56] H. Chen and B. Bhanu, "Human ear recognition in 3D", *IEEE Trans. Pattern Anal. Mach. Intell.*, vol. 29, no. 4, pp. 718-737, Apr. 2007.

[57] H. Chen, H. Valizadegan, C. Jackson, S. Soltysiak and A. K. Jain, "Fake hands: spoofing hand geometry systems", *Biometric Consortium 2005*, Washington DC, 2005.

[58] I. H. Jacoby, A. J. Giordano and W. H. Fioretti, "Personnel identification apparatus," U.S. Patent No. 3648240, 1972.

[59] J. Chen and Y. S. Moon, "Using SIFT features in palmprint authentication", *Proc. ICPR 2008*, pp. 1-4, 2008.

[60] J. Daugman, "Probing the uniqueness and randomness of IrisCodes: Results from 200 billion iris pair comparisons," *Proc. IEEE*, vol. 94, no. 11, pp 1927-1935, 2006.

[61] J. G. Wang, W. Y. Wang, A. Suwandy and E. Sung, "Fusion of palmprint and palm vein images for person recognition based on laplacianpalm feature", *Proc. IEEE Computer Vision and Pattern Recognition Workshop on Biometrics*, pp. 1–8, 2007.

[62] J. G. Wang, W. Y. Yau, A. Suwandy and E. Sung, "Person recognition by fusing palmprint and palm vein images based on Laplacianpalm representation", *Pattern Recognition*, vol. 41, no. 5, pp. 1514–1527, 2008.

[63] J. J. Koenderink and A. J. van Doorn, "Surface shape and curvature scales", *Image Vision Computing*, vol. 10, no. 8, pp. 557–564, Oct. 1992.

[64] J. Kittler, M. Hatef, R. P. W. Duin and J. Matas, "On combining classifiers", *IEEE Trans. Patt. Anal. Machine Intell.*, vol. 20, pp. 226-239, Mar. 1998.

[65] J. S. Chen, Y. S. Moon and H. W. Yeung, "Palmprint authentication using time series", *Proc. Fifth International Conference on Audio- and Video-based Biometric Person Authentication*, pp. 20–22, 2005.

[66] J. You, W. K. Kong, D. Zhang and K. H. Cheung, "On hierarchical palmprint coding with multiple features for personal identification in large databases", *IEEE Trans. Circuits and Systems for Video Technology.*, vol. 14, no. 2, pp. 234–243, 2004.

[67] K. I. Chang, K. W. Bowyer and P. J. Flynn, "An evaluation of multimodal 2D+3D face biometrics", *IEEE Trans. Pattern Anal. Mach. Intell.*, vol. 27, no. 4, pp. 619-624, Apr. 2005.

[68] K. Nandakumar, Y. Chen, A. K. Jain and S. C. Dass, "Quality-based score level fusion in multibiometric systems", *Proc. 18th International Conference on Pattern Recognition (ICPR 2006)*, pp. 473-476, 2006.

[69] K. Veeramachaneni, L. A. Osadciw and P. K. Varshney, "An adaptive multimodal biometric management algorithm", *IEEE Trans. Sys. Man & Cybern., Part-C*, vol. 35, no. 3, pp. 344-356, Aug. 2005.

[70] L. Liu and D. Zhang, "A novel palm-line detector", *Proc. AVBPA 2005*, pp. 563-571, 2005.

[71] L. Shang, D. S. Huang, J. X. Du and C. H. Zheng, "Palmprint recognition using FastICA algorithm and radial basis probabilistic neural network", *Neurocomputing*, vol. 69, pp. 1782–1786, 2006.

[72] L. Wang and G. Leedham, "Near- and far- infrared imaging for vein pattern biometrics", *Proc. IEEE Intl. Conf. on Video and Signal Based Surveillance*, 2006.

[73] L. Wang, G. Leedham and D. S. Y. Cho, "Minutiae feature analysis for infrared hand vein pattern biometrics", *Pattern Recognition*, vol. 41, no. 3, pp. 920-929, 2008.

[74] L. Wong and P. Shi, "Peg-free hand geometry recognition using hierarchical geometry and shape matching", *Proc. IAPR Workshop on Machine Vision Applications*, Nara, Japan, pp. 281–284, 2002.

[75] L. Zhang and D. Zhang, "Characterization of palmprints by wavelet signatures via directional context modeling", *IEEE Trans. Sys. Man & Cybern.: Part B*, vol. 34, no. 3, pp. 1335–1347, 2004.

[76] L. Zhang, Z. Guo, Z. Wang and D. Zhang, "Palmprint verification using complex wavelet transform", *Proc. International Conference on Image Processing*, vol. 2, pp. 417–420, 2007.

[77] M. Clerc and J. Kennedy, "The Particle Swarm-Explosion, Stability, and Convergence in a Multidimensional Somplex space", *IEEE Trans. Evolutionary Comp.*, vol. 6, p. 58-73, 2002.

[78] M. G. K. Ong, T. Connie and A. B. J. Teoh, "Touch-less palm print biometrics: Novel design and implementation", *Image Vision Computing*, vol. 26, no. 12, pp.1551-1560, 2008.

[79] M. Sonka and R. Hlavac, V. Boyle, *Image processing, analysis, and machine vision*, PWS Publishing, 1999.

[80] M. Watanabe, T. Endoh, M. Shiohara and S. Sasaki, "Palm vein authentication technology and its applications" *Proc. The Biometric Consortium Conference*, 2005.

[81] Minolta Vivid 910 noncontact 3D digitizer. <http://www.konicaminolta.com/instruments/products/3d/non-contact/vivid910/index.html>, 2008.

[82] N. Duta, "A survey of biometric technology based on hand shape", *Pattern Recognition*, vol. 42, no. 11, pp. 2797-2806, Nov. 2009.

[83] N. Duta, A. K. Jain and K. V. Mardia, "Matching of palmprints", *Pattern Recognition Letters*, vol. 23, no. 4, pp. 477–485, 2002.

[84] N. K. Ratha, J. H. Connell and R. M. Bolle, "An analysis of minutiae matching strength", *Proc. 3 rd AVBPA*, pp. 223 – 228, 2001.

[85] N. Otsu, "A threshold selection method from gray-level histograms", *IEEE Trans. Sys. Man & Cybern.*, vol. 9, no. 1, pp. 62–66, 1979.

[86] N. Yokoya and M. D. Levine, "Range image segmentation based on differential geometry: a hybrid approach", *IEEE Trans. Pattern Anal. Mach. Intell.*, vol. 11, no. 6, pp. 643-649, Jun. 1989.

[87] P. Besl, "Active, optical range imaging sensors", *Machine Vision and Applications*, vol.1, no. 2, pp. 127-152, 1988.

[88] P. H. Hennings-Yeomans, B. V. K. Vijaya Kumar and M. Savvides, "Palmprint classification using multiple advanced correlation filters and palm-specific segmentation", *IEEE Trans. Inf. Forensics Security*, vol. 2, no. 3, pp. 613-622, Sep. 2007.

[89] P. J. Besl and R. C. Jain, "Segmentation through variable-order surface fitting", *IEEE Trans. Pattern Anal. Mach. Intell.*, vol. 10, no .2, pp. 167-192, Mar 1988.

[90] P. J. Flynn and A. K. Jain, "On reliable curvature estimation", *Proc. CVPR*, pp. 110-116, 1989.

[91] P. K. Varshney, *Distributed Detection and Data Fusion*, Springer, New York, 1997.

[92] P. V. Reddy, A. Kumar, S. M. K. Rahman and T. S. Mundra, "A new antispoofing approach for biometric devices", *IEEE Trans. Biomedical Circuits and Systems*, vol. 2, no. 4, pp. 284-293, Dec. 2008.

[93] P. Yan and K. W. Bowyer, "Biometric recognition using 3D ear shape", *IEEE Trans. Pattern Anal. Mach. Intell.*, vol. 29, no. 8, pp. 1297-1308, Aug. 2007.

[94] P. Yan and K.W. Bowyer, "Multi-biometrics 2D and 3D ear recognition", *Proc. AVBPA 2005*, pp. 503-512, 2005.

[95] R. C. Eberhart and J. Kennedy, *Swarm intelligence*, Morgan Kaufmann, San Diego, 2001.

[96] R. H. Ernst, "Hand ID system," U.S. Patent No. 3576537, 1971.

[97] R. K. Rowe, U. Uludag, M. Demirkus, S. Parthasaradhi and A. K. Jain, "A multispectral whole-hand biometric authentication system", *Proc. Biometric Symposium*, Biometric Consortium Conference, Baltimore, Sept. 2007.

[98] R. P. Miller, "Finger dimension comparison identification system", U.S. Patent No. 3576538, 1971.

[99] R. Sanchez-Reillo, C. Sanchez-Avila and A. Gonzalez- Macros, "Biometric identification through hand geometry measurements", *IEEE Trans. Pattern Anal. Mach. Intell.*, vol. 22, no. 10, pp.168-1171, Oct. 2000.

[100] R. W. Frischholz and U. Deickmann, "BioID: A multimodal biometric identification system", *IEEE Comput.*, vol. 33, no. 2, Feb. 2000.

[101] Recognition Systems. <http://recognitionsystems.schlage.com/products>.

[102] S. Malassiotis, N. Aifanti, and M. G. Strintzis, "Personal authentication using 3-D finger geometry", *IEEE Trans. Info. Forensics & Security*, vol.1, no. 1, pp. 12-21, Mar. 2006.

[103] S. Ribaric and I. Fratric, "A biometric identification system based on Eigenpalm and Eigenfinger features", *IEEE Trans. Pattern Anal. Mach. Intell.*, vol. 27, no. 11, Nov. 2005.

[104] S. Ribaric and I. Fratric, "An online biometric authentication system based on eigenfingers and finger-geometry", *Proc. 13th Eur. Signal Processing Conf.*, Antalya, Turkey, Sep. 2005.

[105] S. T. V. Parthasaradhi, R. Derakhshani, L. A. Hornak and S. A. C. Schuckers, "Time-series detection of perspiration as a liveness test in fingerprint devices", *IEEE Trans. Syst., Man & Cybern.: Part C*, vol. 35, no. 3, pp. 335–343, Aug. 2005.

[106] Savitzky-Golay filters for 2D images. <http://research.microsoft.com/en-us/um/people/jckrumm/savgol/savgol.htm>, 2008.

[107] T. Connie, A. T. B. Jin, M. G. K. Ong and D. N. C. Ling, "An automated palmprint recognition system", *Image and Vision Computing*, vol. 23, no. 5, pp. 501–515, 2005.

[108] T. Matsumoto, H. Matsumoto, K. Yamada and S. Hoshino, "Impact of artificial Gummy fingers on fingerprint systems", *Proc. SPIE*, vol. 4677, pp. 275 – 289, 2002.

[109] T. S. Lee, "Image representation using 2D Gabor wavelet", *IEEE Trans. Pattern Anal. Mach. Intell.*, vol. 18, no. 10, pp. 959 - 971, Oct. 1996.

[110] T. Sim, S. Zhang, R. Janakiraman and S. Kumar, "Continuous verification using multimodal biometrics", *IEEE Trans. Patt. Anal. Machine Intell.*, vol. 29,no. 4, pp. 687-700, Apr. 2007.

[111] V. Kanhangad, A. Kumar and D. Zhang, "Combining 2D and 3D hand geometry features for biometric Verification", *Proc. IEEE Workshop on Biometrics at CVPR 2009*, Miami, Florida, Jun. 2009.

[112] V. Kanhangad, D. Zhang and L. Nan, "A multimodal biometric authentication system based on 2D and 3D palmprint features", *Proc. SPIE Biometric Technology for Human Identification V*, Orlando, pp. 69440C-69440C-9, Mar. 2008.

[113] V. Ruiz-Albacete, P. Tome-Gonzalez, F. Alonso-Fernandez, J. Galbally, J. Fierrez and J. Ortega-Garcia, "Direct attacks using fake images in iris verification", *Proc. COST 2101 Workshop on Biometrics and Identity Management*, BIOID, 2008.

[114] W. H. Press, S. A. Teukolsky, W. T. Vetterling and B. P. Flannery, *Numerical recipes: the art of scientific computing*, Cambridge University Press, 2007.

[115] W. Jia, D. S. Huang and D. Zhang, "Palmprint verification based on robust line orientation code", *Pattern Recognition, vol.* 41, no. 5, pp. 1504–1513, 2008.

[116] W. K. Kong, D. Zhang and W. Li, "Palmprint feature extraction using 2-D Gabor filters", *Pattern Recognition*, vol. 36, pp. 2339–2317, 2003.

[117] W. Li, D. Zhang and Z. Xu, "Palmprint identification by fourier transform", *Int. J. Patt. Recog. & Art. Intell.* , vol. 16, no. 4, pp. 417–432, 2002.

[118] W. Shu and D. Zhang, "Automated personal identification by palmprint", *Optical Engineering*, vol. 38, no. 8, pp. 2359–2362, 1998.

[119] W. Xiong, K. A. Toh, W. Y. Yau and X. Jiang, "Model-guided deformable hand shape recognition without positioning aids", *Pattern Recognition*, vol. 38, no. 10, pp. 1651-1664, Oct. 2005.

[120] X. Lu, A. K. Jain and D. Colbry, "Matching 2.5D face scans to 3D models", *IEEE Trans. Pattern Anal. Mach. Intell.*, vol. 28, no.1, pp. 31-43, Jan. 2006.

[121] X. Wang, H. Gong, H. Zhang, B. Li and Z. Zhuang, "Palmprint identification using boosting local binary pattern", *Proc. International Conference on Pattern Recognition*, pp. 503–506, 2006.

[122] X. Wu, D. Zhang and K. Wang, "Fisherpalms based palmprint recognition", *Pattern Recognition Letters*, vol. 24, no.15, pp. 2829–2838, 2003.

[123] X. Wu, D. Zhang and K. Wang, "Palm line extraction and matching for personal authentication", *IEEE Trans. Sys. Man & Cybern.: Part A*, vol. 36, no. 5, pp. 978-987, Sep. 2006.

[124] X. Wu, K. Wang and D. Zhang, "A novel approach of palm-line extraction", *Proc. the Third International Conference on Image and Graphics*, pp. 230–233, 2004.

[125] X. Wu, K. Wang and D. Zhang, "Palmprint recognition using directional line energy feature", *Proc. ICPR 2004*, vol.4, pp. 475-478, Aug. 2004.

[126] X. Wu, K. Wang and D. Zhang, "Wavelet based palmprint recognition", *Proc. the First International Conference on Machine Learning and Cybernetics*, vol. 3, pp. 1253–1257, 2002.

[127] X. Y. Jing and D. Zhang, "A face and palmprint recognition approach based on discriminant DCT feature extraction", *IEEE Trans. Sys. Man & Cybern.: Part B*, vol. 34, no.6, pp. 2405–2415, 2004.

[128] Y. Hao, T. Tan, Z. Sun and Y. Han, "Identity verification using handprint," *Proc. ICB 2007*, Lecture Notes Springer, vol. 4642, pp. 328-337, 2007.

[129] Y. Hao, Z. Sun, and T. Tan, "Comparative studies on multispectral palm image fusion for biometrics", *Proc. ACCV*, 2007.

[130] Y. Hao, Z. Sun, T. Tan and C. Ren, "Multispectral palm image fusion for accurate contact-free palmprint recognition", *Proc. ICIP 2008*, pp. 281-284, 2008.

[131] Y. L. Lay, "Hand shape recognition", *Opt. Laser Technol.*, vol. 32, no. 1, pp. 1–5, 2000.

[132] Z. Sun, T. Tan, Y. Wang, and S. Z. Li, "Ordinal palmprint representation for personal identification", *Proc. CVPR 2005*, vol. 1, pp. 279- 284, 2005.